Shape observables

CALT-68-723

Gallimaufry

CALT-68-723
DoE RESEARCH AND
DEVELOPMENT REPORT

A Gallimaufry of e^+e^- Annihilation Event Shapes*

by

GEOFFREY C. FOX and STEPHEN WOLFRAM†

California Institute of Technology, Pasadena, California 91125

ABSTRACT

This paper treats several disjointed topics in the study of event shapes in e^+e^- annihilation to hadrons. First, we describe the calculation of the shape parameters $\langle H_\ell \rangle$ in QCD perturbation theory. We show that they suffer $O(\sqrt{m^2/s})$ mass corrections, discuss smearing required near thresholds and consider some effects of hadron formation and of higher-order corrections. For large ℓ, the $\langle H_\ell \rangle$ computed to lowest order in α_s diverge like $\log(\ell)$ or $\log^2(\ell)$. We describe in detail the summation of such leading logarithmic terms to all orders in perturbation theory and emphasize the appearance of single and double logarithmic behavior in different kinematic configurations. Our methods are of general utility in estimating higher order effects in QCD perturbation theory. In particular, we apply them in an analysis of the angular spread of QCD jets and of the transverse momentum distribution of virtual photons from the Drell-Yan process. The second topic considered is energy correlation functions, which give the mean energy incident on two detectors around an e^+e^- annihilation event. Practical methods for calculating energy correlations from measured events are devised. Analytical formulae for energy correlations derived from perturbation theory are presented, but it is found (as expected from their infrared instability) that energy correlations are of little practical utility at foreseeable energies because of large fragmentation corrections. In the third part of the paper, correlations between the final state and the beam direction are considered. We present observables which allow the angular distributions of planes of final particles with respect to the beam to be determined without finding the planes explicitly. Finally, we discuss three-detector energy correlations and their moments, which provide methods for investigating planar structure in e^+e^- annihilation events.

*Work supported in part by the U.S. Department of Energy under Contract No. EY76-C-03-0068. Gallimaufry, n. Heterogeneous mixture, jumble, medley [1].
†Supported by a Feynman fellowship.

CONTENTS

1. Introduction

Footnotes

2. Corrections to the $\langle H_\ell \rangle$

2.1 Introduction

2.2 Thresholds

2.3 Mass Corrections

2.4 Hadronization Effects

2.5 Higher-order Terms in the Perturbation Series

2.6 H_ℓ Distributions, Phase Space Final States, QED Radiative Corrections and an Analogy with Electromagnetic Showers

2.7 Processes with Colored Initial States

Footnotes

Figure

3. The $\langle H_\ell \rangle$ for Large ℓ and their Estimation by Leading Log Summation

3.1 Introduction

3.2 Estimation of $\langle H_\ell \rangle$ for $e^+e^- \to q\bar{q}(G)$ from $\langle F_2^{pt}(\chi) \rangle$

3.3 Choices of Gauge in $e^+e^- \to q\bar{q}G$

3.4 The Leading Log Approximation for $e^+e^- \to q\bar{q}(GG..)$

3.5 Leading Log Estimates for $\langle F_2^{pt}(\chi) \rangle$ near $\chi = -1$ and $\langle H_\ell \rangle$ in $e^+e^- \to q\bar{q}(GG...)$

3.6 Leading Log Estimates for $\langle F_2^{pt}(\chi) \rangle$ near $\chi = +1$ and the $\langle H_\ell \rangle$ in $\zeta \to GGG(GG...)$

3.7 The Width of QCD Jets

3.8 Application to the Drell-Yan Process

3.9 Real Photon Production in e^+e^- Annihilation

Table

Footnotes

Figures

4. Rotationally-averaged Two-detector Energy Correlations

4.1 Formalism and Calculational Techniques

4.2 $\langle F_2 \rangle$ and $1/\sigma\, d\sigma/dF_2$ for Two- and Three-jet Events

4.3 Heavy Quark and Lepton Production Events

Footnotes

Figures

5. Correlations with Respect to the Beam Axis

5.1 Introduction

5.2 General Form of the Angular Dependence of Energy Correlations

5.3 Moments of Angular Correlations

5.4 Some Analytical Results for $\tilde{F}_2^{pt}$

5.5 Some Results on $\tilde{F}_2^{pt}$ and its Moments $\bar{\Pi}_k^\ell$ for Hadronic Events

Tables

Footnotes

Figures

6. Three-detector Energy Correlations

6.1 $F_{3\perp}$ as a Test of Planar Structure

6.2 Moments of Three-detector Energy Correlations

Figures

Appendix A: Analytical Results for Mean Two-detector Energy Correlations in the Free Quark and Gluon Approximation

Appendix B: $2 + \sin^2\theta_N$ Forever?

Appendix C: 'Scalar QCD'

Footnote

Acknowledgments

References

1. Introduction

In a previous paper [2] [F1.1], we introduced the shape parameters (the P_ℓ are the Legendre polynomials, and the sum runs over all pairs of particles)

$$H_\ell = \sum_{i,j} \frac{|\vec{p}_i||\vec{p}_j|}{s} P_\ell(\hat{p}_i \cdot \hat{p}_j) \tag{1.1}$$

which describe the distribution of energy in the final states of e^+e^- annihilation events and whose mean values may be computed from QCD perturbation theory. In this paper, we develop further the calculation of the $\langle H_\ell \rangle$ and also describe other methods for analyzing event shapes.

In Section 2 we consider corrections to the $\langle H_\ell \rangle$ in QCD perturbation theory. We first describe the general picture of e^+e^- annihilation events in QCD and show that the $\langle H_\ell \rangle$ typically probe the structure of final states at distances less than about $\ell/\sqrt{s}$ ($\sqrt{s}$ is the e^+e^- c.m. energy). For small s, we show (in Section 2.3) that the $\langle H_\ell \rangle$ (and other shape parameters) exhibit $O(\sqrt{m^2/s})$ mass corrections, as opposed to the $O(m^2/s)$ ones found in the total cross-section. We discuss (in Section 2.2) the smearing of the $\langle H_\ell \rangle$ required near thresholds. In Section 2.5 we address higher order terms in the perturbation series for the $\langle H_\ell \rangle$ at low ℓ, while in Section 2.7 we describe some difficulties associated with the calculation of the $\langle H_\ell \rangle$ for processes in which the initial state contains colored partons.

For large ℓ, the $\langle H_\ell \rangle$ at each order in α_s develop large logarithms of ℓ. Section 3 is devoted to a detailed discussion of the summation of the leading log terms in the $\langle H_\ell \rangle$ to all orders in perturbation theory. At large ℓ, the $\langle H_\ell \rangle$ probe integrals of energy correlation functions for detectors close to 0° and 180° apart. These give the mean square energy into a small cone in an event and the mean product of energies incident on two back-to-back cones.

In the first case, single logarithms of the cone opening angle (of order $1/\ell$) appear at each order in α_s while in the second case, double logarithms are found. In Section 3.2 we use our explicit calculation of energy correlation functions to $O(\alpha_s)$ given in Appendix A to find the leading behavior of $\langle H_\ell \rangle$ to $O(\alpha_s)$. Sections 3.3 and 3.4 describe the formalism required for leading log summations in the process $e^+e^- \to q\bar{q}(GG\ldots)$ [F1.2]. The results of these summations are given in Section 3.5; the double logarithmic divergences as $\ell \to \infty$ (or $\theta \to 0$) exponentiate to a function which goes smoothly to zero in this limit. The double logarithms summed in Section 3.5 are characteristic of processes in which pairs of jets are produced approximately back-to-back. When this is not the case, the leading log terms come from the behavior of the energy correlations between two detectors close in angle, which exhibit single logarithms at each order. These are summed in Section 3.6 where they are used to provide an estimate for $\langle H_\ell \rangle$ in $\zeta \to GGG(GG\ldots)$ [F1.2] at large ℓ. In Section 3.7 we use results in Section 3.6 to discuss the angular spread of energy in QCD jets. Section 3.8 applies our methods to the calculation of the transverse momentum spectrum of lepton pairs produced in hadron-hadron collisions (Drell-Yan) where double logarithms are found to exponentiate. Finally, in Section 3.9, we make some brief comments on real photon production in e^+e^- annihilation.

We define the two-detector energy correlation function by

$$\tilde{F}_2(\sigma_1,\sigma_2) = \frac{16\pi^2}{|\sigma_1||\sigma_2|} \frac{|\vec{p}_1||\vec{p}_2|}{s} \tag{1.2}$$

where the $|\vec{p}_i|$ are the sum of the moduli of the three-momenta of particles incident on two detectors covering the regions σ_i of total solid angle $|\sigma_i|$. The rotationally-invariant observable F_2 is formed in each event by averaging

$\tilde{F}_2$ over all possible positions for the detectors, while maintaining their relative orientation. F_2 may, therefore, be written as

$$F_2(\chi) = \frac{\langle|\vec{p}_1||\vec{p}_2|\rangle_o}{\langle E_1\rangle_o\langle E_2\rangle_o} \simeq \frac{\langle E_1E_2\rangle_o}{\langle E_1\rangle_o\langle E_2\rangle_o} \tag{1.3}$$

where χ signifies the relative orientation of σ_1 and σ_2, and the averages are over all positions of σ_1 and σ_2 in a particular event which maintain this: F_2 does not depend on the orientation of the final state with respect to the beam axis. Section 4 is devoted to a discussion of F_2. First (in Section 4.1) we give a convenient method for computing the mean value of F_2 and the distribution of events in F_2. We then present (Sections 4.2 and 4.3) some phenomenological estimates for $\langle F_2\rangle$ and $1/\sigma\, d\sigma/dF_2$ in various types of events. We find that hadronic corrections to perturbative results for energy correlations are very severe so that energy correlations are of limited practical utility at foreseeable energies. Nevertheless, for theoretical purposes, such as those of Sec. 2 and 3, it is very convenient to the idealized energy correlation $F_2^{pt}(\chi)$ between two point detectors. This has the useful property that

$$H_\ell = \frac{1}{2}\int_{-1}^{1} F_2^{pt}(\chi)\, P_\ell(\chi)d\chi. \tag{1.4}$$

The energy correlation functions F_2 described in [2] and in Section 4 are explicitly averaged over the direction of the incoming e^+e^- beam axis. However, QCD also makes definite predictions for the dependence of the shapes of final states on their orientation with respect to the beam direction. In Section 5 we give a general treatment of this dependence. We also introduce the observables Ξ_i^ℓ which allow the analysis of the angular distribution of

planes of particles [3] in the final state with respect to the beam axis without requiring a definite axis for the plane to be found (for example, by minimization).

In Section 6 we discuss methods for investigating planar structures in events. Most of the basic results of this section are contained in Ref. [3]; here we give some of the details.

In order to assess to what extent the various predictions presented in this paper constitute tests of QCD, one should compare them with results from other theories. Appendix C gives some predictions which would follow from a theory with colored scalar, rather than vector, gluons.

We apologize for the length of this paper and hope that any potential readers will not be deterred by it but will rather realize that the various sections are designed to suit differing tastes. For those interested by theoretical calculations in QCD perturbation theory, we recommend Section 2 and especially Section 3, where we have tried to present our results and methods in sufficient detail that they may be readily assimilated. Those of more experimental persuasion are directed to Sections 4, 5 and 6 which address more practical matters [F1.3].

Section 1 - Footnotes

F1.1 The background and motivation of the present work is discussed in Ref. [2].

F1.2 As in Ref. [2], $e^+e^- \to q\bar{q}(GG\ldots)$ represents the sum of processes $e^+e^- \to q\bar{q}$, $e^+e^- \to q\bar{q}G$, $e^+e^- \to q\bar{q}GG$ and so on, together with virtual (loop) corrections to these. ζ denotes a $^3S_1$ $Q\bar{Q}$ heavy quark bound state (such as Υ or Υ). Another notation from [2] is the kinematic definition $x_i = 2E_i/\sqrt{s}$.

F1.3 Section 6 contains some unusual mathematics which one of the authors considers a quaint relic of darker ages (at least it must be agreed by all that days of yore were less colorful).

2. Corrections to the $\cdot H_i >$

2.1 Introduction

In a typical e^+e^- annihilation event, the virtual photon decays into a q and $\bar{q}$, which then travel outwards, emitting gluons at a logarithmically-increasing rate until they reach a distance of order $1/\Lambda \sim 2\ \mathrm{GeV}^{-1}$, at which time the expanding system of quarks and gluons begins to condense into hadrons. This transition from a phase consisting of quarks and gluons to one in which these appear only clustered into color-singlet hadrons is beyond the perturbative methods that we discuss here. The purpose of considering infrared stable observables is to avoid these non-perturbative complications.

The most obvious example of an infrared stable observable is the total cross-section (σ). This is the total decay rate of the virtual photon. In the simplest (Born) approximation, one would compute just the process $\gamma^* \to q\bar{q}$, using plane waves for the q, $\bar{q}$ wavefunctions. However, final state interactions modify the q and $\bar{q}$ wavefunctions even at the moment of the decay. (This seemingly acausal behavior is, of course, a standard feature of quantum mechanical processes.) The modification may be found roughly by solving the Dirac equation for the q, $\bar{q}$ wavefunctions in a potential which represents their final state interaction. This interaction has two basic parts: at small distances, it corresponds to the emission and exchange of gluons in a manner amenable to perturbative treatment, while at distances around $1/\Lambda$ and beyond, it must account for the non-perturbative effects by which quarks and gluons are combined into hadrons. Typically, the modification to σ due to final state interactions between the q and $\bar{q}$ is given by (s is the square of the e^+e^- c.m. energy) [4]

$$\sigma(s) \simeq \sigma_o(s)\left|\exp\left[\int_0^\infty \frac{ds'}{\pi}\,\frac{\delta(s')}{s'-s-i\epsilon}\right]_o\right|^2, \qquad (2.1)$$

where $\delta(s')$ is the phase shift for $q\bar{q}$ scattering. For large s', $\delta(s')$ will be dominated by one-gluon processes and will be of order α_s. However, when s' becomes smaller than about Λ^2, the $q\bar{q}$ interaction will become very strong, and $\delta(s')$ will be of order one. The contribution to the integral (2.1) from this second region at energies $s \gg \Lambda^2$ will be of order Λ^2/s, while the contribution from the first (perturbative) region will be of order α_s [F2.1]. Hence, because the wavefunctions of the quarks at the time of the γ^* decay are not significantly affected by final state interactions which occur at much later times, it would be possible to compute σ from perturbation theory considering only quark and gluon final states at least up to terms of order Λ^2/s arising from interactions in the final state at large times. The perturbative final state interactions occurring between the q and $\bar{q}$ should tend to enhance σ over its $O(\alpha_s^o)$ Born approximation value, since in a color singlet state, one-gluon exchange between a q and $\bar{q}$ will be attractive. To order α_s, the result for σ is $\sigma = \sigma_o(1 + \alpha_s(s)/\pi)$, where by using the 'running coupling constant' $\alpha_s(s) \sim 1.5/\log(s/\Lambda^2)$, one has summed up a set of logarithmic terms in higher orders of perturbation theory which are remnants of infrared divergences that canceled because of the color singlet nature of the initial state (γ^*). Note that if the $q\bar{q}$ had been in a color octet state, the final state interactions would have been repulsive, giving $\sigma = \sigma_o(1 - \alpha_s(s)/6\pi)$ to $O(\alpha_s)$ [F2.2]. When $\sqrt{s}$ is of order Λ, $\alpha_s(s)$ becomes large and the perturbation series becomes useless so that σ cannot be estimated reliably [F2.3]. The point at which the perturbation expansion for σ breaks down depends on the actual numerical coefficients at each order in α_s. As discussed in Sec. 2.5, it appears, however, that with

a suitable definition of α_s, the perturbation series for σ should be reliable until α_s becomes of order one. Inasmuch as the result for σ depends on the definition of α_s, it is only useful if the same definition renders the perturbation series for other processes or other measurements similarly reliable, so that the value of α_s may be extracted from experimental data in one case and then used to make predictions in another.

We argued above that the cross-section σ should be well approximated by perturbation theory ignoring hadronic effects for $s \gg \Lambda^2$. However, perturbation theory also ceases to be reliable close to thresholds of, for example, new flavor production. In this case, the energy denominator in eq. (2.1) is modified roughly by $s \to s - 4\,m_Q^2$. In fact, large distance (non-perturbative) effects are probably important in σ for a range in energy ($\sqrt{s}$) of order Λ above each threshold. (The corresponding range in s is therefore of order $4\,m_Q\Lambda$.) Moreover, the perturbation series close to a threshold will be an expansion in α_s/v (v is the relative velocity between the primary particles produced) and so cannot be used. However, as discussed in Sec. 2.2, both these effects, which afflict the $\langle H_\ell\rangle$ as well as σ, may be tamed by averaging both experimental and theoretical results over a range of energies.

In the calculation of the total cross-section, the differential cross-section is integrated over the final state phase space with a uniform weighting. To obtain more information on the structure of e^+e^- annihilation, one must instead perform the integration using the shape parameters H_ℓ as weights so as to obtain the $\langle H_\ell\rangle$. The H_ℓ weighting of phase space is sufficiently smooth that the infrared divergences which canceled in the calculation of σ still cancel in $\langle H_\ell\rangle$. Recalling from (1.1) the definition of the H_ℓ, one sees that as ℓ increases, the H_ℓ vary more rapidly in phase space. For large ℓ, the Legendre polynomials $P_\ell(\cos\phi)$ may be approximated as 1 for $|\phi| \le 2/\ell$, $(-1)^\ell$

for $|\eta - \phi| \leq 2/\ell$ and zero elsewhere. Hence, emissions of particles at angles less than about $2/\ell$ will not affect the values of the H_ℓ for large ℓ, since two particles whose momenta are less than an angle $2/\ell$ apart will act as one particle with the sum of their momenta. At a c.m.s. time τ after the decay of the virtual photon, the energies of the quarks and gluons are such that the typical angles of emission are of order $1/(\tau\sqrt{s})$. The values of the H_ℓ for an event should, therefore, remain roughly unchanged by processes occurring at times greater than about $\ell/\sqrt{s}$. Thus the $\langle H_\ell \rangle$ are sensitive only to the structure of events at distances smaller than about $\ell/\sqrt{s}$ and, hence, for small ℓ and large $\sqrt{s}$ should be insensitive to the formation of hadrons at distances of order $1/\Lambda$. (In practice, a more accurate estimate of the times probed by the $\langle H_\ell \rangle$ is $\ell/(\sqrt{s}\langle z \rangle)$ where $\langle z \rangle$ is the mean momentum of a parton at a time of order $\ell/\sqrt{s}$.) In Sec. 2.4, we make some crude estimates of the onset of fragmentation effects in the $\langle H_\ell \rangle$ at small $\sqrt{s}$. Note that our discussion of the distance scales to which the $\langle H_\ell \rangle$ are sensitive is essentially classical whereas quantum mechanics was required for analogous considerations on σ.

At high $\sqrt{s}$ and sufficiently small ℓ that fragmentation is unimportant, the $\langle H_\ell \rangle$ remain constant with s except for the logarithmic variation of $\alpha_s(s)$. As $\sqrt{s}$ decreases (or ℓ increases), this scaling is violated by the presence of the fixed confinement mass scale Λ. This introduces corrections to the $\langle H_\ell \rangle$ of order $(\Lambda^2/s)^p$. Another cause of scaling violations is the presence of effective masses for quarks and gluons which introduce corrections of order $(m^2(\tau)/s)^p$. For σ, such corrections are always of order m^2/s; but for the mean values of shape parameters, we find in Sec. 2.3 that they are instead typically of order $\sqrt{m^2/s}$.

The sensitivity of the $\langle H_\ell \rangle$ for high ℓ to the structure of events at large times affects perturbative calculations even if the relevant times are less

than those at which fragmentation occurs. Above we found that the $\langle H_\ell \rangle$ are sensitive only to emissions at angles larger than about $1/\ell$. For the q and $\bar{q}$ produced in the continuum e^+e^- annihilation process $e^+e^- \to q\bar{q}(GG\ldots)$, we show in Sec. 3 that the probability for deflection of the q or $\bar{q}$ through an angle greater than θ is of order $\alpha_s \log^2\theta$ to $O(\alpha_s)$ so that the corresponding $\langle H_\ell \rangle$ (which in this case receive their dominant contribution from the q and $\bar{q}$ via the peak in the P_ℓ close to $\cos\theta = -1$) are of order $1 - c\alpha_s \log^2 \ell$. For large ℓ, the logarithms become so large that keeping only a few terms in the perturbation series for $\langle H_\ell \rangle$ becomes unreliable. However, the leading terms of order $[\alpha_s \log^2 \ell]^n$ in the perturbation expansion exponentiate, and may be summed to all orders in α_s, yielding the result $\langle H_\ell \rangle \simeq 1/2\ [1 + (-1)^\ell \exp(-8\alpha_s/3\pi \log^2 \ell) + O(\frac{\alpha_s(s/\ell^2\Lambda^2)}{\alpha_s(s/\Lambda^2)})^p)]$. The leading log part of this goes to zero as ℓ goes to infinity, reflecting the physical result that the probability for the q and $\bar{q}$ in $e^+e^- \to q\bar{q}(GG\ldots)$ to emerge exactly back-to-back vanishes; in this approximation, the q and $\bar{q}$ are always emitted outside the infinitesimal cone sampled by the H_ℓ. Of course, our leading log perturbative calculations of the $\langle H_\ell \rangle$ for large ℓ cannot be trusted unless they probe only times much shorter than $1/\Lambda$; at larger times, hadronization and subleading log effects are important. In practice, therefore, the estimates are relevant only for $\ell \ll \sqrt{s}/\Lambda$. The $\langle H_\ell \rangle$ for $e^+e^- \to q\bar{q}(GG\ldots)$ are dominated by the contribution from the cross-term between the nearly back-to-back q and $\bar{q}$ in the sum (1.1). For processes in which the minimum number of particles produced is more than two (e.g., $\zeta \to GGG(GG\ldots)$), the contribution to the $\langle H_\ell \rangle$ from pairs of particles which are back-to-back within an angle $1/\ell$ (corresponding to the width of the backward peak in $P_\ell(\cos\theta)$) no longer appears, and instead the $\langle H_\ell \rangle$ probe the fraction of the energy in each jet which is within an angle $1/\ell$ about its

axis (they are then dominated by cross-terms in (1.1) between particles in the same jet, and less than an angle $1/\ell$ apart). Whereas the probability for deflection of two back-to-back jets is of order $\alpha_s \log^2\theta$, the probability for most of the energy of a single jet to be restricted to a cone of angle θ is rather of order $\alpha_s \log\theta$. As discussed in Sec. 3, the $[\alpha_s \log\theta]^n$ terms at each order in α_s also exponentiate to a form $[\log(\theta^2 s/\Lambda^2)]^p$. We find that for $\zeta \to GGG$, the $\langle H_\ell \rangle \sim 0.14\ [\log(s/\Lambda^2)/\log(s/\ell^2\Lambda^2)]^{0.61}$ for large ℓ.

As mentioned above, the $\langle H_\ell \rangle$ for large ℓ probe the structure of events at small angular scales corresponding to large times. They can, therefore, provide a characterization of the energy distributions inside jets in a way that does not require the axis of the jet to be found. The $\langle H_\ell \rangle$ should decrease slowly with ℓ as shown in Fig. 3.3 over the region for which perturbation theory (with leading logs summed) is valid and should then level off as the intrinsic scale provided by confinement is probed.

An e^+e^- annihilation event may be considered to consist of three basic regions. At short distances, only a few large-angle gluon emissions may occur, and the system is well-described by low-order perturbation theory. At larger distances, the rate of emissions increases and the leading log terms in the perturbation series must be summed. Finally, when many emissions have degraded the energies of quarks and gluons until they are of order Λ, confinement occurs and the quarks and gluons condense into hadrons. This last stage is entirely universal to all processes: at least locally there is no trace of the nature of the subprocess in which the quarks and gluons were produced. The behavior of the event at the leading log stage is also to some extent universal. Once the energies have been degraded so that leading logs dominate, only small angle emissions occur and the jets of quarks and gluons in the events evolve independently. (Note that, as discussed in Sec. 3, the details of this depend critically on the gauge chosen for the gluon propagator.) Their evolution

depends only on their original energy. This picture of e^+e^- annihilation events suggests a procedure for estimating their structure (which we begin to implement in Sec. 3.7). Since the behavior of events at large distances cannot yet be determined from QCD, one must simply treat it phenomenologically. Therefore, one should fit the parameters of a phenomenological model for the development of jets at some value of $\sqrt{s}$ by considering the events to consist of jets corresponding to each of the partons produced at $\tau < \tau_o$. τ_o should be chosen to be on the boundary between the lowest-order and leading-log regions. Operationally, this may be done by treating particles as being in one jet if they cannot be resolved as separate by a detector of angular resolution $O(1/\tau_o\sqrt{s})$. Then to estimate the structure of events at another value of $\sqrt{s}$, scale τ_o so that $\tau_o\sqrt{s}$ is fixed, compute the jets produced at times $\tau < \tau_o$ and then let each jet evolve according to the phenomenological model fitted to similar jets of various energies at another value of $\sqrt{s}$. For single particle distributions, it is well known that, in fact, τ_o may be chosen differently at two values of $\sqrt{s}$, and the evolution of the jet during the leading log stage may be calculated using a renormalization group equation. The work of Ref. [5] allows this to be extended to n-particle distributions, from which the complete evolution of the jet could, in principle, be reconstructed. However, the leading log approximations necessary are unlikely to be adequate until very high energies ($\sqrt{s} \gtrsim 100$ GeV) are reached.

e^+e^- annihilation is one of the simplest processes to analyze in QCD because its initial state contains no colored particles. Whenever the initial state contains colored partons (albeit collected into color singlet hadrons), there are inevitably low-momentum spectator particles in any interaction, whose effects may become visible beyond the leading log order in perturbation theory, thereby spoiling perturbative predictions. As discussed in Sec. 2.7, however,

the $\langle H_\ell \rangle$ are less sensitive to such effects than is σ. The $\langle H_\ell \rangle$ and $\langle C_\ell \rangle$ for deep inelastic scattering will be discussed in Ref. [6].

2.2 Thresholds

At the threshold of each new channel available for e^+e^- annihilation, the total cross-section and $\langle H_\ell \rangle$ will exhibit bumps. If the new channel corresponds, for example, to having just one extra pion, then the bumps will probably be almost imperceptible. However, the bumps associated with the threshold for production of a new flavor will be much larger: their amplitudes will be of order the asymptotic change in the cross-section associated with the threshold. Perturbation theory cannot, of course, describe the details of the bumps. It, however, exhibits its own peculiar behavior at thresholds. In regions where the observed cross-section is bumpy, neither it nor the $\langle H_\ell \rangle$ should, therefore, be compared directly with perturbation theory predictions at each particular energy. Rather, only when both experimental data and perturbation theory predictions have been suitably averaged over the range of energies where bumps occur may a comparison be meaningful [7].

We first describe the behavior of perturbation theory close to thresholds. Near a threshold, (for example, for the production of a pair of heavy quarks (Q) [F2.4] or for the production of a $Q\bar{Q}$ pair together with, say, four light quarks (q)), the long-range nature of the forces in perturbative QCD introduces $(\alpha_s/v)^i \log^j(v)$ terms at each order where v is the relative velocity between the outgoing particles. The presence of these terms renders perturbation theory useless close to thresholds and presumably leads (directly for QED) to the existence of resonances in the cross-section. The effects of these threshold divergences may be removed (up to a high order in perturbation theory) by

considering only the cross-section smeared over a range of energies rather than at a particular $\sqrt{s}$. If $\Pi(s)$ is the vacuum polarization amplitude, then one suitable smearing of the cross-section is given by [7]

$$\overline{s\sigma}(s,\Delta) = \frac{\Delta}{\pi}\int_0^\infty \frac{s'\sigma(s')ds'}{(s-s')^2+\Delta^2} = \frac{1}{2i}\left[\Pi(s+i\Delta) - \Pi(s-i\Delta)\right], \qquad (2.2)$$

where Δ represents the magnitude of the smearing; typically values of a few GeV (corresponding to $\alpha_s/v \sim 1$ for the minimal set of particles at the threshold) are sufficient. The smearing (2.2) amounts to considering the photon propagator only at complex invariant masses, in which two currents act at times of order $1/\Delta$ apart, so that intermediate particles propagate only for finite time and, therefore, may not encounter the complicated hadronic effects which appear at large distances. In this way, all intermediate particles are held off their mass shells so that no divergences appear. The same avoidance of threshold singularities by smearing for σ may also be used for the $\langle H_\ell \rangle$. The precise threshold behavior of the $\langle H_\ell \rangle$ depends on how the $\langle H_\ell \rangle$ are defined. We usually take the H_ℓ to be weighted with the three-momenta of the particles in an event. In this case, $\langle H_\ell \rangle$ will exhibit zeros, corresponding to isotropic events, at threshold. However, if one considers either $\langle H_\ell/H_0 \rangle$ or $\langle H_\ell \rangle$ defined using energy, rather than momentum weightings, then the $\langle H_\ell \rangle$ will take on a non-zero and extremely unstable value at thresholds. Since all infrared considerations are for massless particles, these do not determine whether energy or momentum weighting should be used.

We discuss first the case in which the $\langle H_\ell \rangle$ are defined using the momenta of the final state particles as weights. Here thresholds will correspond to

zeros of $\langle H_\ell \rangle$. The primary reason for this is that threshold divergences appear only when particles have close to zero momentum (so that they are near in space for long enough to allow many exchanges), while in the $\langle H_\ell \rangle$ the contribution of a given particle is weighted by its momentum. Consider first the process $e^+e^- \to Q\bar{Q}(GG\ldots)$ where Q is a heavy quark, and an arbitrary number of gluons are emitted. Relative to the cross-section in the absence of strong interaction corrections, the rate for $e^+e^- \to Q\bar{Q}(GG\ldots)$ near threshold is

$$\sigma = \sigma_o\left(1 + \frac{2\pi\alpha_s}{3v} + O(\alpha_s^2)\right),$$
$$v = \sqrt{1 - 4\, m_Q^2/s}. \tag{2.3}$$

In the ladder approximation, the result near threshold to all orders is known (in analogy to the 'Sommerfeld factor' for QED [8])

$$\sigma_{\text{ladder}} = \sigma_o\left(1 + \frac{2\pi\alpha_s}{v} + \frac{4\pi^2\alpha_s^2}{27v^2} - O(\alpha_s^4)\right) = \left(\frac{\xi}{1 - \exp(-\xi)}\right)\sigma_o,$$
$$\xi = \frac{4\pi\alpha_s}{3v}. \tag{2.4}$$

Some terms not included in this approximation will contain $\log^k(v)$. On the other hand, the H_ℓ (with momentum weighting) for the heavy quark pair near threshold will be given roughly by (here $|\vec{p}_Q| \simeq m_Q \frac{v}{2}$)

$$H_\ell \simeq \tfrac{1}{2} v^2[1 + P_\ell(\cos\phi)] \simeq v^2. \qquad (\ell \text{ even})$$
$$\simeq 0 \qquad (\ell \text{ odd}). \tag{2.5}$$

The presence of extra soft gluons introduces $O(v^3)$ corrections to this. In $e^+e^- \to Q\bar{Q}(GG\ldots.)$, therefore, the 1/v threshold singularities are damped in

the $\langle H_\ell \rangle$, which go smoothly to zero, corresponding to isotropic particle production, as $v \to 0$. The same phenomenon will clearly occur at all other thresholds, such as $e^+e^- \to Q\bar{Q}q\bar{q}(GG\ldots)$ [F2.5].

Both the pathologies of perturbation theory close to thresholds and the obvious non-perturbative nature of the bumps in σ (and the $\langle H_\ell \rangle$) in these regions make it imperative to smear both perturbative theoretical predictions and experimental results for σ and the $\langle H_\ell \rangle$ in s before comparing them. However, our results for the $\langle H_\ell \rangle$ of continuum e^+e^- annihilation in Ref. [2] were computed for $q\bar{q}(G)$ with $m_q = 0$ and for $Q\bar{Q}$ production (and decay) only to $O(\alpha_s^o)$. Hence the calculations were not hampered by $(\alpha_s/v)^k$ threshold singularities, and the smearing need be applied only to the experimental data. In higher orders, the perturbative calculations would also require smearing. Equation (2.2) gives a possible form for the smeared total cross-section. One can use a similar definition for the smeared $\langle H_\ell \rangle$:

$$\overline{\langle H_\ell \rangle}(s,\Delta) = \frac{\Delta}{\pi}\int_0^\infty \frac{\langle H_\ell(s')\rangle ds'}{(s-s')^2 + \Delta^2}. \tag{2.6}$$

It is for these observables that experimental results and theoretical calculations should be free of complications associated with heavy quark thresholds. In the case of σ, the smeared σ was essentially the difference between the vacuum polarization amplitude evaluated at two points in the complex s plane: one $i\Delta$ above the real s axis and one $i\Delta$ below. Of course, it is trivial to define a function which is analogous in this respect for the $\overline{\langle H_\ell \rangle}$. However, unlike $\Pi(s)$, this function will admit no direct physical interpretation and cannot be computed using ordinary Feynman diagrams.

2.3 Mass Corrections

In Sec. 2.1 we argued that the $\langle H_\ell \rangle$ were typically sensitive to the structure of events at times less than about $\ell/\sqrt{s}$, so that for large $\sqrt{s}$ and small ℓ, hadronic effects occurring at large distances should be irrelevant. In the next two sections, we discuss two residual corrections of order $(\Lambda^2/s)^p$ to the $\langle H_\ell \rangle$ from large distance effects. In this section, we consider corrections which arise from the fact that hadronic effects occurring at times of order $1/\Lambda$ should modify quark and gluon wavepackets even at short distances, imposing a lower limit on their momenta as if they were confined in a region of radius $1/\Lambda$ [10]. This phenomenon will give the quarks and gluons effective masses, and in the remainder of this section, we consider the effects of such masses on the $\langle H_\ell \rangle$ and other shape parameters. Most of the effects which we find arise simply from kinematics, and do not depend on the way in which the effective masses enter matrix elements.

The infrared finiteness of the total cross-section (σ) and of the $\langle H_\ell \rangle$ means that when they are computed in QCD perturbation theory, all terms of the type $[\log(m^2/s)]^k$ (which diverge as $m \to 0$) are arranged to cancel. In this section we consider the residual effects of finite effective masses for final state quarks and gluons, which introduce corrections of order $(m^2/s)^p$ (or $(m^2/s)^p[\log(m^2/s)]^k$) to σ and the $\langle H_\ell \rangle$. These mass corrections cause σ and $\langle H_\ell \rangle$ to have a (non-scaling) dependence on s over and above that associated with the effective coupling $\alpha_s(s)$. We find that, whereas the leading correction to σ is of order (m^2/s), the leading corrections to the mean values of shape parameters tend rather to be of order $\sqrt{m^2/s}$. That mass corrections are more important for shape parameters than for the total cross-section is to be expected, since, in the integration over the possible final state configurations,

weighting with the H_ℓ (or other shape parameters) will probe to a greater extent (more for higher ℓ) the regions of phase space in which the particles have low energy than will a uniform weighting as used in the calculation of σ. It is, of course, for these low energy particles that a finite mass will be most important. If the differential cross-section has infrared divergences when some of the particles become soft, then these regions of phase space will be further accentuated.

The dependence of the shape parameters $\langle 1 - H_2 \rangle$, $\langle H_3 \rangle$, $\langle 1 - H_{10} \rangle$, $\langle 1 - T \rangle$ and $\langle S \rangle$ [F2.6] for the process $e^+e^- \to q\bar{q}G$ on the effective gluon mass, $\sqrt{\varepsilon s}$, is shown in Fig. 2.1. The introduction of a finite gluon mass makes nearly back-to-back $q\bar{q}$ production relatively less probable, so that the events become more isotropic, and the mean values of shape parameters decrease. All these parameters (except perhaps spherocity, which has many other problems) are seen to exhibit significant $\sqrt{\varepsilon}$ mass corrections for small ε. The total cross-section σ is, however, required from power-counting theorems on the real part of the vacuum polarization amplitude to suffer only $O(\varepsilon)$ corrections. For example, with quarks of effective mass $\sqrt{\gamma s}$, the total cross-section for $e^+e^- \to q\bar{q}(G)$ at large s is [11]

$$\sigma \simeq \sigma_0\Big(1 + \frac{\alpha_s}{\pi}\Big(1 + 12\gamma - \frac{4\beta}{3}\Big(\frac{2\pi^2}{3} - 1 - 2\log^2\beta - \log\varepsilon\Big) + 2(5 - 12\log\gamma)\gamma^2 + O(\beta^2,\beta\gamma) + \ldots\Big) + O(\alpha_s^2)\Big). \tag{2.7}$$

(The mass corrections may be obtained by computing diagrams with mass insertions on the relevant lines; if the modified diagram is infrared divergent, then logs appear [12].) No such result holds for the mean values of shape parameters, and, in fact, for small β:

$$\langle H_2\rangle \simeq 1 + \frac{2\alpha_s}{3\pi}\,(33 - 4\pi^2 + 12\pi\sqrt{\beta} + O(\sqrt{\gamma}) + \ldots) + O(\alpha_s^2), \tag{2.8}$$

$$\langle B_2\rangle = \frac{1}{10} - \frac{\alpha_s}{\pi}\,(\frac{3}{10} - \frac{2\pi}{5}\sqrt{\beta} + O(\sqrt{\gamma}) + \ldots) + O(\alpha_s^2) \tag{2.9}$$

while for thrust

$$\langle T\rangle \simeq 1 + \frac{2\alpha_s}{3\pi}\,(\frac{3}{4}\log 3 + \frac{1}{18} + \pi^2 - 2\log^2(\frac{4}{3}) - 4(\mathrm{Li}_2(\frac{3}{4}) + \mathrm{Li}_2(\frac{2}{3})) - 8\sqrt{\beta} + O(\sqrt{\gamma}) + \ldots) + O(\alpha_s^2), \tag{2.10}$$

$$\mathrm{Li}_2(x) = \int_x^0 \frac{\log(1-u)}{u}\,du = \sum_{i=1}^{\infty} \frac{x^i}{i^2}.$$

Note that in most of these cases, the next order mass corrections contain $O(\beta\log\beta)$ and $O(\gamma\log\gamma)$, as well as $O(\beta)$ and $O(\gamma)$ terms. The origin of the $\sqrt{\beta}$ terms is in all cases somewhat subtle. Essentially they arise from the fact that the constraint $2\sqrt{\beta} < x_3 < 1 + \beta$ on the gluon energy in a $q\bar{q}G$ final state involves $\sqrt{\beta}$. (The quark energies satisfy $0 < x_{1,2} < 1 - \beta$, not involving $\sqrt{\beta}$.) Then, when x_1 and x_2 are close to one, the mean value of almost any observable

which is proportional to particle energies will receive contributions of order $\sqrt{\beta}$. For $\langle H_2\rangle$, the integral which gives the $\sqrt{\beta}$ term is

$$\int \frac{dx_1\,dx_2}{x_1\,x_2\,x_3} \sim \int_0^{1-\beta} \frac{\log[(1-x_1)^2 + \beta]}{(x_1-2)x_1}\,dx_1 = \frac{\pi^2}{4} - \pi\sqrt{\beta} + O(\beta) + O(\beta\log\beta). \tag{2.11}$$

In the $\langle H_\ell\rangle$, the leading mass corrections are of order $\sqrt{\beta}$ for all $\ell > 2$. In Sec. 2.6 we show that for large ℓ, the $O(\alpha_s)$ terms in the $\langle H_\ell\rangle$ go roughly as $\log^2(1/\ell)$. When $\beta \neq 0$, this becomes roughly $\log^2(1/\ell + \sqrt{\beta}/2)$, so that the coefficients of $\sqrt{\beta}$ in the $O(\alpha_s)$ terms of the $\langle H_\ell\rangle$ grow roughly linearly with ℓ. The $\sqrt{\beta}$ terms are larger in the $\langle H_{2\ell}\rangle$ by a factor around 4 compared to those in the corresponding $\langle H_{2\ell-1}\rangle$. $\sqrt{\beta}$ terms apparently do not appear in the $\langle H_{2\ell-1}\rangle$ if one approximates the differential cross-section and the form for $H_{2\ell-1}$ by those obtained in the limit $\beta = 0$. This is in contrast to, for example, $\langle H_2\rangle$, in which the $\sqrt{\beta}$ term comes solely from use of the correct ($\beta \neq 0$) limits for the $x_{1,2}$ integration. Note that in no case is the $\sqrt{\beta}$ term affected by the use of momentum, rather than energy weightings in the definitions of the shape parameters.

The presence of $\sqrt{\gamma}$ corrections to the mean values of most shape parameters for final states containing massive quarks is again essentially a consequence of the fact that the minimum quark energies are proportional to $\sqrt{\gamma}$ for small γ: $2\sqrt{\gamma} \leq x_{1,2} \leq 1$ ($0 \leq x_3 \leq 1 - 4\gamma$).

The existence of $\sqrt{m^2/s}$ mass corrections to shape parameters for $e^+e^- \to q\bar{q}(G)$ is related to the presence of infrared divergences in the differential

cross-section in regions where the energies of some final state particles are dominated by their masses. In processes such as $\zeta \to GGG$, where, to lowest order, no infrared divergences appear, $\sqrt{\beta}$ mass corrections are absent, at least in $\langle H_2 \rangle$, despite the presence of $\sqrt{\beta}$ terms in kinematic constraints ($2\sqrt{\beta} \le x_i \le 1 - 3\beta$).

It appears that large mass corrections are an inevitable feature of the mean values of any observables which are sensitive to the structure of final states.

2.4 Hadronization Effects

The argument given in Sec. 2.1 for the insensitivity of the $\langle H_\ell \rangle$ to the structure of events at large distances was based on the fact that they are sensitive only to large angle ($\theta \gtrsim 2/\ell$) emissions, which do not occur at large times. The condensation of quarks and gluons into hadrons typically leads to emissions of roughly fixed average transverse momentum ($\sim \Lambda$). These emissions are therefore at angles $O(\Lambda/\sqrt{s})$, leading to corrections to the $\langle H_\ell \rangle$ of order $(\Lambda^2/s)^p$. To estimate these corrections for $\langle H_2 \rangle$, we approximate a jet as a cylinder of particles distributed symmetrically in azimuth, and all with transverse momentum k_T. Then

$$H_2 \simeq \frac{1}{4} \left| \sum_i \left(z_i - \frac{3}{2} \left(\frac{2k_T}{z_i\sqrt{s}} \right)^2 z_i \right) \right|^2, \tag{2.12a}$$

where

$$z_i = \frac{2E_i}{\sqrt{s}}, \quad \frac{2k_T}{z_i\sqrt{s}} \le 1. \tag{2.12b}$$

To obtain $\langle H_2 \rangle$, one must average over the longitudinal momentum spectrum:

$$\int_{2k_T/\sqrt{s}}^{1} dz \, \frac{1}{z} \, D(z) \simeq \frac{\sqrt{s}}{2k_T} \langle n \rangle / \log(\sqrt{s}/2k_T) \tag{2.13}$$

where $\langle n \rangle$ is the mean multiplicity of the jet. Hence

$$\langle H_2 \rangle \simeq 1 - 6\sqrt{\frac{k_T^2}{s}} \langle n \rangle / \log(\sqrt{s}/2k_T). \tag{2.14}$$

Note that the origin of the $\sqrt{k_T^2/s}$ was similar to the origin of the $\sqrt{\beta}$ in eq. (2.7): it came from integration over the angle made by the particle ($\simeq 2k_T/z\sqrt{s}$)) down to the kinematic lower limit. As ℓ increases, the coefficient of $\sqrt{k_T^2/s}$ increases: for $\sqrt{k_T^2/s} \le 0.1$ the 6 in the estimate (2.14) becomes roughly $\ell(\ell + 1)$. This considerably overestimates the effects of fragmentation for large ℓ found with a more realistic model [2].

For large ℓ, the $\langle H_\ell \rangle$ probe the structure of events on angular scales of order $1/\ell$. In perturbation theory, the mean energy in a hadron jet within an angle θ diverges logarithmically as $\theta \to 0$. However, both fragmentation and finite quark/gluon masses introduce an intrinsic scale (cutoff) in the jet, so that the $\log(\theta)$ terms are damped at small θ roughly like $\log(\theta + \delta)$ or $\log(\theta + \sqrt{\beta})$, where δ is the 'resolution' or angular spread associated with fragmentation, which is presumably of order $\sqrt{\Lambda^2/s}$. From these considerations, we expect that at large ℓ, the $\langle H_\ell \rangle$ for hadronic events will tend to a constant value which characterizes the angular 'resolution' associated with the process of fragmentation into hadrons. This limit should depend only on the energies of the jets in the events, and not on the details of the subprocess which produced them. An experimental measurement of the $\langle H_\ell \rangle$ for large ℓ can be considered as determining the energy distributions inside jets, but without explicitly finding their axes.

2.5 Higher-order Terms in the Perturbation Series

We now discuss the third basic correction to estimates of σ and the $\langle H_\ell \rangle$ derived from low-order perturbation theory: the effect of higher-order terms in the perturbation series. For the total cross-section, the perturbation series is

$$\sigma = \sigma_0 (1 + \frac{\alpha_s(s)}{\pi} + c(\frac{\alpha_s(s)}{\pi})^2 + O(\alpha_s^3)) \tag{2.15a}$$

where (F is the number of active quark flavors) [13]

$$c \simeq 2.0 - 0.1\,F \tag{2.15b}$$

$$\alpha_s(s) \simeq \frac{4\pi}{[(11 - \frac{2}{3}F)\log(s/\Lambda^2) + (\frac{306-38F}{33-2F})\log\log(s/\Lambda^2)]}. \tag{2.15c}$$

The value of c depends on the renormalization prescription used in obtaining it. Equation (2.15b) is for the truncated minimal subtraction scheme [13] [F2.8]. The parameter Λ obtained by fitting data to the form (2.12) and ignoring yet uncalculated $O(\alpha_s^3)$ and higher terms should be close to the value deduced from studies of other processes (e.g., deep inelastic scattering) by fitting to analogous forms, and with the analogous constants c calculated using the same renormalization prescription. This provides an important test of perturbative methods in QCD. Note that the values of Λ deduced from different processes using forms such as (2.15) but with the $O(\alpha_s^2)$ terms ignored need not even be nearly equal. The effective values of Λ deduced by this procedure will differ by exponentials of the $O(\alpha_s^2)$ coefficients. Instead of considering the effective

values of Λ to differ, one may, of course, keep Λ fixed, but evaluate α_s at an energy given by some number times s.

By using $\alpha_s(s)$ in eq. (2.15a), one has implicitly summed all the leading logarithmic terms ($\sim [\alpha_s \log(s/\mu^2)]^k$, where μ is a renormalization mass) in the cross-section as calculated by perturbation theory. The form of these leading logarithmic terms is determined by the renormalization group equation (independence of μ^2) once the coefficient of α_s (in this case $1/\pi$) in the perturbation series is known. Knowledge of the constant c (together with the $\log\log(s/\Lambda^2)$ terms in (2.15c) from $\beta(g)$ to $O(g^5)$) is sufficient to allow correct account to be taken also of subleading logarithmic terms ($\sim \alpha_s^k \log^{k-1}(s/\mu^2)$), again using the renormalization group equation.

For the $\langle H_\ell \rangle$ a similar perturbative calculation may be made. For example, for $\langle H_2 \rangle$ the result is

$$\langle H_2 \rangle = 1 + \frac{\alpha_s(s)}{\pi}\frac{2}{3}(33 - 4\pi^2) + c_2(\frac{\alpha_s(s)}{\pi})^2 + O(\alpha_s^3), \tag{2.16}$$

where the constant c_2 is not yet known [F2.9]. A knowledge of c_2 is necessary to obtain a value of Λ from measurements of $\langle H_2 \rangle$ which can be compared with values deduced in other ways (for example, from the total cross-section for e^+e^- annihilation). For a perturbative estimate of $\langle H_2 \rangle$ to be reliable, it is necessary that successive terms in the perturbation series be, on average, smaller. At sufficiently high values of $\sqrt{s}$, $\alpha_s(s)$ will be so small that this is inevitable. However, at practical values of $\sqrt{s}$, $\alpha_s(s)$ may not be small enough that perturbation theory is useful. The numerical size of the coefficients of α_s^k at each order in the perturbation series determine its domain of applicability. We shall ignore the eventual $k!\,\alpha_s^k$ divergence of perturbation theory in very high orders, and hope that precursors of this behavior

in low orders will not affect our calculations. The first indication as to the accuracy of perturbation theory comes from the coefficient of α_s in the perturbation series. For $\langle H_2 \rangle$, this coefficient is tolerably small (~ -1.4), but for the $\langle H_\ell \rangle$ with large ℓ it becomes uncontrollably large, growing like $\log^2(\ell)$. In the next section, we describe a method for summing the leading offensive $(O((\alpha_s \log^2 \ell)^k))$ terms in $\langle H_\ell \rangle$ to all orders in α_s, thereby finding $\langle H_\ell \rangle \underset{\ell\to\infty}{\sim} \frac{1}{2}(1 + (-1)^\ell \exp(-8\alpha_s/3\pi \log^2(\ell)) + O\left((\frac{\alpha_s(s/\ell^2)}{\alpha_s(s)})^p\right)$, whose leading term goes to zero as ℓ goes to infinity, quite contrary to the divergent behavior of each term in the perturbation series. However, as discussed in Sec. 3, the leading terms do not provide accurate estimates of all higher order effects as $\ell \to \infty$. In addition, we have no firm guarantee that the higher-order terms in $\langle H_2 \rangle$ do not conspire to be numerically important. The fact that the coefficients of α_s and α_s^2 in σ given in eq. (2.15) are both small in the 'truncated minimal subtraction scheme' [F2.8] inspires some hope that the relevant $O(\alpha_s^3)$ and higher terms will also be small, and that the $O(\alpha_s^2)$ estimate for σ will be accurate. Note that the coefficient of α_s^2 in σ or in the $\langle H_\ell \rangle$ depends on the renormalization prescription used in its calculation. The 'truncated minimal subtraction' scheme was chosen for σ because it gave a reasonably small value for c, so that neglect of higher order terms was sensible. If the value of Λ deduced from experimental measurements of σ using calculations in this scheme is to be used in estimating the $\langle H_\ell \rangle$, then it is necessary that the coefficients of α_s^2 for the $\langle H_\ell \rangle$ calculated in the scheme are small enough that neglect of higher order terms is reasonable. Some indication that the $\langle H_\ell \rangle$ for small ℓ do not receive large $O(\alpha_s^2)$ contributions comes from the result that $O(\alpha_s^2)$ terms appear to lead only to small modifications to the $O(\alpha_s)$ two and three jet structure in e^+e^- annihilation. In particular, calculations indicate that $e^+e^- \to q\bar{q}GG$ and $q\bar{q}q'\bar{q}'$ events at $O(\alpha_s^2)$ are mostly nearly coplanar [15].

2.6 H_ℓ Distributions, Phase Space Final States, QED Radiative Corrections and An Analogy with Electromagnetic Showers (the Gallimaufry Within)

In Sec. 3, we discuss the $\langle H_\ell \rangle$ for large ℓ, and show that to $O(\alpha_s)$, the $\langle H_\ell \rangle$ for $e^+e^- \to q\bar{q}(G)$ behave like $1 - (4\alpha_s/3\pi)\log^2(\ell)$. This decrease in the $\langle H_\ell \rangle$ at large ℓ is reflected in a broadening of the distribution of events in H_ℓ $(1/\sigma_0 d\sigma/dH_\ell)$ at large ℓ. These distributions for ℓ from 2 to 10 were given in Fig. 30 of Ref. [2]; the movement of events from around the peak (at $H_\ell = 1(0)$ for ℓ even(odd)) to other values of H_ℓ as ℓ increases is evident there. This behavior may be understood qualitatively from the fact as ℓ increases, the H_ℓ probe the structure of events on smaller and smaller angular scales. The distributions of events in H_ℓ represent roughly the distributions of energy within jets (see Sec. 3 for a more precise discussion) [F2.10]. As ℓ becomes larger, the distributions in H_ℓ give a progressively magnified representation of the jet energy distributions. Despite the increase of the width of the peak in H_ℓ distributions for $e^+e^- \to q\bar{q}(G)$ at large ℓ, the extreme value of H_ℓ away from the peak does not change significantly with ℓ. One finds that for large ℓ, $\mathrm{Min}[H_{2\ell}] \to 0.18$ while $\mathrm{Max}[H_{2\ell-1}] \to 0.61$. These limits are approached quickly as ℓ increases. They are determined by the extremal values of the Legendre polynomials, and, for example, $\mathrm{Min}[H_{2\ell}] \to (1 + 2\mathrm{Min}[P_{2\ell}(x)])$ [F2.11]. These results hold, of course, only for three-particle final states. For larger numbers of particles, the range of the H_ℓ extends rapidly to fill the interval [0,1].

In general, the basic structure of the final states from any QCD process roughly preserves the structure obtained at the lowest order in α_s, since infrared divergences tend to concentrate the higher-order emissions into jets along the directions of the partons at lowest order. The structure of events at the lowest order in α_s is usually well-approximated by distributing the

final state particles uniformly in the available phase space (appropriate for their multiplicity). For two-particle final states, only one point in phase space is, of course, allowed and, as usual, $H_\ell = O(1)$ for ℓ odd(even). The processes $e^+e^- \to q\bar{q}(GG\ldots)$ usually lead to two jets and, therefore, roughly preserve the lowest-order results for the $\langle H_\ell \rangle$. However, as ℓ increases, the $\langle H_\ell \rangle$ become progressively more sensitive to the detailed structure of the events and probe the internal constitution of the jets so that the lowest order structure is lost. For three-particle events, a phase space distribution gives

$$\langle H_2 \rangle = (3\pi^2-29) \simeq 0.61$$

$$\langle H_3 \rangle = (75\pi^2-740) \simeq 0.22 \qquad (2.17)$$

$$\langle H_\infty \rangle = 3/8 = 0.375.$$

Note the extreme similarity between these results and those for $\zeta \to GGG$ at lowest order ($\langle H_2 \rangle \simeq 0.62$, $\langle H_3 \rangle \simeq 0.22$, $\langle H_\infty \rangle \simeq 0.3751$). In higher orders of α_s, the $\langle H_\ell \rangle$ for large ℓ again deviate significantly from the lowest-order results or from the phase space approximation to them. For an n particle final state distributed uniformly in phase space, the $\langle H_\ell \rangle$ are approximately 1/n so that as $n \to \infty$, the usual result $\langle H_\ell \rangle = 0$ ($\ell \neq 0$) for a genuinely isotropic system is regained.

For a three-particle final state generated uniformly in phase space, the energy correlation function is given by (compare the results for QCD processes given in Appendix A)

$$\langle F_2^{pt}(\chi) \rangle = \frac{24}{(\chi-1)^5} \{(\chi^2+10\chi+13)\log(\tfrac{1+\chi}{2}) + 3(1-\chi)(\chi+3)\}$$

$$+ \frac{3}{4}\,\delta(1-\chi), \qquad (2.18)$$

$$\langle F_2^{pt}(0) \rangle = 24(13\log 2-9) \simeq 0.26.$$

Near $\chi = -1$, $\langle F_2^{pt}(\chi) \rangle$ in this case becomes

$$-3[\log(\tfrac{1+\chi}{2}) + 3 + \ldots]. \qquad (2.19)$$

This integrable divergence has its origins in the Jacobian from the differential cross-section in (x_1, x_2) to that in (x_1, χ). Near $\chi = +1$, the regular part of $\langle F_2^{pt}(\chi) \rangle$ tends to 1/10. These results are again very similar to those for $\zeta \to GGG$ at lowest order, given in Appendix A. When a phase-space generated final state contains more than three particles, the Jacobian divergence at $\chi = -1$ visible in eq. (2.19) (and which becomes $\delta(1+\chi)$ for a two-particle final state) disappears. This occurs even for the rather constrained 6 particle final state discussed in Appendix A (eq. A.16). $\langle F_2^{pt}(\chi) \rangle$ becomes progressively flatter as the multiplicity of the final state increases and for a truly isotropic final state containing an infinite number of particles, $F_2^{pt}(\chi) = 1$.

Although it is unfortunately not especially apposite, we now make a brief digression regarding electromagnetic radiative corrections. For σ, one must consider QED corrections due to emission from both the initial (e^+e^-) state and from the final state, together with corrections to the virtual photon propagator [F2.12]. For the $\langle H_\ell \rangle$, only QED corrections which change the configuration of the final state need be considered. These are of two types:

photon emission from the final state and photon emission from the initial state, giving the virtual photon a non-zero three-momentum in the e^+e^- c.m. system. The interference between these two processes is negligible. The first type of correction may be computed to first order in direct analogy to gluon emission corrections. For $e^+e^- \to q\bar{q}$, photon emission from the final state modifies $\langle H_2 \rangle$ to $\langle H_2 \rangle \simeq 1 + \alpha_{em}(s)/(2\pi)(33-4\pi^2) + O(\alpha^2)$, while for large ℓ, the $\langle H_{2\ell} \rangle$ become roughly (see Sec. 3) $\langle H_{2\ell} \rangle \simeq 1 - \frac{\alpha_{em}(s)}{\pi} \log^2(2\ell)$. (These estimates are probably less accurate than those for gluon emissions since, whereas the final state is a color singlet, it still contains charged particles which continue to emit photons at all times.) Photon emission from the initial state boosts the final state by giving the γ^* a non-zero three-momentum in the e^+e^- c.m.s. and corrects $\langle H_{2\ell} \rangle$ by an amount of order $\alpha_{em}(s)\log(s/\epsilon^2)$ and roughly independent of ℓ, where ϵ is the energy resolution of the incoming e^+, e^- beams (c.f., some of the discussion of colored initial states in the next section). Note that all these QED radiative corrections to event shapes are usually much smaller than the QCD ones.

Our discussion of the development of a jet in QCD bears many qualitative similarities to the standard treatment [16] of the development of electromagnetic showers in matter. Here we make a very brief exploration into this analogy. An electromagnetic shower is initiated by the entry of a high-energy electron or photon into material. At first, electrons lose energy by Bremsstrahlung and photons by pair creation (or Compton scattering, at lower energies). The secondary particles produced by these processes then themselves radiate, as do their progeny, and a cascade or shower of electrons and photons is formed. Eventually, when the energies of individual electrons or photons have been degraded by radiations to below some critical energy, governed by the binding energies (inverse sizes) of atoms in the particular material, but

independent of the original constitution of the shower, they will be absorbed (through atomic excitation or ionization) and will disappear from the shower. The development of a QCD jet as described in Sec. 2.1 is in many respects very similar to the formation of an electromagnetic shower in matter. A quark or gluon produced in the primary (short distance) interaction radiates its energy into a shower of partons which presumably condense into hadrons in a universal manner when their energies have been degraded below about Λ (which gives the inverse size of the hadrons formed). This final step may picturesquely be considered as the dissipation of the jet's energy in the QCD vacuum. The longitudinal development of a QCD jet (in the perturbative (or non-dissipative) region) is described by Altarelli-Parisi or diffusion differential equations which are extremely similar to those used in calculations of longitudinal electromagnetic shower shapes (in fact, 'anomalous dimensions' and the method of moments were introduced for shower analyses [17] long before their use in QCD). The transverse distribution of energy in electromagnetic showers is also roughly analogous to that expected for QCD jets (see Sec. 3), although there is no direct analogue of the multiple Coulomb scattering of single electrons (which is irrelevant for longitudinal considerations) in the QCD case. The photons emitted by an electron in Bremsstrahlung usually have wavelengths much smaller than the distance between emissions, and may, therefore, be assumed independent and incoherent. Similarly, the dominant emissions of gluons by a quark are independent (leading log approximation), since their energies are of rough order $\sqrt{s}$, whereas the invariant mass of the intermediate quark line is typically of rough order Λ or $\sqrt{s\ell^2}$. (The first few gluons emitted may be at distances $\sim 1/\sqrt{s}$, and must therefore be considered coherently.)

2.7 Processes with Colored Initial States

e^+e^- annihilation is probably the simplest process to analyze in QCD, because there is no color in the initial state, so that, at least immediately after the decay of the virtual photon, the final state will consist only of a $q\bar{q}$ pair. (In fact, two other processes with colorless initial states are also available, but are experimentally less accessible than e^+e^- annihilation. The first is $\tau \to \nu_\tau$ + hadrons, in which a virtual W rather than a virtual photon decays to hadrons, and the second is $\gamma\gamma \to$ hadrons, which should be accessible from $e^+e^- \to e^+e^-$ + hadrons.) In a process such as deep inelastic scattering ($\gamma^*N \to$ hadrons), the initial state contains colored particles. For a QCD analysis of deep inelastic scattering, it is convenient to make the idealization that the initial state consists of a single isolated quark, rather than of a nucleon, so that it is not a color singlet. This idealization leads to difficulties, however. In e^+e^- annihilation, the total cross-section remains finite when infrared cutoffs are taken to zero, so long as all possible final states have been included in its calculation. This is not the case for the γ^*q total cross-section: even when all possible final states are included, infrared divergences remain. They are canceled only if processes with extra particles in the initial state, such as $\gamma^*qG \to q$, are also taken into account. Any colored object will always develop around itself a polarization cloud which serves to screen its color. For example, a quark with high energy produced in, say, $\gamma^* \to q\bar{q}$, will emit gluons which form a 'jet' around its direction, and spread its energy and color out into a cone of finite angle. Eventually, at times of order $1/\Lambda$, many gluons are exchanged between the q and $\bar{q}$ jets, so that their color is completely canceled, and the system condenses into hadrons.

Infrared stable observables are, of course, designed to be insensitive to this large distance behavior.

For deep inelastic scattering, the idealization that the initial state consists simply of an isolated quark suffices in the calculation of σ or the $\langle H_L \rangle$ if one works only to $O(\alpha_s^0)$. However, at $O(\alpha_s(Q^2))$, one must include the possibility that the initial quark carried with it a gluon. The idealization that the initial state has survived as an isolated quark for an infinite time is no longer sufficient. As higher orders of perturbation theory are considered, so it is necessary to include the possibility that the initial state consisted of a whole jet of quarks and gluons. This is the best approximation that perturbation theory can muster to the actual physical case in which the initial state is a nucleon. Just as at large times, the structure of a final state jet is governed by nonperturbative hadronic phenomena, so too will the structure of an initial jet, which has propagated from the infinite past (in the perturbative, plane wave idealization), be determined by nonperturbative effects. The typical spread in energies and angles of the initial state jet which is supposed to represent a nucleon will be determined by the size of the nucleon.

If no extra initial particles are considered, then the total cross-section for γ^*q scattering at $O(\alpha_s)$ (obtained by adding real gluon emission diagrams $\gamma^*q \to qG$ with virtual corrections to $\gamma^*q \to q$) contains terms of order $\alpha_s \log(s/\mu^2)$, where μ is some finite (say, quark) mass retained to regularize infrared divergences. If new processes involving extra initial particles (such as $\gamma^*qG \to qG$) are included, but the initial state is taken to have only a finite spatial extent (e.g., ~ 1 fm), so that particles in it are kept off their mass shells by a small amount p^2, then $\alpha_s \log(\mu^2/p^2)$ terms will be introduced, and the leading terms in the total cross-section become $O(\alpha_s \log(s/p^2))$ [F2.13]. The

$\log(p^2/\mu^2)$ terms arise from the propagation of nearly on-shell intermediate particles. Their behavior is approximately independent of the hard scattering process (the propagation of the particles is unaffected by disturbances at distances much smaller than their wavelength) [F2.14]. Hence, the $\log(s/p^2)$ terms in σ (whose coefficients are the same as those of the $\log(p^2/\mu^2)$ terms) are also independent of the short distance structure of the interaction. There are $O(\log(s/p^2))$ terms associated with each of the initial 'jets' of partons corresponding to each colored initial particle. These terms depend only on the energy and nature of the corresponding initial particle and are unaffected by the short distance structure of the interaction which the particle undergoes (e.g., the structure of the γ^* coupling to the quark in deep inelastic scattering). The universal $\log(s/p^2)$ terms may thus be determined from a study of one reaction at a particular energy and then factorized out in comparisons with another energy or another process. When cross-sections at two energies are compared, $\log(s_1/s_2)$ terms appear which may be summed to all orders using the renormalization group equation.

It has been proved [18] that all terms in total cross-sections involving colored initial particles which are singular in the limit p^2 (or ϵ) tend to zero are universal and may be factorized out in comparisons between different processes. One may therefore hope that in comparisons between processes, only their short distance structure will be probed, and there will be no dependence (at least up to terms of order p^2/Q^2) on the detailed construction of the initial hadrons (perhaps represented by boxes of quarks and gluons in perturbation theory). It is clear that because of their close association with divergent contributions to σ, some details of the initial state will be irrelevant. For example, doubling the diameter of the initial box, so that $p^2 \to p^2/4$, will lead to $\log(4)$ terms which factorize just like the $\log(Q^2/p^2)$

terms. However, we cannot prove that all features of the initial state do not contribute to comparisons between processes [F2.15]; there may still be terms, even at $O(\alpha_s)$ (only the $\alpha_s \log(s/p^2)$ terms are known to be universal), which depend on the construction of the incoming wavepackets in a different way in each process thereby rendering calculations on reactions involving colored initial states (but taking unaccompanied incoming partons) irrelevant. Such effects are potentially very damaging since they could depend on the amplitudes (rather than just probabilities) for quarks and gluons in the initial state to share their momenta in different ways. Nevertheless, one may hope that such terms are of order p^2/Q^2 as they appear to be for deep inelastic scattering.

For the $\langle H_i \rangle$, the structure of the initial state has a somewhat smaller effect that on σ. In σ, the $O(\alpha_s)$ term in the perturbation expansion for a process with initial color already has a divergent coefficient of order $\log(s/p^2)$. However, in $\langle H_i \rangle$ the $O(\alpha_s)$ term remains finite, and only at $O(\alpha_s^2)$ do divergences appear. Note that because of the infrared stability of the $\langle H_i \rangle$, these divergent terms should factorize in comparisons between different processes, just as they do in σ. It is the non-logarithmic terms which accompany these universal divergences that may be sensitive to details of the initial state. The fact that these appear only at order α_s^2 in $\langle H_i \rangle$ renders them less important than in σ. Note that, just as there were $\sqrt{\tau}$ mass corrections to the $\langle H_i \rangle$ in e^+e^- annihilation, so now we expect $\sqrt{p^2/s}$ corrections to the $\langle H_i \rangle$ in deep inelastic scattering. These terms will violate scaling for the $\langle H_i \rangle$ to a greater extent than the p^2/s terms in σ.

Section 2 - Footnotes

F2.1 Antiquaries (a term of respect according to one of the authors) may object that rescattering corrections due to pomeron exchange do not fall off with s. The conventional pomeron should presumably be regarded as a sum of gluon exchanges, each of which has a sufficiently small momentum transfer that the effective coupling associated with it is large. In the e^+e^- annihilation total cross-section, the same sum of gluon exchanges presumably contributes. However, gluon exchanges at small times will transfer momenta of order $\sqrt{s}$, so that their effective couplings will be small, and will not build up the conventional pomeron behavior. Of course, gluons exchanged at large times will have small invariant masses and large couplings, but as described in the text, their contribution is of order Λ^2/s. On the other hand, in hadron collisions, there exist wee partons at all times, and exchanges between them will have large effective couplings, so that the conventional pomeron behavior is generated.

F2.2 If the final state in the process $e^+e^- \to q\bar{q}(G)$ is a color singlet, then the color factor is c_F, while if it were a color octet, the color factor would be $c_F(c_F - c_A/2)$, where c_F (c_A) are the quadratic Casimir invariants for the quark (gluon) $SU(3)_{color}$ representations, and usually $c_F = 4/3$, $c_A = 3$. Care must, of course, be taken to maintain gauge invariance with a color octet $q\bar{q}$ source.

F2.3 By employing the analytic properties of the complete photon propagator, of which σ is the imaginary part, it is, nevertheless, possible to use perturbation theory to compute integrals of σ over s which run right down to $s = 0$.

F2.4 In the actual case of heavy quark pair production, the observed final states will presumably consist of the quark's decay products, as discussed in detail in [2].

F2.5 One might guess that in the process $e^+e^- \to Q\bar{Q}q\bar{q}(GG...)$ the cross-section (and $\langle H_\ell \rangle$) would exhibit $(\alpha_s/v)^k$ divergences whenever the $q\bar{q}$ relative velocity could be zero. This could occur in the materialization of a high momentum gluon with invariant mass $4m_q^2$ into a q and a $\bar{q}$ with equal three-momenta. However, in the calculation of the diagrams, one must integrate over all momenta and invariant masses of the gluon, so that the power singularities associated with process $G^* \to q\bar{q}$ when the gluon mass was fixed externally to be close to $4m_q^2$ (as in $\gamma^* \to Q\bar{Q}$) will be damped to the usual logarithmic ones.

F2.6 For three-particle final states, thrust (T) and spherocity (S) are given respectively by (e.g., [9])

$$T = \max(x_1, x_2, x_3)$$

$$S = \frac{64}{\pi^2}(1 - x_1)(1 - x_2)(1 - x_3)/T^2.$$

For an $e^+e^- \to q\bar{q}$ event, $T = 1$ and $S = 0$.

F2.7 It is clear from Fig. 2.1 that this point is only of formal relevance: the actual mass corrections in this case are quite as large as for other shape parameters.

F2.8 Despite the fact that in a renormalizable theory, no physical predictions can depend on the prescription for factorizing out ultraviolet divergences (renormalization), it is, of course, first necessary to determine the coupling constant. This may be done by fitting a theoretical calculation of some cross-section, obtained using a particular renormalization prescription, to an experimental result for the cross-section. The value of the coupling constant

(characterized by Λ) deduced will depend on the prescription used for the calculation but should be the same as that obtained from another process using the same method. (In QED, there is an obvious definition of α: the low energy limit of a process such as Compton scattering, where low-energy theorems require that all higher-order terms in the perturbation series vanish. For massless fermions, or for a theory with large coupling in the infrared regime, this convenient definition fails, and one must resort to more arbitrary methods.) In the truncated minimal subtraction scheme, infrared and ultraviolet divergences are regularized by taking the dimensionality of spacetime as $4 - \epsilon$ (so that the Coulomb potential $e^2/[4\pi r]$ becomes $e^2(\mu r)^\epsilon/[(2\pi^{3/2-\epsilon}/\Gamma(\frac{3}{2} - \epsilon))r]$ (where μ is a renormalization mass), which is regular in the infrared (ultraviolet) region when ϵ is negative (positive)), and then essentially subtracting all results at $s = \mu^2$ (i.e., factorizing off ultraviolet logs arising from distances $\lesssim 1/\mu$). In the usual minimal subtraction scheme, for which only $1/\epsilon$ terms are subtracted off, terms in $\gamma(\sim 0.577)$ and $\log(4\pi)$ appear, which are absent in the truncated scheme. This usual scheme gives $c \sim 7.4 - 0.4\,F$.

F2.9 Its calculation would not be particularly simple. The trick of evaluating the log divergent $(O(1/\epsilon))$ term in the real part of the vacuum polarization amplitude to obtain the constant c in eq. (2.15) for σ can, of course, not be used here. Instead one must explicitly integrate over phase space using H_2 as a weight for the various possible final states: $q\bar{q}GG$, $q\bar{q}q'q'$ and $q\bar{q}G$. One need not consider the $q\bar{q}$ final state, since it does not contribute to $\langle H_2\rangle - 1$. For the $q\bar{q}G$ final state, the amplitude must be known to the one-loop level, and an infrared cutoff (e.g., ϵ = difference of number of dimensions from 4; a gluon mass naively introduced will destroy gauge invariance irreparably at this order) must be retained so as to regularize the divergences

arising from integration over phase space for the four-particle final states. The mass introduced by the regularization procedure (subtraction point, mass parameter in coupling away from $\epsilon = 0$) will appear as the 'argument' of α_s, and at $O(\alpha_s^2)$ there will be an explicit $\log(s/\mu^2)$ term, whose coefficient corresponds to the expansion of $\alpha_s(s)$ in terms of $\alpha_s(\mu^2)$ at $O(\alpha_s^2(\mu^2))$. Setting $\mu^2 = s$, the tower of terms $O(\alpha_s \log(s/\mu^2))^k$ are summed to all orders, and the log at $O(\alpha_s^2)$ disappears.

The calculation required to obtain c_2 is not beyond the capabilities of modern algebraic and numerical computer programs. For example, the fully differential cross-section for the four particle final state written in terms of dot products of momenta as generated by GAMALG [14] occupies about 300 lines of FORTRAN.

F2.10 Of course, this interpretation is not precise. For example, the spectacular Jacobian peaks visible in the H_ℓ distributions do not in any way correspond to features of jet energy distributions. Note that beyond $O(\alpha_s)$, the complete distributions in H_ℓ become generalized functions, as discussed in Sec. 4.2 for $\langle F_2^{pt}(x)\rangle$; only when smeared over a small range are they physically meaningful.

F2.11 For large ℓ, $\mathrm{Min}[P_{2\ell}(x)]$ tends to a limit of approximately -0.40, which is the value of $J_0(x)$ at the first zero of $J_1(x)$.

F2.12 Most of the QED corrections to σ, in fact, cancel out when $\sigma(e^+e^- \to \text{hadrons})/\sigma(e^+e^- \to \mu^+\mu^-)$ is considered. However, close to the energies of resonances in the hadron system, there will exist large QED corrections even in this case. Just as for QCD corrections, theoretical predictions and experimental results in this region must be smeared over energy before comparison.

F2.13 Note that in this picture scaling violations are a simple consequence of the fact that the proton is a collection of partons whose transverse momenta rather than angles, with respect to the direction of the total momentum, are bounded (i.e., it is a cylinder of partons rather than a cone of them). This leads to terms in the cross-section of order $\log(Q^2/k_T^2)$. If only the angles of the incoming partons were bounded, these would instead be $\log(Q^2/(Q^2\delta^2))$ and would not change with Q^2. Note that the presence of logs in the first place arises from the fact that the transverse momenta of particles emitted in the final state are limited only by kinematics and may, therefore, run up to Q^2 yielding $\log(Q^2/(k_T)^2_{initial})$ terms.

F2.14 This is analogous to the case of ultraviolet logs. Their renormalization is similar to the factorization of infrared logs. The structure of the field around a point charged particle at very short distances is essentially unaffected by the interactions of the particle occurring on much larger distance scales. Hence the logarithmic divergences associated with the field at very short distances will be universal to all interactions of the particle, and may be factorized out, so that they will not appear in suitable comparisons between processes. (Usually one chooses to take the charge and mass as the standard 'processes' with which to compare others.) The renormalization mass (subtraction point) typically gives the inverse distance below which log terms contributing to a process will be factorized out.

F2.15 It is well known that use of different infrared (and ultraviolet) regularization schemes can lead to different results for a particular process. However, once the coupling constant and the necessary distribution or fragmentation functions have been defined, unambiguous predictions for other processes should be possible. It is believed, on the basis of calculations which sum

over degenerate final, but not initial, states, that comparisons between processes are independent of infrared regularization scheme. We point out that this result has been proved only for infrared divergent terms and could perhaps fail in a complete calculation which includes a sum over many possible initial states.

Section 2 - Figure Captions

2.1 The mean values of various shape parameters for $e^+e^- \to q\bar{q}(G)$ as a function of the mass $\sqrt{\beta s}$ assumed for the gluon. S denotes spherocity and T, thrust [9].

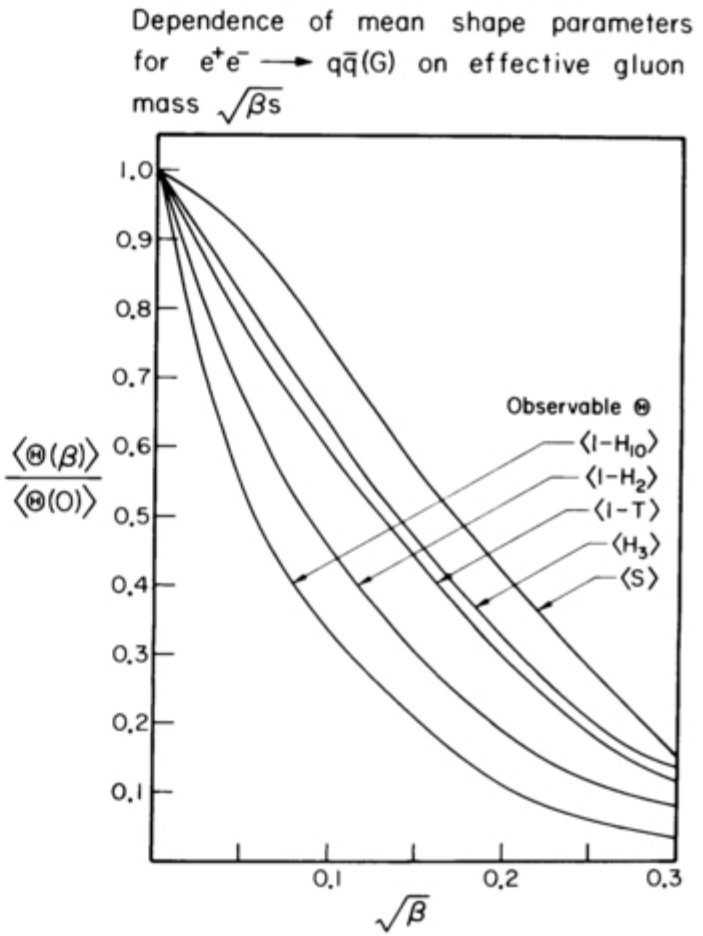

Fig. 2.1

3. The $\langle H_\ell \rangle$ for Large ℓ and their Estimation by Leading Log Summation

3.1 Introduction

As discussed at length in [2], all $\langle (H_\ell)^p \rangle$ are infrared stable: when computed in QCD perturbation theory, they will remain finite at each order when infrared cutoffs used to regularize the contributions of individual diagrams are taken to zero. (This is in contrast to, for example, $\langle \sum_i E_i^2 \rangle$ (i.e., $\langle F_2^{pt}(1) \rangle$), which diverges like $\log^2(\delta)$ as the angular resolution parameter δ is taken to zero.) However, the finite numerical results for the coefficient of, say, α_s in the perturbation series for the $\langle (H_\ell)^p \rangle$ may be numerically so large as to render the expansion useless. That such terms will be larger than in the total cross-section is to be expected, since, in integration over final state phase space, the H_ℓ give higher weight to regions in which the differential cross-section is large (corresponding to kinematic configurations close to those in which it is divergent) than would the uniform weighting of phase space used to calculate σ. For larger ℓ, the H_ℓ vary more rapidly in phase space, and give higher weight to configurations in which particles are nearly collinear, and for which the differential cross-section is close to a divergence. While this behavior causes the terms in the perturbation series for $\langle H_\ell \rangle$ to become very large at large ℓ, it also allows a simple estimate for the $\langle H_\ell \rangle$ at all orders in perturbation theory. The reason for this is that for large ℓ, the $\langle H_\ell \rangle$ probe the structure of events at very small angular scales so that they sample the cores of jets, which may be well described by a leading logarithmic approximation. Of course, this small-scale structure is the most sensitive to fragmentation into hadrons, and it is only at very high energies (see below) that our perturbative calculation of the $\langle H_\ell \rangle$ for large ℓ will be at all accurate.

In Sec. 3.2 we obtain an estimate of the $\langle H_\ell \rangle$ for large ℓ in the process $e^+e^- \to q\bar{q}(G)$ (to $O(\alpha_s)$) from the form of $\langle F_2^{pt}(\chi) \rangle$. We find that $\langle H_{2\ell} \rangle \sim 1-(4\alpha_s/3\pi)\log^2\ell$ for large ℓ in this case. In Sec. 3.5 we calculate $\langle H_\ell \rangle$ for $e^+e^- \to q\bar{q}(GG\ldots)$ to all orders in $\alpha_s \log^2\ell$ and find the exponentiated form $\langle H_\ell \rangle \sim \frac{1}{2}(1+(-1)^\ell \exp(-8\alpha_s/3\pi \log^2\ell))$. The leading log techniques used are derived in the preceding two sections. We also discuss there the gauge dependence of the physical interpretation described in Sec. 2.1 which underlies the calculation of Sec. 3.5. The $(\alpha_s \log^2\ell)^k$ terms in the $\langle H_\ell \rangle$ for $e^+e^- \to q\bar{q}(GG\ldots)$ arise from the region $\chi \simeq -1$ in $\langle F_2^{pt}(\chi) \rangle$. In Sec. 3.6, we discuss the $(\alpha_s \log\ell)^k$ terms associated with the region $\chi \simeq +1$, and obtain a leading log estimate for the $\langle H_\ell \rangle$ at large ℓ from the decay $\zeta \to GGG(GG\ldots)$. Some of these results have also been derived using the 'jet calculus' of Ref. [5]. Our results in Sec. 3.6 are used in Sec. 3.7 to discuss the average angular spread of jets produced in any process. Unfortunately (see especially Sec. 3.8), uncertainties concerning subleading logarithmic terms severely limit the precision of absolutely-normalized predictions. Nevertheless, in Sec. 3.8 we apply our methods in estimating the p_T spectrum of γ^* produced in hadron-hadron collisions and related processes. Finally, in Sec. 3.9, we give a brief discussion of the use of hard photons to probe the structure of e^+e^- annihilation events.

3.2 Estimation of $\langle H_\ell \rangle$ for $e^+e^- \to q\bar{q}(G)$ from $\langle F_2^{pt}(\chi) \rangle$

In estimating the behavior of the $\langle H_\ell \rangle$ for large ℓ, it is convenient to consider the point-detector energy correlation function $F_2^{pt}(\chi)$ discussed in Ref. [2] and defined by eqs. (1.2) and (4.9). We use the relation

$$\langle H_\ell \rangle = \frac{1}{2} \int_{-1}^{1} P_\ell(\chi) \langle F_2^{pt}(\chi) \rangle d\chi. \tag{3.1}$$

For large ℓ, $P_\ell(\cos\theta)$ may be roughly approximated by

$$P_\ell(\cos\theta) = 1 \qquad |\theta| < 2/\ell$$

$$= (-1)^\ell \qquad |\pi-\theta| < 2/\ell \tag{3.2}$$

$$= 0 \qquad \text{otherwise.}$$

Hence to obtain an estimate for the $\langle H_\ell \rangle$ at large ℓ, one requires only the behavior of $\langle F_2^{pt}(\chi)\rangle$ for χ close to ± 1, corresponding to energy correlations between detectors which are either close together or back-to-back (anticollinear). The exact form of $\langle F_2^{pt}(\chi)\rangle$ for the process $e^+e^- \to q\bar{q}(G)$ (given in Appendix A) to order α_s is

$$\langle F_2^{pt}(\chi)\rangle = \{\delta(1+\chi) + \delta(1-\chi)\} + \frac{16\alpha_s}{3\pi}\frac{(\chi+2)}{(1+\chi)(1-\chi)^5}$$

$$\times \{4(\chi^2+4\chi+1)\log(\tfrac{1+\chi}{2}) + 3(1-\chi)(1+3\chi)\} \tag{3.3}$$

$$+ \{C_{-1}\delta(1+\chi) + C_{+1}\delta(1-\chi)\}.$$

The first term here arises from the lowest-order process $e^+e^- \to q\bar{q}$. The second term accounts for the three-particle final state process $e^+e^- \to q\bar{q}G$. For $\chi \simeq -1$, this term becomes

$$-\frac{2\alpha_s}{3\pi}\{\frac{2\log(\frac{1+\chi}{2})}{(1+\chi)} + \frac{3}{(1+\chi)} + \ldots\}, \tag{3.4}$$

while for $\chi \simeq +1$, the term is approximately

$$\frac{\alpha_s}{\pi}\{\frac{1}{(1-\chi)} + \frac{19}{30} + \ldots\}. \tag{3.5}$$

The third term in eq. (2.19) has two sources. First, it gives the contribution from $O(\alpha_s)$ one-loop corrections to $e^+e^- \to q\bar{q}$, and second, at $\chi = +1$, it receives contributions from $e^+e^- \to q\bar{q}G$ events in which one of the final particles passes through both coincident detectors. The constants $C_{\pm 1}$ both diverge logarithmically as the infrared regulator (e.g., a fictitious gluon mass μ) is taken to zero. The coefficient C_{+1} of the delta function at $\chi = +1$ is given simply by

$$C_{+1} = \langle \sum_i \frac{2E_i^2}{s} \rangle, \tag{3.6}$$

where the average is taken over both $q\bar{q}$ and $q\bar{q}G$ final states at $O(\alpha_s)$. The nonlinearity of the form (3.6) in the energies of the final particles means that in averaging over possible final state configurations, collinear pairs of particles will be weighted differently from single particles which carry the sum of their momenta. For this reason, the collinear divergences from $q\bar{q}$ and $q\bar{q}G$ final states will not cancel in (3.6), and C_{+1} will diverge like $\log(s/\mu^2)$ as μ^2 goes to zero. One finds, in fact, that ($\beta = \mu^2/s$ and $\zeta(2) = \pi^2/6$)

$$C_{+1} \simeq \frac{\alpha_s}{\pi}\ [\log(\beta) + \frac{77}{18}]$$

$$(+ \frac{2\alpha_s\beta}{9\pi}\ [6\log^2(\beta) + 21\ \log(\beta) - 12\zeta(2) - 41] + O(\beta^2)). \tag{3.7}$$

However, the integral over χ of the second term in eq. (3.3) (regularized by the introduction of a finite δ) for $\langle F_2^{pt}(\chi)\rangle$, which arises from $q\bar{q}G$ final states, also has a logarithmic divergence in δ close to $\chi = +1$. This divergence cancels against C_{+1} when $\langle F_2^{pt}(\chi)\rangle$ is integrated over χ with a (nonsingular) weight function, such as $P_\ell(\chi)$. This is, of course, necessary in

order that the $\langle H_\ell \rangle$ obtained from $\langle F_2^{pt}(\chi)\rangle$ using eq. (3.1) should be infrared finite as $\mu \to 0$.

The coefficient of the $O(\alpha_s)$ delta function in the backward direction ($\chi = -1$) is given by

$$C_{-1} = \langle \sum_i \frac{2E_i E_{i'}}{s} \rangle, \tag{3.8}$$

where i' is a particle exactly back-to-back with i. This receives contributions only from loop corrections to $e^+e^- \to q\bar{q}$; in fact, it is simply the total cross-section for the process $e^+e^- \to q\bar{q}$ (or, equivalently, the quark electromagnetic form factor) [F3.1]:

$$C_{-1} \simeq \frac{-2\alpha_s}{3\pi}\left[\log^2(\beta) + \frac{3}{2}\log(\beta) - \frac{7}{2} + 2\zeta(2)\right] \\ \left(+ \frac{4\alpha_s \beta}{3\pi}\left[\log^2(\beta) + \log(\beta) - 1 - 2\zeta(2)\right] + O(\beta^2)\right). \tag{3.9}$$

Once again, in integrals of $\langle F_2^{pt}(\chi)\rangle$, these divergences are canceled by corresponding divergences in integrals of the $q\bar{q}G$ contribution (3.4) to $\langle F_2^{pt}(\chi)\rangle$ around $\chi = -1$. The presence of a $\log^2$ divergence in the individual terms around $\chi = -1$ is a consequence of the fact that a $q\bar{q}G$ final state becomes indistinguishable from $q\bar{q}$ if either one of the particles becomes soft or a pair of them are collinear. The introduction of a finite quark mass regularizes the collinear divergences to $O(\alpha_s)$, so that C_{+1} would then exhibit no divergence. However, a single log divergence would remain in C_{-1}, which could only be regularized by taking a finite gluon mass (see [F3.1]).

Using the approximation (3.2) for the Legendre polynomials in eq. (3.1), we obtain for large ℓ

$$\langle H_\ell \rangle \simeq \frac{1}{2}\int_{1-2/\ell^2}^{1} \langle F_2^{pt}(\chi)\rangle d\chi + \frac{(-1)^\ell}{2}\int_{-1}^{-1+2/\ell^2} \langle F_2^{pt}(\chi)\rangle d\chi. \tag{3.10}$$

To $O(\alpha_s^0)$, this gives for $e^+e^- \to q\bar{q}(GG\ldots)$ as usual

$$\begin{aligned} \langle H_\ell \rangle &= 1 \quad (\ell \text{ even}) \\ &= 0 \quad (\ell \text{ odd}). \end{aligned} \tag{3.11}$$

The $O(\alpha_s)$ corrections to this are found by taking the $O(\alpha_s)$ terms in $\langle F_2^{pt}(\chi)\rangle$. The integral of $\langle F_2^{pt}(\chi)\rangle$ over χ with unit $(P_o(\chi))$ weight is simply 2 ($= 2H_o$) and has no $O(\alpha_s)$ corrections. We may, therefore, evaluate the integrals required in (3.10) by computing the integral of $\langle F_2^{pt}(\chi)\rangle$ only up to $\chi = \pm 1 \mp 2/\ell^2$, and subtracting the result from 2, thereby avoiding complications associated with the cancellation of divergences at $\chi = \pm 1$ and allowing us to use only the second term in (3.3) for the calculation. The most singular terms in $\langle F_2^{pt}(\chi)\rangle$ are at $\chi \simeq -1$; we keep only these terms, since they will dominate in the limit $\ell \to \infty$ with which we are here concerned. (In Sec. 3.7 we give the exact result for the integral.) Then using eq. (3.4), we obtain simply

$$\begin{aligned} \langle H_\ell \rangle &\simeq 1 - \frac{4\alpha_s}{3\pi}\log^2\ell + O(\alpha_s \log\ell) \quad (\ell \text{ even}) \\ &\simeq \frac{4\alpha_s}{3\pi}\log^2\ell + O(\alpha_s \log\ell) \quad (\ell \text{ odd}) \end{aligned} \tag{3.12}$$

for large ℓ. This leading behavior for the $\langle H_\ell \rangle$ at large ℓ came from the terms in $\langle F_2^{pt}(\chi)\rangle$ which dominate for small angle emissions. These terms have a simple structure at $O(\alpha_s)$ and in higher orders. Below, we make use of their simplicity to obtain an approximation to the $\langle H_\ell \rangle$ for large ℓ summed to all

orders in α_s. At $O(\alpha_s)$, subleading terms in the large ℓ limit arise both from retaining the complete form of $\langle F_2^{pt}(\chi)\rangle$, rather than simply the part most singular as $\ell \to \infty$, and from using exact forms for the Legendre polynomials rather than the simple approximation (3.2). In fact, it turns out that, at least for even ℓ, the approximation (3.12) gives an accurate result for the variation of the $\langle H_\ell\rangle$ with ℓ right down to $\ell = 2$. In Table 6 of [2], we gave numerical results for the $\langle H_\ell\rangle$ in the process $e^+e^- \to q\bar{q}G$ with ℓ up to 10. For even ℓ, the formula

$$\langle H_\ell\rangle \simeq 1 - \alpha_s(1.32 + 0.43 \log^2\ell), \qquad (\ell \text{ even}) \tag{3.13}$$

provides a good fit to these results. For odd ℓ, a significant $\log\ell$ is also required to obtain a satisfactory fit, although

$$\langle H_\ell\rangle \simeq \alpha_s(0.07 + 0.30 \log^2\ell) \qquad (\ell \text{ odd}) \tag{3.14}$$

gives a rough fit. According to the leading log approximation (3.12), the coefficient of $\log^2\ell$ should, in both cases, be $\simeq 0.42\ \alpha_s$. The fact that the $\langle H_{2\ell}\rangle$ are better approximated by leading log terms than the $\langle H_{2\ell-1}\rangle$ is presumably because the subleading log terms $O(\alpha_s \log\ell)$ cancel between the backward ($\chi \simeq -1$) and forward ($\chi \simeq +1$) direction in the former but not the latter case. From eq. (3.13), one sees that the leading log terms in $\langle H_\ell\rangle$ dominate for $\ell \gtrsim 10$. This indicates that the leading log approximation to perturbative results should be reasonable for emissions at angles $\lesssim 10°$.

3.3 Choices of Gauge in $e^+e^- \to q\bar{q}G$

The picture of e^+e^- annihilation events introduced in Sec. 2.1 took the evolution of the various jets in an event to be independent at times sufficiently

large that the leading logarithmic terms, which correspond to soft or collinear emissions, dominate. This picture emerges naturally from the relevant Feynman diagrams when evaluated in an axial gauge. In this section, we discuss how the details of the picture depend importantly on the particular gauge chosen for the gluon propagator using the example of the process $e^+e^- \to q\bar{q}G$.

In Table 3.1 we give the differential cross-section derived from each of the three classes of diagrams for the square of the amplitude in the process $e^+e^- \to q\bar{q}G$ with various choices for the gluon polarization sum (gauge). Of course, the gauge invariance of the complete amplitude implies that the complete cross-section ($x_{1,2} = 2E_{1,2}/\sqrt{s}$, where 1 and 2 are the q and $\bar{q}$):

$$\frac{d\sigma}{dx_1 dx_2} = \frac{2\alpha_s}{3\pi}\,\frac{x_1^2 + x_2^2}{(1-x_1)(1-x_2)} \tag{3.15}$$

obtained by summing the contributions from each diagram which should be independent of the form chosen for the gluon polarization sum. Nevertheless, the choice of gauge affects the diagrammatic interpretation of the results [20]. For example, in some gauges (e.g., gauge vector $n = q - p_1/x_1$), the gluon may be viewed in the leading log approximation as being emitted solely from one of the quarks, whereas in other gauges (e.g., $n = q$), it appears to be emitted with equal probability from each of the quarks. In $e^+e^- \to q\bar{q}G$ (as in any quantum mechanical process) interferences between amplitudes do not allow one to determine unambiguously from which quark the gluon was emitted. The choice of gauge may be considered to associate (at least to leading log accuracy) each emitted gluon with a particular quark. (Note that, to obtain positive partial cross-sections in Table 3.1, we have not included axial gauges such as $n = p_1 - p_2$ in which $n.k$ changes sign in the physical region.)

Physical predictions are obtained by integrating the differential cross-section (3.15) over the region $1 - x_1 \le x_2 \le 1$, $0 \le x_1 \le 1$. For example, the

energy distribution of quark 1 is given by integrating over x_2, inserting a suitable cutoff near the collinear divergence $x_2 = 1$. The leading terms found will be of order $\log(s/\mu^2)$, where μ is the cutoff. It is possible to choose a gauge in which all such leading log terms come from diagrams containing gluon emissions only from quark 2, allowing a simple probabilistic interpretation of the process. As discussed in Sec. 3.4, the total probability for the q and $\bar{q}$ in the process $e^+e^- \to q\bar{q}G$ to be emitted more than an angle θ from back-to-back is of order $\log^2(\theta)$. Once again, it is possible to choose gauges in which all contributions to these double logarithmic terms come only from a single term in the squared amplitude.

The gauges which admit the clearest physical interpretation are axial gauges, in which $n.\epsilon = 0$, where n is some fixed four-vector which specifies the gauge, and ϵ is the gluon polarization vector. In these gauges, the gluon polarization sum (numerator of propagator) is

$$P_{\mu\nu} = \sum_{\text{pols.}} \epsilon_\mu \epsilon^*_\nu = g_{\mu\nu} - \frac{n_\mu k_\nu + n_\nu k_\mu}{(n.k)} + \frac{n^2 k_\mu k_\nu}{(n.k)^2}, \tag{3.16}$$

where k is the gluon momentum. Note that $k_\mu P_{\mu\nu} = 0$, indicating that one may consider the gluon polarization vector ϵ to be orthogonal to the hyperplane defined by n and k, so that the gluon has only its rightful two transverse polarization states [F3.2]. This if, of course, manifest in the fact that at $k^2 = 0$, $P_{\mu\mu} = 2$ in axial gauges, recording the two polarization states. (In contrast, Feynman gauge gives $P_{\mu\mu} = 4$.) It is clear that the third term in the axial propagator (3.16) cannot give a leading log contribution; however, since all but one of the axial gauge entries in Table 3.1 have $n^2 = 0$, it appears only in one case, for which we have given results obtained with and without the term.

The amplitude for an off-shell quark with invariant mass $\sqrt{t}$ to emit a physical massless spin 1 gluon vanishes like $\sqrt{t}$ as $t \to 0$. The spin non-flip nature of the γ_μ coupling implies that the emission of a helicity ± 1 gluon from an on-shell massless quark is forbidden. In axial gauges, only such helicity ± 1 gluons appear so that collinear divergences are suppressed. In the emission of unphysical helicity 0 (Coulomb-like) gluons, the collinear divergences are not damped [F3.3]. In gauges (such as Feynman gauge) where the sum over polarization states includes contributions from helicity 0 gluons, spurious divergences are introduced into individual diagrams although these naturally cancel out in the complete gauge-invariant cross-section. This discussion allows one to understand the singularity structure of the partial cross-sections for $e^+e^- \to q\bar{q}G$ contributed by the various diagrams given in Table 3.1. Three types of singularities, which we denote C_1, C_2 and G, are apparent. $C_{1,2}$ has the form $1/(k+p_{1,2})^2 = 1/(1-x_{2,1})$ and corresponds to the collinear infrared divergence associated with the emission of the gluon nearly parallel to quark 1 or 2. G is a 'gauge' singularity arising from the (n.k) denominator in the definition (3.16). Let us consider first a general axial gauge in which the vector n is not parallel to the four-momentum which either of the quarks in the final state has when the gluon becomes collinear (two-jet limit). The choices $n = q$ and $n = q - p_3/x_3$ made in Table 3.1 are examples of this case. Here, the diagrams D_{11} and D_{22} (which correspond to the squares of the amplitudes for the gluon to be emitted from quarks 1 and 2, respectively) exhibit the singularities C_1G and C_2G. The appearance of C_1, rather than $(C_1)^2$ $(= 1/(1-x_1)^2)$ is a consequence of the suppression of collinear physical gluon emission mentioned above. This same suppression insures that the interference diagram D_{12} exhibits only the gauge singularity G. Now consider choices of n that become parallel to the q or $\bar{q}$ direction in the collinear gluon limit

('collinear gauges'). Examples of this in Table 3.1 are $n = p_1$, for which G coincides with C_1, and $n = q - p_1/x_1$, for which C_2 and G are the same. For definiteness, we discuss the latter case. It is clear that in this gauge, D_{11} exhibits both C_1 and C_2 (i.e., G) singularities while D_{12} and D_{22} exhibit only C_2 singularities. One might naively have expected a $(C_2)^2$ (from the propagator and gauge singularities) singularity in D_{22}, but this cannot be present because it is absent in the sum of the diagrams (3.15). In this gauge, therefore, the double singularity appearing in the total cross-section is completely accounted for by the single diagram D_{11}. The partial cross-section D_{11} here, in fact, represents the complete leading log estimate for the $e^+e^- \to q\bar{q}G$ cross-section; the gauge choice $n = q - p_1/x_1$ allows the gluon to be considered as emitted only from quark 1 in the leading log approximation. A 'non-collinear' choice of axial gauge, such as $n = q$, associates leading log contributions with emissions from both the outgoing quarks (diagrams D_{11} and D_{22}). This is perhaps more natural physically (especially when n is chosen to be symmetric in p_1 and p_2) but is more complicated in calculations. (The calculations of Sec. 3.4 involve more complicated integrals in such a gauge but require no conceptual changes.) On the other hand, in Feynman gauge, the diagram D_{11} exhibits the singularity C_1, D_{22}, C_2, and D_{12}, C_1C_2. The appearance of the double singularity in the interference diagram D_{12} is due to the inclusion of unphysical helicity 0 gluons in the polarization sums, as discussed above.

The extraction of singly-logarithmic predictions, such as the single quark energy distribution, from the partial cross-sections in Table 3.1 is in all cases simple. One may immediately identify which terms will lead to single logarithms of the infrared cutoff when integrated over x_1 or x_2. However, one must note that x_3 denominators may lead to log terms whose coefficients

contain $\delta(1-x_{1,2})$. One might naively expect that only terms proportional to $1/(1-x_1)(1-x_2)$ would contain $\log^2$ when integrated over x_1 and x_2. However, it is clear that these terms do not give the complete $\log^2$ results (e.g., they appear to differ in the various gauges of Table 3.1). To obtain the correct $\log^2$ results, one must also retain $1/[(1-x_{1,2})x_3]$ terms whenever the region of integration includes the point $x_1 = x_2 = 1$ in the limit that any infrared cutoffs go to zero.

In investigations of the diagrammatic structure of deep inelastic scattering, it is often convenient to choose an axial gauge so that leading log contributions (away from $x = 1$) come only from the squares of amplitudes involving gluon emissions from the incoming rather than the outgoing quark [21]. One possible gauge for this purpose is defined by $n = xp + q$, where p is the incoming quark momentum, q is the photon momentum, and $x = |q^2|/2p.q$. The analogue of this gauge in e^+e^- annihilation is $n = q - p_1/x_1$ (or $n = q - p_2/x_2$), for which the leading log contributions will come solely from diagrams involving gluon emissions from quark 1 (or 2). We will often use this gauge below since it is convenient for calculations. The result that it identifies all gluon emissions as being from one of the outgoing quarks survives to all orders in α_s, although the proof that essentially uncrossed ladder diagrams dominate the squared amplitude (necessary to derive our exponentiation results) is slightly complicated but quite analogous to the case of deep inelastic scattering [21].

3.4 The Leading Log Approximation for $e^+e^- \to q\bar{q}(GG...)$

We consider first the $O(\alpha_s)$ process $e^+e^- \to q\bar{q}G$ in order to introduce the methods to be used in higher orders. Let the q, $\bar{q}$ and G momenta be p_1, p_2 and p_3, respectively, and take $x_i = 2E_i/\sqrt{s}$. Then the differential cross-section

for $\gamma^* \to q\bar{q}G$ is given by

$$\frac{d\sigma}{dx_1 dx_2} = \frac{2\alpha_s}{3\pi} \frac{(x_1^2+x_2^2)}{(1-x_1)(1-x_2)}. \tag{3.17}$$

This can be cast into a form suitable for extension to higher orders by defining the Sudakov (light cone) variables (with the 3-axis defined by $\vec{p}_2 + \vec{p}_3$)

$$\begin{aligned} p_i^o + p_i^3 &= z_i\sqrt{s} \\ p_i^o - p_i^3 &= y_i\sqrt{s}. \end{aligned} \tag{3.18}$$

The Sudakov variables for particles 2 and 3 satisfy

$$\begin{aligned} & z_2 + z_3 = 1 \\ & y_2 + y_3 = \hat{t} = (1-x_1), \quad \hat{t}Q^2 = (p_2+p_3)^2 \\ & z_2y_2 = z_3y_3 = z_2(1-z_2)\hat{t} = k_T^2/s \\ & z_2 = x_2 - \hat{t}(1-x_2)/(1-\hat{t}), \end{aligned} \tag{3.19}$$

where k_T is their transverse momentum with respect to $\vec{p}_2 + \vec{p}_3$, which here is simply the direction of particle 1. Then the differential cross-section (3.17) may be rewritten in terms of z_2 and the 23 invariant mass squared $\hat{t}Q^2$ as

$$\frac{d\sigma}{dz_2 d\hat{t}} = \frac{2\alpha_s}{3\pi} \left[\frac{(1+z_2^2)}{\hat{t}(1-z_2)} - \frac{2(1-z_2(1-z_2))}{(1-z_2)} + \frac{\hat{t}(1+(1-z_2)^2)}{(1-z_2)}\right]. \tag{3.20}$$

This differential cross-section is largest when the gluon is emitted with small transverse momentum and in this region the first term in eq. (3.20) dominates.

For any weighting of phase space which is not especially insensitive to the small k_T region, the differential cross-section (3.20) may, therefore, be approximated by its first term. This is a convenient approximation because at higher orders in α_s, terms with the form of the first term in eq. (3.20) iterate in a simple manner (at least when a prudent gauge is chosen) representing the independent emissions of many gluons from the q, $\bar{q}$ or both. The second two terms in eq. (3.20) are important for large k_T gluon emission and are the precursors of correlations between gluons emitted at higher orders in α_s. These terms may be dropped if only small k_T emissions are considered.

From Table 3.1 and the discussion in the previous section, it is clear that one may choose a gauge for the gluon propagator (e.g., an axial one with $n = q - p_2/x_2$) in which the leading log (i.e., first) term in eq. (3.20) arises only from the diagram (D_{22} in Table 3.1) where the gluon is emitted from quark 2. Terms in the cross-section arising from diagrams involving gluon emissions from quark 1 do not contribute to leading log accuracy. One may then identify the leading log part of the cross-section (3.20) as the probability that a quark of invariant mass $\sqrt{\hat{t}s}$ will propagate from its production in the γ^* decay and emit a gluon so that its final energy is approximately z_2 times its original energy. Integrating over the possible invariant masses $\hat{t} \approx \beta$ to 1 for the virtual quark, the total probability for its energy to be degraded by a factor z in the emission of the gluon becomes

$$\approx \frac{2\alpha_s}{3\pi} \left(\frac{1+z^2}{1-z}\right) \log\left(\frac{s}{\mu^2}\right), \tag{3.21}$$

where μ is an infrared regulator which imposes a lower limit on the virtual quark invariant mass (e.g., allows only propagation for a finite time). The probability (3.21) is the standard Altarelli-Parisi [22] kernel which describes

the degradation of the energy of a quark by gluon emissions. When more than one gluon is emitted, eq. (3.21) gives the probability that at each emission (of a nearly collinear gluon) the quark energy will decrease by a factor z.

Instead of using an axial gauge in which all gluons may be taken to be emitted from a single quark, one may choose a gauge (such as those specified by $n = q$ or $n = q - p_3/x_3$) in which diagrams involving emission from both of the quarks contribute leading log terms. This makes for a more difficult analysis but allows the physical interpretation of some radiation from each of the quarks.

The cross-section (3.20) is only for the process $e^+e^- \to q\bar{q}G$. However, at $O(\alpha_s)$ there can also be one-loop corrections to $e^+e^- \to q\bar{q}$ which contribute to the total $e^+e^- \to q\bar{q}(G)$ cross-section only at $\hat{t} = 0$, $z_2 = 1$ (in higher orders, they contribute at $\hat{t}_{i+1} = \hat{t}_i$ and the relative longitudinal Sudakov variable $z_{i+1} = 1$). By introducing Sudakov variables analogous to (3.19) in the internal loop integrations in these diagrams, one may write this leading contribution to the total cross-section as

$$-\frac{2\alpha_s}{3\pi}\int_{\sim\beta}^{s}\frac{d\hat{t}}{\hat{t}}\int_0^{\sim 1-\beta}\left(\frac{1+z^2}{1-z}\right)dz, \tag{3.22}$$

where β is an infrared regulator (e.g., $\beta = \mu^2/s$, with μ a fictitious gluon mass). It is often permissible to include the virtual corrections by modifying the form of the differential cross-section (3.20). The leading part of the modified cross-section is simply

$$\frac{d\sigma}{dz_2 d\hat{t}} = \frac{2\alpha_s}{3\pi\hat{t}}\left(\frac{1+z_2^2}{1-z_2}\right)_+ = \frac{2\alpha_s}{3\pi\hat{t}}\left[\frac{(1+z_2^2)}{(1-z_2)_+} + \frac{3}{2}\delta(1-z_2)\right]$$

$$= \frac{\alpha_s}{2\pi\hat{t}}P_{qq}(z_2) \tag{3.23}$$

$$\int_0^1 (h(z))_+ f(z)dz = \int_0^1 h(z)(f(z)-f(1))dz.$$

This modified form suffices in most practical cases. The form (3.23) will only give the correct result for the contribution of virtual diagrams (involving no explicit gluon emission) at $z_2 = 1$ if $\hat{t}$ at this point is permitted to run right up to 1. For our applications, and for any case in which only the k_T of the gluon, rather than its angle, is considered, this condition will be satisfied, and the form (3.23) may be used without reservation.

The leading log approximation to cross-sections for $e^+e^- \to q\bar{q} + n$ gluons (and the associated virtual diagrams) may be obtained by simple iteration of the result (3.23). First, however, we must define the Sudakov variables for the process. We take the ith gluon emitted from the $q(\bar{q})$ to have momentum $k_i^{1(2)}$ and the quark after the emission to have momentum $p_i^{1(2)}$ (see Fig. 3.1) and invariant mass $\sqrt{\hat{t}_{i+1}s}$. Then the Sudakov variables are given by the formulae analogous to (3.19) where now $\vec{p}_{i-1}$ defines the 3-axis. The transverse momentum of the ith gluon emitted with respect to the $i-1^{th}$ quark link is given by

$$(k_T)_i^2 = s(1-z_i)(z_i\,\hat{t}_i - \hat{t}_{i+1}), \tag{3.24}$$

with $z_i = (p_i^o + p_i^3)/(p_{i-1}^o + p_{i-1}^3)$. For our leading logarithmic approximations to be valid, we must require at least

$$\Lambda^2/s \ll (k_T)_i^2/s \ll 1. \tag{3.25}$$

We now choose a gauge (e.g., $n = q - p_i/x_i$) in which only diagrams involving gluon emissions from one of the outgoing quarks give leading logarithmic contributions. In this case, it is clear that the differential cross-section for the emission of n gluons may be written to leading log accuracy (independent emission approximation) in the simple product form

$$\frac{1}{\sigma_o}\frac{d\sigma}{dz_1\ldots dz_n d\dot{t}_1\ldots d\dot{t}_n} = \left(\frac{2}{3\pi}\right)^n \left[\left(\frac{1+z_1^2}{1-z_1}\right) + \frac{\alpha_s(t_1)}{\dot{t}_1}\right]\ldots\ldots \left[\left(\frac{1+z_n^2}{1-z_n}\right) + \frac{\alpha_s(t_n)}{\dot{t}_n}\right]. \tag{3.26}$$

For our double logarithmic applications, it will be formally sufficient to approximate all the $\alpha_s(t_i)$ by $\alpha_s(s)$. The cross-section (3.26) is the standard result for independent small angle emissions and also describes, for example, the radiation of many photons by an electron (c.f., Sec. 2.6).

If instead we considered the radiation of gluons from a gluon line (forming a gluon jet), then in eq. (3.23), P_{qq} is replaced by the $G \to G$ kernel which, for our doubly logarithmic purposes, may be taken as

$$P_{GG}(z) = 3\left(\frac{z}{1-z}\right)_+. \tag{3.27}$$

This will be relevant for estimates of the $\langle H_\ell\rangle$ in events containing gluon jets (e.g., decays of $Q\bar{Q}$ bound states; see eq. (3.42) et seq).

3.5 Leading Log Estimates for $\langle F_2^{pt}(\chi)\rangle$ near $\chi = -1$ and $\langle H_\ell\rangle$ in $e^+e^- \to q\bar{q}(GG\ldots)$

In this section, we shall use the approximation (3.26) to the differential cross-section for $e^+e^- \to q\bar{q}(GG\ldots)$ to obtain leading log estimates for the behavior of $\langle F_2^{pt}(\chi)\rangle$ around $\chi = -1$ and hence for the $\langle H_\ell\rangle$ at large ℓ. $\langle F_2^{pt}(\chi)\rangle$ for χ close to -1 is given in the leading log approximation simply by the probability that the q and $\bar{q}$ produced in $e^+e^- \to q\bar{q}(GG\ldots)$ should be at angle χ. Gluons do not contribute to $\langle F_2^{pt}(\chi)\rangle$ (except inasmuch as they are responsible for the deflection of the quarks) since their energies may be neglected in the leading log approximation; they give subleading log terms which we must ignore in view of our other approximations.

Recall the definition (1.1) of the H_ℓ. Since we ignore the energies of the gluons, the $\langle H_\ell\rangle$ for $e^+e^- \to q\bar{q}(GG\ldots.)$ is given simply by (see also (3.1), (3.2))

$$\langle H_\ell\rangle \simeq \frac{1}{2}\langle P_\ell(\chi_{q\bar{q}})\rangle \simeq \frac{1}{2}(-1)^\ell \frac{1}{\sigma}\int_{-1}^{-1+2/\ell^2} \frac{d\sigma}{d\chi_{q\bar{q}}}\, d\chi_{q\bar{q}} \tag{3.28}$$

where $\chi_{q\bar{q}}$ is the cosine of the angle between the final directions of the q and $\bar{q}$, and the second equality follows on using the approximation (3.2) for $P_\ell(\chi)$ at large ℓ. Note that our leading log approximation for the $e^+e^- \to q\bar{q}(GG..)$ differential cross-section is valid only for small angle emissions so that it could not give the $\langle H_\ell\rangle$ at small ℓ even if a more exact form for $P_\ell(\chi)$ were used. Equation (3.28) implies that at large ℓ the $\langle H_\ell\rangle$ in $e^+e^- \to q\bar{q}(GG\ldots)$ are approximately proportional to the total probability $\mathcal{F}_B(\theta)$ that the q and $\bar{q}$ produced are back-to-back (anticollinear) within an angle $\theta = 2/\ell$. This condition implies that the emission of gluons by the q and $\bar{q}$ produced in $\gamma^* \to q\bar{q}$ must radiate a transverse momentum less than $\lesssim \theta^2 s/4$. This requires that any gluons emitted must be both soft and nearly collinear with the q, $\bar{q}$ and, therefore, leads to double-log $O([\alpha_s \log^2\theta]^k)$ terms in $\mathcal{F}_B(\theta)$ and $\langle H_\ell\rangle$.

In calculating $\mathcal{F}_B(\theta)$ from the differential cross-section (3.26), it is convenient to compute the total probability that gluon emissions deflect the q and $\bar{q}$ by an angle more than θ away from the anticollinear configuration and then to subtract this from one. In this way, one avoids the infrared difficulties associated with a direct calculation in the small angle region. Such a procedure is satisfactory for the calculation of any infrared finite observable. To $O(\alpha_s)$, then $\mathcal{F}_B(\theta)$ may be obtained from the differential cross-section (3.23):

$$\mathcal{F}_B(\theta) \simeq 1 - \frac{2\alpha_s}{3\pi}\int_{\theta^2/4}^{1}\frac{d\tilde{t}}{\tilde{t}}\int_0^{1-\theta^2/4\tilde{t}}\frac{x_1x_2(1+z_2^2)}{(1-z_2)}\,dz_2 \tag{3.29}$$

$$\simeq 1 - \frac{8\alpha_s}{3\pi}\log^2\theta,$$

in agreement with eq. (3.12). (The exact form is given in eqs. (3.67) and (3.69).) The energy correlation (3.4) near $\chi = -1$ is given (to leading log accuracy) simply by the derivative of $\mathcal{F}_B(\theta)$ with respect to $\chi = -\cos(\theta)$. In eq. (3.29) we could have taken the numerator in the z_2 integral to be simply 2; only terms singular in the limit $z_2 \to 1$ contribute to our leading double log approximation for $\mathcal{F}_B(\theta)$. Note that $1 - z_2$ gives the energy of the gluon emitted, while $\tilde{t}$ gives its angle ($d\tilde{t}/\tilde{t} = 2d\eta/\eta$, where η is the angle between the initial quark and the emitted gluon) so that the region $z_2 \simeq 1$, $\tilde{t} \simeq 0$ corresponds to emissions that are both soft and nearly collinear. In eq. (3.29) we ignored the variation of the coupling constant $\alpha_s(t)$ across the region of the $\tilde{t}$ integration since the corrections introduced at each order by allowing a logarithmic variation of α_s with t are of order $\log(\theta^2)/\log(s/\Lambda^2)$ relative to the leading terms and may, therefore, formally be neglected in our leading double log approximation. When we treat $\langle P_2^{pt}(\chi)\rangle$ near $\chi = +1$ in Sec. 3.5,

the leading terms in each order will be singly logarithmic so that the variation of α_s with t must be included.

We now extend the estimate (3.29) to all orders in α_s using the leading log approximation (3.26) for the $e^+e^- \to q\bar{q}(GG\ldots)$ differential cross-section. To do this, we integrate the cross-section over z_i and $\tilde{t}_i$ with the constraint (dropping the irrelevant factor 4 dividing θ^2)

$$\sum_{i=1}^{n}(1-z_i)\tilde{t}_i \le \theta^2, \tag{3.30}$$

where n is the total number of gluons emitted. Equation (3.30) is the condition that the transverse momentum radiated by the q, $\bar{q}$ is less than $\theta^2 s$. (As discussed above, one may choose a gauge so that only diagrams involving gluon emissions from one of the quarks need be considered in the leading log approximation.) Equation (3.24) shows that in the region $z_i \simeq 1$ relevant for our leading log approximation, the $\tilde{t}_i$ satisfy $\tilde{t}_{i-1} \gg \tilde{t}_i$. In fact, our approximations should only be valid if $\lambda\tilde{t}_{i-1} \gg \tilde{t}_i$ where $\lambda \ll 1$. However, the difference between choosing these two kinematic constraints will be of order $\log(\lambda)/\log(\theta)$, which is formally of subleading log order, although in practice perhaps not particularly small (see below). We may, therefore, use the simpler constraint $\tilde{t}_{i-1} \ge \tilde{t}_i$ to the level of our approximations. The integration over the kinematic region (3.30) must be done with care. Consider the ith emission and define

$$\theta_c^2 = \theta^2 - \sum_{j=1}^{i-1}(1-z_j)\tilde{t}_j. \tag{3.31a}$$

Then, according to eq. (3.30), the required integration region is bounded by

$$0 \leq z_i \leq 1, \qquad \Lambda^2/s \leq \dot{t}_i \leq \dot{t}_{i-1} \tag{3.31b}$$

$$(1-z_i)\dot{t}_i \leq \theta_c^2 \tag{3.31c}$$

which includes the point $z_i = 1$, where virtual diagrams (involving virtual corrections to gluon emission, or to the propagation of the quarks) as well as real gluon emissions, contribute. To integrate over the kinematic region (3.31b,c), correctly accounting for these virtual diagrams, is somewhat complicated. It is simpler to use the analogue of the method of eq. (3.29) for one gluon emission, which avoids direct integration over the difficult region. For this purpose recall that, by the arguments given above, the leading double log contributions from the ith gluon emission cancel their 'soft' logarithms against those from the virtual corrections to the corresponding quark line when integrated over the full kinematic region (3.31b), without the restriction (3.31c), leaving only single collinear log terms. Hence the double log contribution subject to the restriction (3.30) is given simply by minus the integral of the differential cross-section (3.26) over the region (3.31b), but outside the boundaries (3.31c). The limits of this complementary region are just

$$0 \leq z_i \leq 1 - \theta_c^2/\dot{t}_i, \qquad \theta_c^2 \leq \dot{t}_i \leq \dot{t}_{i-1}. \tag{3.31d}$$

In fact, one may take the θ_c in these constraints as θ to leading double log accuracy. Now one may easily integrate the differential cross-section (3.26) over the regions (3.31d) for each gluon emission. Then, introducing the requisite $(-1)^n$ to account for the fact that the integrals were done over the regions (3.31d), complementary to the required region (3.30), the probability that the q and $\bar{q}$ will be deflected from anticollinearity by an angle less than θ by the emission of n gluons (with possible virtual corrections to these or to the propagation of the quarks) becomes

$$\frac{(-1)^n}{2^n n!}\left(\frac{4\alpha_s}{3\pi}\right)^n \log^{2n}(\theta^2). \tag{3.32}$$

Note that the 1/n! factor in this result is due to the kinematical ordering of the t_i which restricts the phase space for gluon emission (operationally, each double integral of $\log^{2k}(t_i)$ gives a factor $1/(2k+1)$). When summed over n to account for all possible numbers of gluon emissions, the form (3.32) becomes an exponential, giving

$$\mathcal{F}_B(\theta) \simeq \exp[-\frac{8\alpha_s}{3\pi}\log^2(\theta)]. \tag{3.33}$$

The leading log approximation to the energy correlation is determined from this to be [F3.4]

$$\begin{aligned}\langle P_2^{pt}(\chi)\rangle \simeq\ & \delta(1+\chi) - \frac{4\alpha_s}{3\pi}\frac{1}{1+\chi}\log(1+\chi) \\ & \times \exp[-\frac{2\alpha_s}{3\pi}\log^2(1+\chi)] + \delta(1-\chi).\end{aligned} \tag{3.34}$$

We have added here the $O(\alpha_s^0)$ contribution of $e^+e^- \to q\bar{q}$ at $\chi = 1$. In higher orders, the dominant terms in $\langle P_2^{pt}(\chi)\rangle$ for $e^+e^- \to q\bar{q}(GG\ldots)$ around $\chi = +1$ are of subleading logarithmic order compared to those around $\chi = -1$. The expansion of the leading log result (3.34) clearly agrees with the leading log term in the exact $O(\alpha_s)$ result (3.4). In the $O(\alpha_s)$ result, the logarithmic term is $\log[(1+\chi)/2]$ rather than $\log(1+\chi)$ as suggested by (3.34). (The argument of the logs in (3.34) would have been $(1+\chi)/2$ if we had not dropped a factor of 4 in (3.30).) Of course, there is no difference between these forms at leading log order (i.e., for χ very close to -1 so that $|\log(1+\chi)| \gg 1$). Nevertheless, one might speculate that by replacing $\log(1+\chi)$ with $\log[(1+\chi)/2]$,

one might be able to account for much of the subleading log corrections to (3.34) near $\chi = -1$. However, the explicit $O(\alpha_s)$ result (3.4) shows that this is not the case: the subleading log term appearing there is not dominated by the log(2) from the difference of these forms and, in fact, the complete correction is opposite in sign to it. The leading log result (3.34) gives higher-order corrections to any $q\bar{q}$ final state regardless of how it was produced. However, the subleading log terms depend on the process by which the $q\bar{q}$ were produced ($\gamma^* \to q\bar{q}$, $\gamma\gamma^* \to q\bar{q}$, $W^* \to q\bar{q}$, etc.) and so cannot be universally included [F3.5]. It would be of great interest to compute the subleading log terms at $O(\alpha_s^2)$ in order to investigate whether, for example, they obey some simple differential equation, perhaps with the appearance of a renormalization group equation in θ. Another subleading log contribution is associated with the choice of the 'argument' of α_s. Although formally negligible, the numerical difference between taking $\alpha_s(s)$ and, say, $\alpha_s(s/10)$, or worse $\alpha_s(s(1+\chi))$, is rather large at conceivable values of s. These difficulties are discussed further in Sec. 3.7.

The $O(\alpha_s)$ result (3.29) for the total probability that the q and $\bar{q}$ from $e^+e^- \to q\bar{q}(GG....)$ are produced back-to-back within an angle θ (or equivalently, to leading log accuracy, the integral of the energy correlation function $\langle F_2^{pt}(\chi)\rangle$ around $\chi = -1$) exhibits a double logarithmic divergence as $\theta \to 0$. However, the exponentiated form, in which the double logarithmic divergences appearing at each order in α_s have been summed up, goes smoothly (faster than any power of θ) to zero as $\theta \to 0$, reflecting the fact that the q and $\bar{q}$ will never be produced exactly back-to-back: they will always emit some gluons and be deflected. While this result implies that a summation of leading log perturbative terms is apparently sufficient to obtain a physically reasonable form, one should not forget that in practice the small θ region will be dominated by non-perturbative and subleading log QCD effects and, in fact, the behavior of leading log perturbation theory there may well be entirely irrelevant.

In addition, the damping exhibited by the summed leading log terms will probably not be shared by subleading perturbative terms which may well even diverge like $\alpha_s(\theta^2 s)$ as $\theta \to 0$.

The exponentiated double log form (3.33) is reminiscent of several well-known results in QED (e.g., [24]) and of some in QCD [25]. However, it appears that none of these are exactly equivalent to (3.33). The usual results come from investigating exclusive reactions and requiring a fixed kinematic configuration for the final (and initial) state but inserting a non-zero mass for some of the particles involved in the scattering in such a way as to avoid mass singularities (infrared divergences). In our result (3.33), all regularization masses have been taken to zero, and we do not consider a fixed kinematic configuration: we derive the total probability for inclusive $q\bar{q}$ production with the q and $\bar{q}$ deviating from anticollinearity by an angle less than θ. The simplest example of a fixed angle result is probably the 'Sudakov' form factor for an electron in QED:

$$|F_{(p^2)}(s)|^2 \simeq \exp[-\tfrac{\alpha}{\pi}\log^2(s/p^2)], \tag{3.35}$$

which gives the probability that a massless electron initially off-shell by an amount p^2 will emit no photons, however soft, when it is struck by a hard photon of invariant mass $\sqrt{s}$. Alternatively, one may find the form factor for an on-shell massless electron ($p^2 = 0$), taking a small regularization mass ν for the photons:

$$|F_{(\nu^2)}(s)|^2 \simeq \exp[-\tfrac{\alpha}{2\pi}\log^2(s/\nu^2)]. \tag{3.36}$$

The difference in the coefficients of $\log^2$ in eqs. (3.35) and (3.36) reflects

the different infrared regularization schemes used (see [F3.1]). Equation (3.36) (with the substitution $\alpha \to c_F\alpha_s = 4\alpha_s/3$) gives the cross-section for the process $e^+e^- \to q\bar{q}$ when no real gluons are produced, which is the form factor for a quark in the timelike region [F3.6]. The $O(\alpha_s)$ term in the expansion of (3.36) was obtained in the explicit $O(\alpha_s)$ calculation of $e^+e^- \to q\bar{q}$ given in eq. (3.9). Any form factor or fixed angle scattering cross-section in QCD will be given to leading double log accuracy by the lowest order (Born) term, multiplied by an exponential like those in eqs. (3.35) and (3.36). The coefficient in the exponent is proportional to $\sum_i c_i$, where the c_i are the color Casimir invariants (4/3 for quarks, 3 for gluons) associated with each of the incoming or outgoing partons in the exclusive reaction. (There is a further factor associated with the method of infrared regularization.) Several exclusive processes in QCD have been calculated in detail to subleading log order; the resulting cross-sections are found to obey 'infrared renormalization group equations' in the regularization mass. The equations contain β function terms [25] which suggest the use of a running coupling $\alpha_s(s)$ in the exponentiated forms (3.35) or (3.36) to account for some of the subleading (single) log terms in the perturbation series.

In our derivation of $\langle F_2^{pt}(\chi)\rangle$ for $e^+e^- \to q\bar{q}(GG..)$ near $\chi = -1$, we require the inclusive cross-section for $q\bar{q}$ production rather than an exclusive cross-section. For exclusive processes, there can be no extra real gluon emissions, and so only virtual exchanges contribute to the cross-section. However, in obtaining the integral of $\langle F_2^{pt}(\chi)\rangle$ for $\chi > \chi_0 = \cos(\pi-\theta) \simeq -1$, real emissions make the dominant contribution. Since the total cross-section integrated over all χ must be finite, one might expect that the leading contribution of the relevant real emissions could be obtained simply by replacing the infrared cut-off in the results (e.g., (3.7)) for the virtual exchanges by the cut-off $\simeq \theta^2 s$ on the real emissions. However, this cannot be done directly because the

cut-offs provided by the introduction of non-zero particle masses are somewhat different than those imposed by a minimum transverse momentum cut (see [F3.1]). (At the leading log level, a translation between the results may be possible but at the subleading log level, they will differ in a fundamental way.) We do not understand the kinematic cut-offs used in Ref. [20], and our results differ from those obtained there.

Equation (3.34) gives the leading log form for $\langle F_2^{pt}(\chi)\rangle$ summed to all orders in α_s which is equivalent (in the leading log approximation) to the $q\bar{q}$ inclusive cross-section in $e^+e^- \to q\bar{q}(GG...)$ as a function of the $q\bar{q}$ angle, $\cos^{-1}(\chi)$. This is plotted in Fig. 3.2 together with the exact lowest-order result (3.3). At each order in α_s, $\langle F_2^{pt}(\chi)\rangle$ diverges like $\log^k(1+\chi)/(1+\chi)$ as $\chi \to -1$. However, the sum (3.34) of the leading log terms in $\langle F_2^{pt}(\chi)\rangle$ around $\chi = -1$ no longer diverges as $\chi \to -1$ (ignoring, of course, the lowest order $\delta(1+\chi)$ term). Instead, it rises steadily roughly like $1/(1+\chi)$ until χ becomes of order

$$1 + \chi_{peak} \simeq \exp[-3\pi/(4\alpha_s(s))] \simeq \left(\frac{\Lambda^2}{s}\right)^{25/16} \tag{3.37}$$

at which point

$$\langle F_2^{pt}(\chi_{peak})\rangle \simeq \exp[3\pi/(8\alpha_s(s))] \simeq \left(\frac{s}{\Lambda^2}\right)^{25/32}, \tag{3.38}$$

where we have taken the unsupported liberty of replacing α_s by $\alpha_s(s)$. In deriving (3.34), we specifically limited our discussion to the region $\theta^2 \gg \Lambda^2/s$ since for smaller θ, $\alpha_s(t)$ becomes so large that our perturbative methods and neglect of subleading logarithmic and genuinely non-perturbative terms can no longer be trusted. The damping of the $q\bar{q}$ inclusive cross-section which (3.34)

implies for $\chi < \chi_{peak}$ should, therefore, probably not be taken seriously. In this region, entirely non-perturbative effects will undoubtedly swamp our perturbative terms. This is very clear from the $\langle F_2(\chi)\rangle$ for simulated hadronic events given in Sec. 4. In fact, the vanishing of $\langle F_2^{pt}(\chi)\rangle$ at $\chi = -1$ when summed to all orders in perturbation theory is an example of the common phenomenon of radiation damping. Another example is the suppression of the high-energy end of the electron spectrum in muon decay [26]. Here, the infrared stability of the QED coupling with finite electron mass means that the result may be trusted [F3.7], but the smallness of α means that it appears only in a region (of order $\Lambda^2_{QED}/m^2_\mu \sim e^{-1/\alpha}$ from the kinematic boundary) entirely irrelevant for practical considerations.

In Fig. 3.2, we show the summed leading log result (3.34) for $\langle F_2^{pt}(\chi)\rangle$ in $e^+e^- \to q\bar{q}(GG...)$ together with the explicit $O(\alpha_s)$ result for $e^+e^- \to q\bar{q}(G)$. Note that at intermediate angles, the two forms agree rather well especially at small α_s. However, inspection of the results in Sec. 4 (e.g., Fig. 4.2) shows that until very high energies are reached, the form of $\langle F_2^{pt}(\chi)\rangle$ will be entirely dominated by hadronic (and subleading log) effects, and it will certainly not be possible to distinguish the summed and $O(\alpha_s)$ results close to the backward direction. (We discuss this in more detail in Sec. 3.8.) At energies where hadronization is unimportant, $\alpha_s(s)$ will be sufficiently small that no higher order corrections to the $O(\alpha_s)$ results will be visible. In fact, the result (3.37) for the position of the backward peak in the summed form of $\langle F_2^{pt}(\chi)\rangle$ shows that this will always be lost in the region hidden by the 'resolution' associated with fragmentation to hadrons.

If one attempted to extend the curves for $\langle F_2^{pt}(\chi)\rangle$ beyond $O(\alpha_s)$ or beyond the leading log approximation, one would find that, as explained in Sec. 4.2, they would become undefined at each value of χ, and would only have a meaning

when smeared in χ (as for the calculation of $\langle H_\ell\rangle$). However, the contributions to χ integrals of $\langle F_2^{pt}(\chi)\rangle$ from the terms responsible for the difficulties are of subleading log order and thus formally insignificant. It is probably best to use $\langle F_2^{pt}(\chi)\rangle$ only as an intermediate in finding the infrared finite $\langle H_\ell\rangle$ and not to consider its own properties in detail.

From the result (3.34) for $\langle F_2^{pt}(\chi)\rangle$, we may now estimate the $\langle H_\ell\rangle$ in $e^+e^- \to q\bar{q}(GG...)$ at large ℓ using the approximation (3.10). We find

$$\langle H_\ell\rangle \simeq \frac{1}{2}\{1 + (-1)^\ell \exp[-(8\alpha_s/3\pi)\log^2\ell]\} \tag{3.39}$$

for large ℓ. The $O(\alpha_s)$ results in eqs. (3.13) and (3.14) suggest that a correction term $C\alpha_s$ should be added to (3.39), where $C = -1.32\,\alpha_s$ (ℓ even), $\simeq 0$ (ℓ odd). In Fig. 3.3 we show the form (3.39) with this correction added for even ℓ, as a function of ℓ and in Fig. 3.4 as a function of α_s. We also show the corresponding $O(\alpha_s)$ result (3.12). The cross-hatched barriers represent very rough (and optimistic) limits of applicability of our perturbative approximation. Beyond them, the typical angles of $2/\ell$ probed by the $\langle H_\ell\rangle$ are smaller than the angular spread of order $\Lambda/(\langle z\rangle\sqrt{s})$ associated with the formation of hadrons. Hadronic effects should be unimportant only when $\sqrt{s} \gg 5\ell$ GeV. (3.39) implies that when $\ell \to \infty$, $\langle H_\ell\rangle \to 1/2$ in the leading double log approximation. This limit is approached when $\ell \gg 1/(1+\chi_{peak}) \sim (s/\Lambda^2)$, so that the $\langle H_\ell\rangle$ are sensitive only to the behavior of the $q\bar{q}$ inclusive cross-section at angles so small that the exponentiated doubly logarithmic terms are strongly damped. In this region, the singly logarithmic terms in $\langle F_2^{pt}(\chi)\rangle$ both around $\chi = -1$ and also around $\chi = +1$ should become important in determining the $\langle H_\ell\rangle$ through eq. (3.10), and leading log methods no longer suffice. In the next section we discuss the behavior of $\langle F_2^{pt}(\chi)\rangle$ for χ close to +1 where the singly

logarithmic terms are leading. For $\gamma \simeq -1$, a treatment of the subleading singly logarithmic terms does not appear to be easy.

Using the methods described above, we may estimate the $\langle H_\ell \rangle$ for a final state consisting of two gluon jets as might arise, for example, from the decay of a spin 0 or spin 2 $Q\bar{Q}$ state. We use the differential cross-section (3.26) but with the longitudinal kernel (3.27). The doubly logarithmic estimate for the probability that the leading gluons in the two jets will be back-to-back within an angle θ is then

$$\mathcal{S}_B(\theta) \simeq \exp[-\frac{6\alpha_s}{\pi}\log^2(\theta)]. \tag{3.40}$$

The larger exponent in this case than in the case of $q\bar{q}$ jets (3.34) implies that the leading GG are more likely to be found at larger angles than the $q\bar{q}$ by a factor of order 9/4 ($= c_A/c_F$). It has been suggested [27] that this result implies that gluon jets are broader than quark jets. A more relevant treatment of this point, based on the angles between particles in the same jet rather than with respect to a recoil jet, is given in the next section. The result turns out to be numerically very similar. The leading logarithmic energy correlation function for two gluon jets is

$$\langle F_2^{pt}(\chi)\rangle \simeq \delta(1+\chi) - \frac{3\alpha_s}{\pi}\frac{1}{1+\chi}\log(1+\chi)\exp[-\frac{3\alpha_s}{2\pi}\log^2(1+\chi)] + \delta(1-\chi). \tag{3.41}$$

This yields a large ℓ estimate for the $\langle H_\ell \rangle$ in this case:

$$\langle H_\ell \rangle \simeq \frac{1}{2}\{1 + (-1)^\ell \exp[-(6\alpha_s/\pi)\log^2\ell]\} + O(\alpha_s). \tag{3.42}$$

The explicit $O(\alpha_s)$ term depends on the short-distance (large-angle) structure of the final state and for a $Q\bar{Q}$ decay will be affected by the spin of the initial state. The $\langle H_\ell \rangle$ to $O(\alpha_s)$ for the decay of a scalar $Q\bar{Q}$ bound state (χ) may be obtained from the differential cross-sections for the decays $\chi \to GGG$, $Gq\bar{q}$ from a scalar ($F_{\mu\nu}F_{\mu\nu}$) source given in [28]. We find

$$\begin{aligned}
\langle H_2 \rangle &\simeq 1 - \frac{\alpha_s}{\pi}[(3\pi^2-20) + \frac{F}{12}(212-21\pi^2)] \\
&\simeq 1 - (3.1+0.1F)\alpha_s \\
\langle H_3 \rangle &\simeq \frac{\alpha_s}{3\pi}[(2230-225\pi^2) + \frac{145F}{12}(15\pi^2-148)] \\
&\simeq (1.0+0.1F)\alpha_s,
\end{aligned} \tag{3.43}$$

where F is the number of light quark flavors. These may be compared with the results for $q\bar{q}G$ production from a scalar photon [F3.8]

$$\begin{aligned}
\langle H_2 \rangle &\simeq 1 - \frac{\alpha_s}{3\pi}(83-8\pi^2) \\
&\simeq 1 - 0.43\,\alpha_s \\
\langle H_3 \rangle &\simeq \frac{20\alpha_s}{3\pi}(5\pi^2-49) \\
&\simeq 0.74\,\alpha_s.
\end{aligned} \tag{3.44}$$

In Sec. 3.8, we consider briefly the application of methods and results in this section to the transverse momentum spectrum of massive photons produced in the Drell-Yan process where we also give a discussion of their region of validity.

3.6 Leading Log Estimates for $\langle F_2^{pt}(\chi)\rangle$ near $\chi = +1$ and the $\langle H_\ell\rangle$ in $\zeta \to GGG(GG\ldots)$

Recalling the definition (1.1) of the H_ℓ, the approximation (3.2) for the Legendre polynomials implies that for large ℓ, the H_ℓ may be computed by lumping together all assemblies of particles with an angular spread less than about $2/\ell$ and treating them as single 'jets'. Then the vanishing of the $P_\ell(\cos\theta)$ outside an angle $2/\ell$ (in the approximation (3.2)) means that there are only diagonal and 'back-to-back' contributions (E_i^2 and $E_iE_{i'}$) to the H_ℓ for the system of jets. Hence the $\langle H_\ell\rangle$ for large ℓ may be written as (the sum over 'jets' is over all assemblies of particles separated by angles much greater than $2/\ell$)

$$\langle H_\ell\rangle \simeq \frac{1}{2}\left\{\mathcal{S}_F(2/\ell) + (-1)^\ell \mathcal{S}_B(2/\ell)\right\}, \qquad \ell \gg 1$$

$$\text{where} \qquad \mathcal{S}_F = 2\sum_{\text{jets } i} \frac{E_{jet}^2}{s}\left(S_F(2/\ell)\right)_i \tag{3.45}$$

and $(\mathcal{S}_F(\theta))_i$ is the mean square fractional energy which is not radiated outside a cone of half-angle θ around a jet i [F3.9] while $\mathcal{S}_B(\theta)$ was defined in Sec. 3.5 as the mean product of the energies, for all pairs of back-to-back (anti-collinear) jets i and i', at angles less than θ from the axis of the jets. In the leading log approximation, $\mathcal{S}_B(\theta)$ is simply the probability that the leading partons in the jets are anticollinear within an angle θ. This probability goes like $[\alpha_s \log^2\theta]^n$ in each order of perturbation theory but exponentiates to the form (3.33) when summed to all orders. However, the $\mathcal{S}_B(\theta)$

term in eq. (3.43) contributes to the $\langle H_\ell\rangle$ only for processes which give dominantly two-jet final states such as $e^+e^- \to q\bar{q}(GG\ldots)$. In other processes (such as $\zeta \to GGG$), pairs of anticollinear partons are not usually produced, and the $\mathcal{S}_B(\theta)$ term in eq. (3.43) may be ignored leaving only the diagonal $\mathcal{S}_F(\theta)$ term. It is, therefore, the energy distribution inside a single jet which determines the large ℓ behavior of the $\langle H_\ell\rangle$ for final states usually containing more than two jets.

The estimate (3.43) for the $\langle H_\ell\rangle$ may be rewritten in terms of integrals over the energy correlation function $\langle F_2^{pt}(\chi)\rangle$ around $\chi = \pm 1$ as in eq. (3.10). The first terms in eqs. (3.10) and (3.45) probe the behavior of $\langle F_2^{pt}(\chi)\rangle$ for χ close to +1. The result for $\langle F_2^{pt}(\chi)\rangle$ in the $O(\alpha_s)$ process $e^+e^- \to q\bar{q}(G)$ is given by eq. (3.3). Its behavior close to $\chi = +1$ given by eq. (3.5) yields (the exact form is in eq. (3.67))

$$\mathcal{S}_F(\theta) \simeq 1 + \frac{2\alpha_s}{\pi}\log(\theta) \tag{3.46}$$

in this case. This result is to be compared with the $\mathcal{S}_B(\theta)$ for $e^+e^- \to q\bar{q}(G)$ given in eq. (3.26) which exhibits a $\log^2(\theta)$ divergence as $\theta \to 0$. In fact, we find that in general the leading log terms in $\mathcal{S}_F(\theta)$ are of order $[\alpha_s \log\theta]^n$ in contrast to the $[\alpha_s \log^2\theta]^n$ terms in $\mathcal{S}_B(\theta)$.

We now discuss the calculation of $\mathcal{S}_F(\theta)$ (or equivalently, the integral of $\langle F_2^{pt}(\chi)\rangle$ for $\chi \simeq +1$) for a quark-initiated jet [F3.9]. We shall refer to the leading particle in the jet as the quark and consider the successive emission of gluons from it (although, in fact, one must account for 'mixing', in which the role of leading particle is transferred from a quark to a gluon and so on). A typical jet, together with some of the kinematics to be used, is depicted in Fig. 3.1. Consider the contribution to $\mathcal{S}_F(\theta)$ from emissions

at angles of about $\chi = \cos^{-1}(\chi)$ (giving directly a smeared result for $\langle F_2^{pt}(\chi)\rangle$). If the kth gluon emitted is at an angle $\sim \phi \le \theta$ to the leading quark, then its contribution to $\mathcal{F}_F(\theta)$ will be given by the product of its fractional energy with that of the quark. In terms of the variables $\hat{t}_k$ and z_k introduced in Sec. 3.4, we may express the angle η_k between the quark and gluon as

$$\eta_k^2 \simeq 4\,\hat{t}_k/[(z_1\ldots z_{k-1})^2 z_k(1-z_k)]. \tag{3.47}$$

Here we see the critical difference from the calculation of $\mathcal{F}_B(\theta)$ given in Sec. 3.4. In the present calculation of $\mathcal{F}_F(\theta)$, η_k vanishes only when $\hat{t}_k \to 0$, whereas in the computation of $\mathcal{F}_B(\theta)$ the relevant angle was proportional to $\sqrt{(1-z_k)\hat{t}_k}$ and so vanished when the emitted gluon was either soft ($z_k \to 1$) or collinear ($\hat{t}_k \to 0$). In $\mathcal{F}_B(\theta)$, constraints on η_k, therefore, implied constraints on z_k. For $\mathcal{F}_F(\theta)$, constraints on η_k do not prevent z_k from running up to 1, thus allowing virtual loop corrections to cancel soft gluon emission divergences and leading only to single rather than double logarithms of θ at each order in α_s. Since we only retain leading logarithmic terms (in $\hat{t}$), eq. (3.47) may be approximated by

$$\eta_k^2 \sim \hat{t}_k. \tag{3.48}$$

It is certainly disturbing that eq. (3.47) and (3.48) differ by a large factor (~ 20 for $k = 1$ and more for larger k). However, it would not be consistent with our leading log approximations to insist on the complete eq. (3.47); the resulting factor could be canceled by other subleading terms that we have neglected. This point will be discussed further in Sec. 3.7.

The approximation (3.48) leads to a simple algorithm for calculating $\mathcal{F}_F(\theta)$. First note that the kinematic ordering of the $\hat{t}_i$ (c.f. eq. (3.32)) implies in this case that the emission angles η_i are also ordered:

$$\eta_1 \ge \eta_2 \ldots \ge \eta_{k-1} \ge \eta_k \ge \eta_{k+1}. \tag{3.49}$$

Hence if $\eta_k = \phi$, then all previous emissions must have been at angles $\ge \phi$. Moreover, all emissions after the kth must be at angles smaller than ϕ so that they may be neglected. The contribution to $\mathcal{F}_F(\theta)$ from the kth gluon emission which is at an angle $\phi \le \theta$ (which is approximately $\langle F_2^{pt}(\chi = \cos\phi)\rangle$)

$$\begin{aligned}\langle F_2^{pt}(\chi)\rangle \simeq & \int_{\phi^2}^{1} \frac{d\hat{t}_1}{\hat{t}_1}\frac{\alpha_s(t_1)}{2\pi} \ldots \int_{\phi^2}^{\hat{t}_{k-2}} \frac{d\hat{t}_{k-1}}{\hat{t}_{k-1}}\frac{\alpha_s(t_{k-1})}{2\pi} \\ & \times \int_0^1 dz_1 P(z_1)\ldots\int_0^1 dz_{k-1}P(z_{k-1}) \\ & \times \int_0^1 dz_k P(z_k)(z_1z_2\ldots z_{k-1})^2 z_k(1-z_k)\,\frac{\alpha_s(t_k = s\phi^2)}{2\pi\hat{t}_k}\frac{d\hat{t}_k}{d\chi}\end{aligned} \tag{3.50}$$

where we have used the form (3.26) for the differential cross-section and multiplied by (twice) the product of the final quark and gluon fractional energies ($z_1\ldots z_k$ and $z_1\ldots z_{k-1}(1-z_k)$, respectively). The $P(z)$ are the standard longitudinal evolution (Altarelli-Parisi) kernels in the relative 'longitudinal Sudakov variable' z (as in e.g., eq. (3.23)). Note that in eq. (3.50), we have retained the variation of α_s in the t integrations; for the calculation of $\mathcal{F}_B(\theta)$ this could be dropped to double logarithmic accuracy. On summing eq. (3.50) over k, we find that the contributions of the first (k-1) emissions exponentiate, giving, to leading log accuracy,

$$\langle F_2^{pt}(\chi)\rangle \simeq \frac{\alpha_s(s(1-\chi))}{\pi(1-\chi)} V \exp[-\int_0^1 dz\, z^2 P(z)\log(T(\chi))/2\pi b],$$

$$V = \int_0^1 dz\, z(1-z)P(z),$$

$$T(\chi) = \frac{\alpha_s(s)}{\alpha_s(s(1-\chi))} \tag{3.51}$$

$$b = (33-2F)/12\pi.$$

To find the corresponding $\mathcal{F}_F(\theta)$, we use the same method as for $\mathcal{F}_B(\theta)$ above, computing the energy radiated outside a cone of angle θ and then subtracting this from one, and write

$$\mathcal{F}_F(\theta) \simeq \int_{1-\theta^2/2}^{1} \langle F_2^{pt}(\chi)\rangle d\chi \simeq 1 - \int_{\sim 0}^{1-\theta^2/2} \langle F_2^{pt}(\chi)\rangle d\chi. \tag{3.52}$$

In the calculation (3.51), we have not included any contribution due to the emissions of the gluons after the kth one. These serve to spread out the energies of the quark and gluon we consider into cones but with opening angles much less than ϕ, so that all their component particles may be lumped together for our leading log purposes. Nevertheless, if one explicitly multiplies the cross-section (3.50) by the differential cross-section for the (k+1),.... emissions and then integrates over their possible angles and energies, one, of course, finds that they contribute a factor of one [F3.10].

To order α_s, the exponential factor in (3.48) does not contribute and

$$\langle F_2^{pt}(\chi)\rangle \simeq \frac{\alpha_s}{\pi(1-\chi)} V, \tag{3.53}$$

where we have dropped the argument of α_s since formally it cannot affect the $O(\alpha_s)$ result. The corresponding $\mathcal{F}_F(\theta)$ is then

$$\mathcal{F}_F(\theta) \simeq 1 - \frac{\alpha_s}{\pi}\int_0^{1-\theta^2/2} V \frac{d\chi}{1-\chi}$$

$$\simeq 1 + \frac{2\alpha_s}{\pi} V \log(\theta). \tag{3.54}$$

To $O(\alpha_s)$, the spreading of a quark jet arises solely from the emission of a single gluon from the quark so that the corresponding V is given by

$$V_{q\to qG} = \int_0^1 P_{qq}(z)z(1-z)dz = \frac{4}{3}\int_0^1 \left(\frac{1+z^2}{1-z}\right)_+ z(1-z)dz = 1, \tag{3.55}$$

giving, to leading log accuracy,

$$(\mathcal{F}_F(\theta))_q \simeq 1 + \frac{2\alpha_s}{\pi}\log\theta. \tag{3.56}$$

This is in agreement with eq. (3.46) which was derived by integrating the $\langle F_2^{pt}(\chi)\rangle$ for $e^+e^- \to q\bar{q}(G)$ given in eq. (3.4) from $\chi = 1$ to $\chi \simeq 1 - \theta^2/2$. Since $\theta \ll 1$, eq. (3.56) implies that, as expected, the emission of gluons depletes the energy contained in a cone of angle θ around a jet. To $O(\alpha_s)$, a gluon jet can spread by the gluon emitting either a gluon or a $q\bar{q}$ pair, giving

$$V_{G\to GG} = \frac{1}{2}\int_0^1 P_{GG}(x)x(1-x)dx = \frac{21}{10}$$

$$V_{G\to q\bar{q}} = \int_0^1 P_{qG}(x)x(1-x)dx = \frac{F}{20} \tag{3.57}$$

where F is the number of quark flavors with masses << $\theta\sqrt{s}$. Hence for a gluon jet

$$(\mathcal{F}_F(\hat{\tau}))_G = 1 + \frac{2\alpha_s}{\pi}(V_{G\to GG} + V_{G\to q\bar{q}})\log\theta$$
$$= 1 + \left(\frac{42+F}{10}\right)\frac{\alpha_s}{\pi}\log\theta. \tag{3.58}$$

On comparing this with eq. (3.56), we see that gluon jets should be broader than quark jets by a factor of order (42+F)/20 ≃ 2.3. Note that this result is numerically very similar to the ratio 9/4 = 2.25 found in eqs. (3.41) and (3.34) for the mean deviation from anticollinearity of pairs of gluons and of quarks produced in back-to-back jets. Notice that eq. (3.58) implies that $q\bar{q}$ production contributes negligibly to the spreading of a gluon jet. In our later numerical estimates, we take F = 4 although all our results are extremely insensitive to this choice.

The result (3.58) allows us to obtain an estimate for the $\langle H_\ell\rangle$ in the process $\zeta \to GGG(GG..)$ at large ℓ to $O(\alpha_s)$. In this case, the first term in eq. (3.45) contributes, and we obtain (for both even and odd ℓ)

$$\langle H_\ell\rangle \simeq \frac{3}{8}\left(1 - \left(\frac{42+F}{20}\right)\frac{\alpha_s}{\pi}\log(\ell)\right)$$
$$\simeq 0.375(1 - 0.73\,\alpha_s\log(\ell)). \tag{3.59}$$

Here we have approximated the $O(\alpha_s^0)$ result for $\sum_{\text{jets}}(E_i^2/s)$ by the phase space value (see Sec. 2.6). The result (3.59) is to be compared with the corresponding $O(\alpha_s)$ results (3.12) for the process $e^+e^- \to q\bar{q}(GG...)$ which contains a pair of back-to-back jets, leading to a $\log^2(\ell)$ term at $O(\alpha_s)$. The two cases

are plotted in Fig. 3.3 where the slower variation of the $\langle H_\ell\rangle$ for $\zeta \to GGG(GG...)$ than for $e^+e^- \to q\bar{q}(GG...)$ is evident. One may be concerned that the quantum numbers of the ζ state ($^3S_1$) might invalidate our analysis based on the evolution of individual jets. However, as mentioned elsewhere, $\zeta \to GGGG$ is not forbidden (as would the decay of orthopositronium to $\gamma\gamma\gamma\gamma$) because the gluons can be antisymmetric in color.

In going beyond $O(\alpha_s)$, we must consider mixing. In a jet initiated by a quark, any of the gluons emitted by the quark may carry off much of its energy thereby taking its place as the leading particle in the jet. The spreading of the jet energy will then be determined by emissions from the gluons, and so on. To account for these effects, the longitudinal evolution (Altarelli-Parisi) kernels P in eq. (3.51) must be taken as matrices, and the V as vectors (with components $V_{q\to X}$, $V_{G\to X}$) in the basis q, G (q here represents a 'singlet quark' (i.e., $\sum_{i=1}^{F}(q_i+\bar{q}_i)$); 'non-singlet quarks' do not contribute to jet spreading. After the exponential factor appears a two-component vector (1,0) or (0,1) for a quark or gluon jet, respectively. The integrals over P appearing in the exponential factor in eq. (3.51) give simply the matrix of n = 3 anomalous dimensions familiar from analyses of deep inelastic scattering. Using standard methods (e.g., [29]), we find for a quark jet

$$\langle F_2^{pt}(\chi)\rangle \simeq \frac{\alpha_s(s(1-\chi))}{\pi(1-\chi)}\{1.48[T(\chi)]^{0.61} - 0.48[T(\chi)]^{1.39}\}, \tag{3.60}$$

while for a gluon jet

$$\langle F_2^{pt}(\chi)\rangle \simeq \frac{\alpha_s(s(1-\chi))}{\pi(1-\chi)}\{1.84[T(\chi)]^{1.39} + 0.46[T(\chi)]^{0.61}\}. \tag{3.61}$$

These results are plotted in Fig. 3.2 where they are compared both with form obtained in the backward direction and, for quark jets, with the complete $O(\alpha_s)$ results. Figure 3.5 gives the corrections to the $O(\alpha_s)$ leading log result (3.5) due to the inclusion of higher order terms. Results for two choices for the argument of α_s (see next section) are given. The cross-hatched barriers in Fig. 3.2 indicate the angles beyond which our perturbative methods can definitely not be trusted. In practice, inspection of Fig. 4.2 shows that hadronic effects will entirely swamp our perturbative calculations for all χ until rather high values of $\sqrt{s}$ are reached, where higher order corrections are probably irrelevant. Note that, as discussed in Sec. 3.5, subleading log delta functions at all values of χ do not appear in the approximations used for Figs. 3.2 and 3.3. From eqs. (3.60) and (3.61), we obtain leading log approximations for $\mathcal{E}_F(\theta)$:

$$(\mathcal{E}_F(\theta))_q \simeq \left(\frac{12}{33-2F}\right)\left\{\frac{1.48}{0.61}\,[T(\chi)]^{0.61} - \frac{0.48}{1.39}\,[T(\chi)]^{1.39}\right\}$$
$$\simeq 1.17[T(\chi)]^{0.61} - 0.17[T(\chi)]^{1.39} \tag{3.62}$$

$$(\mathcal{E}_F(\theta))_G \simeq 0.64[T(\chi)]^{1.39} + 0.36[T(\chi)]^{0.61}. \tag{3.63}$$

When $\theta \simeq 1$ so that $T(\chi) = 1$, these results reduce simply to $\mathcal{E}_F(\theta) = 1$, the total energy of the jets [F3.11], exhibiting the consistency of our approximations. The consequences of the results (3.60) through (3.63) for the size of jets will be discussed in the next section. Here, we use eq. (3.45) to obtain a leading log estimate for the $\langle H_\ell\rangle$ at large ℓ in $\zeta \to GGG(GG\ldots)$. We find

$$\langle H_\ell\rangle \simeq 0.24[T(1-\ell^2)]^{1.39} + 0.14[T(1-\ell^2)]^{0.61}$$
$$\simeq 0.24\left[\frac{\log(s/\ell^2\Lambda^2)}{\log(s/\Lambda^2)}\right]^{1.39} + 0.14\left[\frac{\log(s/\ell^2\Lambda^2)}{\log(s/\Lambda^2)}\right]^{0.61}. \tag{3.64}$$

This estimate should be reliable for $1 \ll \ell \ll \sqrt{s}/\Lambda$. Notice that whereas for $e^+e^- \to q\bar{q}(GG\ldots)$ the $\langle H_\ell\rangle$ went to zero as $\ell \to \infty$ in the summed loading double log approximation, the $\langle H_\ell\rangle$ for $\zeta \to GGG(GG\ldots)$ diverge logarithmically as $\ell \to \infty$. In neither case can our perturbative methods be used as a reliable guide. The divergence for $\zeta \to GGG(GG\ldots)$ reflects the infinite value of α_s found at $s/\ell^2 \le \Lambda^2$ in perturbation theory. In practice, this divergence is presumably avoided by the non-perturbative hadronic effects which dominate at such values of s/ℓ^2 and perhaps give $\alpha_s(t) \sim 1/\log((t+\Lambda^2)/\Lambda^2)$. The result (3.64) is plotted in Fig. 3.3. Note that the variation with ℓ of the $\langle H_\ell\rangle$ for $\zeta \to GGG(GG\ldots)$ is expected to be much less rapid than for $e^+e^- \to q\bar{q}(GG\ldots)$.

From eq. (3.61) one may also, in principle, find $\langle F_2^{pt}(\chi)\rangle$ for $\zeta \to GGG(GG\ldots)$ by convoluting this with the lowest order result given in eq. (A.A2). However, it is clear that in this procedure, the unknown region around $\chi = 1$ in eq. (3.61) will be sampled at all points. As expected from the discussion in Sec. 4.2, divergences appear in $\langle F_2^{pt}(\chi)\rangle$ to $O(\alpha_s^k)$ at all values of χ which were populated at $O(\alpha_s^{k-1})$. For $e^+e^- \to q\bar{q}(GG\ldots)$ these divergences potentially appear only at $\chi = \pm 1$ in the leading log approximation, but for $\zeta \to GGG(GG\ldots)$ they inevitably appear at all values of χ rendering a direct result for $\langle F_2^{pt}(\chi)\rangle$ in this case meaningless. Of course, when one integrates over χ as in the construction of the $\langle H_\ell\rangle$, the divergences are suitably tamed.

3.7 The Width of QCD Jets

The results in Sec. 3.6 can be used to obtain leading log estimates for the average energy distributions inside jets. Since in the leading log approximation, the structures of jets do not depend on the processes by which they were generated but only on their total energies, our results are also applicable to jets produced in reactions other than e^+e^- annihilation. In practice, it turns out that our predictions are rather sensitive to subleading logarithmic effects which have not yet been calculated and will not be entirely universal.

The H_ℓ were designed to study the distribution of energy in events in their center of mass system. In investigating the structure of single jets, it is convenient to use observables similar to the H_ℓ:

$$J(f,\eta) = \sum_{i,j} \frac{|\vec{p}_i||\vec{p}_j|}{s} f(\phi_{ij})\theta(\cos\phi_{ij}-\eta)$$
$$= \int_\eta^1 \langle F_2^{pt}(x)\rangle f(\cos^{-1}(x))dx, \qquad (3.65)$$

where angles are measured in the rest frame of the complete event, not of a particular jet. The θ function is designed to sample only pairs of particles 'in the same jet'. For processes such as $e^+e^- \to q\bar{q}(GG\ldots)$ in which only two jets are produced, it is convenient to take $\eta = 0$ thereby sampling only pairs of particles in the same hemisphere. For leading log estimates, the precise choice of η will be irrelevant.

The simplest observable based on the definition (3.65) is

$$\mathcal{F}_F(\cos^{-1}\eta) = \langle J(1,\eta)\rangle = \langle \sum_{i,j} \frac{|\vec{p}_i||\vec{p}_j|}{s} \theta(\cos\phi_{ij}-\eta)\rangle$$
$$= \int_\eta^1 \langle F_2^{pt}(x)\rangle dx. \qquad (3.66)$$

This gives essentially the fraction of the energy squared in a jet contained within the cone of full angle $\cos^{-1}(\eta)$ about its 'axis'. (Of course, no axis need actually be found.) For the process $e^+e^- \to q\bar{q}(G)$, one finds [F3.12]:

$$\langle J(1,\eta)\rangle = 1 - \frac{\alpha_s}{54\pi}[36\log^2 2 - 1632\log 2 + 959]$$
$$- \frac{\alpha_s}{3\pi}\frac{1}{(1-\eta)^4}\{4(1-\eta)^4[Li_2(\tfrac{1+\eta}{2}) - \tfrac{1}{2}(\log^2(2)+\zeta(2))]$$
$$- \log(\tfrac{1+\eta}{2})[2(1-\eta)^4(\log(\tfrac{1+\eta}{2}) - 2\log(\tfrac{1-\eta}{2})) \qquad (3.67)$$
$$- 3\eta^4 + 4\eta^3 - 18\eta^2 - 124\eta - 3]$$
$$- 2(1-\eta)(\eta^2 - 33\eta - 4) - 3\log(\tfrac{1-\eta}{2})(1-\eta)^4\}$$

where $Li_2(x)$ is the dilogarithm function defined (for our purposes) in eq. (2.10). For $\eta \simeq +1$, eq. (3.67) becomes

$$\langle J(1,\eta)\rangle = \mathcal{F}_F(\cos^{-1}\eta) \simeq 1 + \frac{\alpha_s}{\pi}\{\log(1-\eta) + (\frac{3156\log 2 - 72\zeta(2) - 2113}{108})$$
$$+ \ldots\} \qquad (3.68)$$
$$\simeq 1 + (0.32\log(1-\eta) - 0.13 + \ldots)\alpha_s.$$

The leading term here agrees with the leading log result (3.46). Notice that in this case, the subleading log terms could be roughly accounted for by replacing $\log(1-\eta)$ with $\log((1-\eta)/1.5)$. In the backward direction, eq. (3.67) gives an exact result for $\mathcal{F}_B(\theta)$ to $O(\alpha_s)$. For $\eta \simeq -1$, one finds

$$\mathcal{F}_B(\cos^{-1}\eta) \simeq 2 - \langle \underset{\sim}{J}(1,\eta)\rangle = 2 - \mathcal{F}_F(\cos^{-1}\eta)$$

$$\simeq 1 - \frac{2\alpha_s}{3\pi}\left(\log^2\left(\frac{1+\eta}{2}\right) + 3\log\left(\frac{1+\eta}{2}\right)\right.$$

$$\left. + \left(\frac{408\log 2 + 9\zeta(2) - 206}{9}\right) + \ldots\right) \qquad (3.69)$$

$$\simeq 1 - \left(0.21\log^2\left(\frac{1+\eta}{2}\right) + 0.64\log\left(\frac{1+\eta}{2}\right) + 2.16 + \ldots\right)\alpha_s$$

$$\simeq 1 - (0.21\log^2(1+\eta) + 0.34\log(1+\eta) + 1.82 + \ldots)\alpha_s .$$

The leading log term here was given in eq. (3.10). It is clear that no replacement for $(1+\eta)$ in the logarithms of eq. (3.69) can remove all the subleading terms (the relevant quadratic equation, in fact, has no real roots). In particular, as mentioned below (3.34), use of $(1+\eta)/2$ is not better than $1+\eta$ as the argument of log. Finally, we give $\langle J(1,0)\rangle$ which represents roughly the average fraction of energy squared produced in one hemisphere of $e^+e^- \to q\bar{q}(G)$ events:

$$\mathcal{F}_F(\pi/2) = \langle J(1,0)\rangle \simeq 1 + \left(\frac{16321\log 2 - 1103}{54}\right)\frac{\alpha_s}{\pi}$$

$$\simeq 1 + 0.17\,\frac{\alpha_s}{\pi}. \qquad (3.70)$$

The rather small deviation from 1 indicates that the gluon is rarely produced at a large angle to both of the quarks so that nearly all the energy which could possibly be attributed to one of the quark jets is contained in one hemisphere of the event.

In Sec. 3.6 we obtained leading log estimates for $\mathcal{F}_F(\theta)$ (or $\langle J(1,\cos\theta)\rangle$) to all orders in α_s valid for small θ. These results for quark and gluon jets together with the exact $O(\alpha_s)$ result for a 'quark' jet produced in $e^+e^- \to q\bar{q}(G)$

are shown in Fig. 3.6 for $\sqrt{s} = 20$ GeV, corresponding to $\alpha_s(s) \simeq 0.2$. In the summed leading log estimates, we only account for terms with the form of the $\log(1-\eta)$ in the $O(\alpha_s)$ result (3.68). However, it is clear from eq. (3.68) that terms which are formally subleading in the limit $\eta \to 1$ may, nevertheless, effectively serve to change the scale of the argument of the logarithm and have important consequences for numerical estimates. In higher orders, lack of knowledge of such terms prevents the determination of the correct 'argument' of α_s to be used in the integrals (3.50). This uncertainty is just the indeterminacy in the effective value of Λ^2 without subleading terms discussed in Sec. 2.5 for the $\langle H_t\rangle$ and σ. It can only be resolved by calculations of subleading terms which must be done for each particular process since they are not universal to jets produced in different reactions. One might suspect (although for little reason) that the correct argument for α_s in the integrals (3.50) would be exactly t. To leading log accuracy, this may be approximated just by $s(1-\chi)$, but if one attempts to account for some subleading terms, one must include the numerical factor in t, implying that the α_s appearing in eq. (3.61), etc., should be $\simeq \alpha_s(s(1-\chi)/20)$ rather than $\alpha_s(s(1-\chi))$ as discussed in Sec. 3.6. The difference between these two choices may be considered as a difference in the effective value of Λ^2 chosen in the absence of exact calculations. The $O(\alpha_s)$ result (3.68) perhaps favors $\alpha_s(s(1-\chi)/1.5)$, but the $O(\alpha_s^2)$ result would be necessary before claiming that this would give accurate estimates. It is clear from Fig. 3.6 that the choice of the argument of α_s has a rather large numerical effect. Note that the curves in Fig. 3.6 depend on s only in the combination $s(1-\chi)$ so that other values of s may be found from the curves by rescaling χ. It is clear from Fig. 3.6 that gluon jets should be broader than quark jets. Note that the convergence of the leading log curves at $\chi = 0$ is artificial - it results from the assumption of a form

proportional to $(1-\chi)$ in the argument of α_s. This cannot be justified past the leading log approximation.

A good measure of the width of jets is provided by [30]

$$\langle\phi\rangle_E = \left\langle \frac{J(\phi,0)}{J(1,0)} \right\rangle, \tag{3.71}$$

which gives the mean angle between pairs of particles in the same hemisphere weighted by the product of their energies. In Fig. 3.7 we give $\langle\phi\rangle_E$ together with

$$\sqrt{\langle\phi^2\rangle_E} = \sqrt{\left\langle \left(\frac{J(\phi,0)}{J(1,0)}\right)^2 \right\rangle} \tag{3.72}$$

for quark and gluon jets as a function of their energy. We give the results obtained from the leading log approximation (3.62, 63) using both $\alpha_s(s(1-\chi))$ and $\alpha_s(0.05\ s(1-\chi))$ where we choose $s = 4E^2_{jet}$, together with the exact $O(\alpha_s)$ result for $e^+e^- \to q\bar{q}(G)$ obtained from the form (A.1) for $\langle F_2^{pt}(\chi)\rangle$ in this case. It is clear that until very high energies are reached, formally subleading terms are critical in determining the numerical results for $\langle\phi\rangle_E$ and $\sqrt{\langle\phi^2\rangle_E}$. Nevertheless, even these uncertainties are probably insignificant compared to those associated with the non-perturbative process of hadron formation which correct our leading log estimates at large times. In Fig. 3.7 we also give the predictions of the Field-Feynman model [31] for hadron production in jets, which are based on fits to available data, and take a fixed intrinsic average transverse momentum of order 0.35 GeV with no account of QCD scaling violation effects. The resulting $\langle\phi\rangle_E$, therefore, falls roughly as $k_T/(\sqrt{s}\langle z\rangle)$ where $\langle z\rangle$ is the average fractional energy of a hadron produced in the jet and is typically of order 0.15. In contrast, the $\langle\phi\rangle_E$ contributed by perturbative QCD effects

falls roughly like $\alpha_s(s) \sim 1/\log(s/\Lambda^2)$. The Field-Feynman model was obtained by fitting transverse momenta in jets at comparatively low energies; some of the transverse momentum found should, however, probably be attributed to perturbative QCD effects rather than to hadron formation. One approach to treating this overlap is suggested by the picture described in Sec. 2.1. We choose some definite angle θ_{cut} to delineate the region for which the perturbative estimates (3.62) or (3.63) will be applied. For smaller angles, we use the phenomenological model, while at larger angles we assume that the perturbative results are exact. Our choice of θ_{cut} was twice the mean value of $\langle\phi\rangle_E$ in the Field-Feynman model (i.e., twice solid line in Fig. 3.7). In Fig. 3.7 we show the perturbative estimates for $\langle\phi\rangle_E$ and $\sqrt{\langle\phi^2\rangle_E}$ obtained by considering only $\phi > \theta_{cut}$ and thereby introducing a cutoff $\sim \theta^2_{cut}s \gg \Lambda^2$ into the necessary integrals. It is clear from Fig. 3.7 that hadronization effects will swamp those of perturbative QCD until very high jet energies ($\gtrsim$ 50 GeV) are reached. Nevertheless, jets of such energies should be available from the FNAL collider-doubler and LEP thus allowing the QCD predictions for their properties to be tested. For phenomenological applications, such as those indulged in Ref. [2], it should be sufficient to use the Field-Feynman fit for jet structure until very high energies are reached [F3.13]. Note that, even when an estimate of fragmentation has been included, Fig. 3.7 still predicts that gluon-initiated jets should be broader than quark-initiated ones.

Despite the uncertainty regarding the argument for α_s in eqs. (3.62) and (3.63), the 'correct' argument is presumably proportional to s and probably also to $(1-\chi)$, at least for χ near 1. Hence, although it may not be possible to obtain accurate absolutely-normalized predictions for $\langle F_2^{pt}(\chi)\rangle$, etc., without a knowledge of subleading terms, the leading log estimates should be sufficient to describe the dependence of these observables on s at fixed χ and

probably on χ at fixed s. It should eventually be possible to measure the anomalous dimensions appearing in the exponents of eqs. (3.62) and (3.63) by analyses of jet structure, thereby providing an important test of QCD. In Ref. [5], the production of pairs of hadrons with definite relative transverse momentum was considered by convoluting (evolving) fragmentation functions for the quark and gluon produced according to eq. (3.51) to generate particular hadrons. In that case, no attempt was made to obtain infrared finite results: the divergences associated with the large distance behavior of the final state were factorized off and absorbed into fragmentation functions at some value of s. Hence there was no restriction to consideration of quantities linear in the momenta of the observed particles: any moment of their energies could be used, for which the analogue of eq. (3.51) contains anomalous dimensions with $n > 2$. We have concentrated on observables which are infrared finite and whose mean values should, therefore, be computable purely from QCD perturbation theory.

3.8 Application to the Drell-Yan Process

In Sec. 3.5 we obtained a leading (double) log approximation for the probability that a $q\bar{q}$ pair produced from a γ^* would be deflected through an angle θ from the anticollinear configuration by the emission of gluons. Our results may be applied almost directly to yield a leading log estimate for the transverse momentum spectrum of γ^* produced in hadron-hadron collisions (Drell-Yan process) by $q\bar{q}$ annihilation.

The lowest-order subprocess, $q\bar{q} \to \gamma^*$, for γ^* production gives rise to photons having no transverse momentum with respect to the incoming q, $\bar{q}$ axis. To obtain the cross-section for γ^* production in hadronic collisions, one must convolute the results for $q\bar{q}$ collisions with the probability distributions

$q(x_1)$, $\bar{q}(x_2)$ for the q, $\bar{q}$ to carry fractions x_1, x_2 of the momenta of their parent hadrons. Then, if $\sqrt{s}$ is the c.m. energy for the hadron-hadron collision and $\sqrt{\hat{s}} = \sqrt{x_1 x_2 s}$ that for the $q\bar{q}$ subprocess, the cross-section for the hadroproduction of a virtual photon with invariant mass Q is

$$\sigma = \sigma_o(\tau) = N \iint q(x_1)\bar{q}(x_2)\delta(1-Q^2/\hat{s})dx_1 dx_2, \tag{3.73}$$

where N is an overall normalization factor ($= \frac{1}{3}\sum e_i^2$) which will be irrelevant for our purposes.

At $O(\alpha_s)$, the $2 \to 2$ subprocesses $q\bar{q} \to \gamma^* G$ and $Gq \to \gamma^* q$ lead to γ^* with non-zero transverse momenta (p_T). We consider first $q\bar{q} \to \gamma^* G$ since this will turn out to be most relevant. To $O(\alpha_s)$, the differential cross-section for $q\bar{q} \to \gamma^* G$ is

$$\frac{d\sigma}{d\hat{t}} = N \frac{8\pi\alpha_s}{3\hat{s}^2} \left[\frac{(\hat{t}-Q^2)^2+(\hat{u}-Q^2)^2}{\hat{t}\hat{u}}\right], \tag{3.74}$$

where $\hat{s}$, $\hat{t}$ and $\hat{u}$ are the subprocess kinematic invariants. We require the differential cross-section for γ^* production as a function of p_T where $p_T^2 = \hat{u}\hat{t}/\hat{s}$. For small p_T^2, $\hat{s}$ is close to its $O(\alpha_s^o)$ value of Q^2, and one finds [32] [F3.13]

$$\begin{aligned}\frac{d\sigma}{dp_T^2} &\simeq -N \frac{4\alpha_s}{3\pi} \iint q(x_1)\bar{q}(x_2) \\ &\quad \times \frac{1}{(\hat{s}-Q^2)} \left[\log\left(\frac{2p_T^2\sqrt{\tau}}{s(1-\tau)}\right) + O(\hat{s}-Q^2)\right]dx_1 dx_2 \\ &\simeq -\frac{4\alpha_s}{3\pi} \frac{\sigma_o(\tau)}{p_T^2} \log\left(\frac{2p_T^2\sqrt{\tau}}{s(1-\tau)}\right) + O(\alpha_s).\end{aligned} \tag{3.75}$$

This leading term arises from the region of phase space in which $\hat{s} \approx Q^2$ where the outgoing gluon is both soft and nearly collinear to the incoming q, $\bar{q}$. The corrections to the leading term will not be proportional to $\sigma_o(\tau)$ but will rather depend on new convolutions of the structure functions $\overset{(-)}{q}(x_i)$ which may be written as integrals on derivatives of the s-dependent leading log forms for $\overset{(-)}{q}(x_i)$ with respect to s at $s \approx Q^2$. As expected, the result (3.75) has the same structure as eq. (3.3) which gives the probability that the q and $\bar{q}$ produced in $\gamma^* \to q\bar{q}G$ should be an angle θ from anticollinear, with $\chi = \cos(\pi-\theta)$, so that they have a relative transverse momentum $p_T^2 = \frac{\hat{s}}{2}(1+\chi)$. Note that the subprocess $Gq \to \gamma^* q$ does not give a leading contribution for small p_T.

In Sec. 3.5 we obtained the leading log approximation (3.35) for the probability that the $q\bar{q}$ produced in $\gamma^* \to q\bar{q}(GG\ldots)$ should have a relative transverse momentum $p_T^2 = \hat{s}/2(1+\chi)$. This result may now be used directly to yield the leading log transverse momentum spectrum for γ^* produced in $hh' \to q\bar{q} \to \gamma^*(GG\ldots)$ [F3.15]:

$$\frac{1}{\sigma_o(\tau)}\frac{d\sigma}{dp_T^2} \approx -\frac{4\alpha_s}{3\pi}\frac{1}{p_T^2}\log\left(\frac{p_T^2}{s}\right)\exp\left[-\frac{2\alpha_s}{3\pi}\log^2\left(\frac{p_T^2}{s}\right)\right], \tag{3.76}$$

where we have dropped the irrelevant $\delta(p_T^2)$ terms which arise from loop corrections to $q\bar{q} \to \gamma^*$. Note that the appearance of s rather than Q^2, perhaps multiplied by some function of τ, in eq. (3.76) cannot be justified in the leading log approximation. Subleading corrections to eq. (3.76) will involve nontrivial convolutions of the q, $\bar{q}$ distribution functions. These must be considered in order to determine the correct arguments for the logs and for α_s in eq. (3.76).

Regardless of non-perturbative complications, the leading double log approximation used to derive eq. (3.76) can only be valid if the subleading

log corrections to it are small. The rough form of the perturbation series for $p_T^2/\sigma\, d\sigma/dp_T^2$ is

$$\begin{aligned} &\alpha_s[\omega+1] + \alpha_s^2[\omega^3+\omega^2+\omega+1] + \alpha_s^3[\omega^5+\omega^4+\ldots] + \ldots, \\ &\omega \sim \log(s/p_T^2). \end{aligned} \tag{3.77}$$

It is the first terms at each order in α_s which sum up to the exponential in eq. (3.76). We must now estimate in which regions the terms in (3.77) thus neglected are unimportant. At lowest order, there is a term $O(\alpha_s)$ compared to $O(\alpha_s\omega)$ which arises from consideration of all parts of the differential cross-section (3.74) rather than just those which diverge as $\hat{t}$, $\hat{u} \to 0$. This term is absent from (3.76) but may easily be calculated and included explicitly. However, it will be unimportant so long as

$$\log(s/p_T^2) \gg 1. \tag{3.78}$$

We may take the exponential factor in eq. (3.76) to be O(1) for our present estimates (see below for justification). Then the requirement that the subleading log term $O(\alpha_s^2\omega^2)$ should be unimportant becomes

$$\alpha_s(s')\log(s/p_T^2) \ll 1. \tag{3.79}$$

It is clear that the constraints (3.78) and (3.79) for the validity of the leading double log approximation (3.76) overlap only at very high energies. In particular, if we require that the corrections due to $O(\alpha_s)$ and $O(\alpha_s^2\omega^2)$ terms be of rough order f (say 10%), then eqs. (3.78) and (3.79) imply

$$p_T^2 \leq s e^{-1/f} \tag{3.80a}$$

$$p_T^2 \gtrsim \begin{cases} s^{1-f}(\Lambda^2)^f & (s' = s) \\ s^{1/(1+f)}(\Lambda^2)^{f/(1+f)} & (s' = p_T^2), \end{cases} \tag{3.80b}$$

where we have made two plausible choices for the optimal argument of $\alpha_s(s')$; its best value can, of course, only be determined by a complete subleading log calculation. Equation (3.80) shows that at present energies, there is no region in which all corrections to (3.76) should be small.

Now let us consider the still higher order terms in (3.77) demanding that all subleading log corrections be small. At $O(\alpha_s^3)$, we then require $\alpha_s^2\omega^3 \ll 1$, while, in general, at $O(\alpha_s^k)$, the condition for $O(f)$ subleading log corrections becomes [F3.16]

$$\alpha_s^{k-1}\omega^{2k-3} \leq f \qquad (k > 1). \tag{3.81}$$

Then in the limit $k \to \infty$, this implies,

$$\alpha_s \log^2(s/p_T^2) \leq f^{1/k} \sim 1. \tag{3.82}$$

This constraint is essentially the requirement that the series (3.77) be convergent. It justifies the statement made earlier that the exponential in (3.76) must be $O(1)$ and implies the condition

$$p_T^2 \gtrsim s \exp[-1/\sqrt{\alpha_s}]. \tag{3.83}$$

Equation (3.80a) then implies that an accuracy better than $f \sim \sqrt{\alpha_s}$ can never be expected from eq. (3.76).

The discussion of the last two paragraphs implies that eq. (3.76) (and corresponding results for $\langle F_2^{pt}(\chi)\rangle$ in e^+e^- annihilation) should suffer rather large corrections even in perturbation theory in accessible kinematic regions. The failure of (3.76) at large p_T may be cured without difficulty simply by including the complete $O(\alpha_s)$ result. In fact, one of the most significant conclusions from our discussion of $\langle F_2^{pt}(\chi)\rangle$ above is that at large angles (p_T), higher order corrections to the lowest-order result are small. To improve the approximation (3.76) at small p_T is more difficult. The main reason for the inadequacy of the leading double log result there is that at small p_T, these terms suffer radiation damping, and subleading contributions may become important as implied by eq. (3.80b). Of course, these subleading terms may also exponentiate and be damped as $p_T \to 0$ so that we may have overestimated their contribution by considering only their lowest-order member. We suspect, however, that, like the $\langle F_2^{pt}(\chi)\rangle$ for $\chi \simeq +1$, but unlike the p_T spectrum in QED, the subleading log terms will probably diverge as $[\alpha_s(p_T^2)]^p$ for small p_T, thereby precluding complete perturbative treatment. The best hope for controlling subleading term appears to be in the derivation of a differential equation analogous to that from the renormalization group, but in p_T rather than μ. A complete treatment of subleading log terms cannot entirely remove the condition (3.82) but would increase the size of the right-hand side.

At each order perturbation theory, the γ^* transverse momentum spectrum diverges as $p_T \to 0$. For moderate p_T, the leading log sum (3.76) exhibits the usual $1/p_T^2$ behavior found at $O(\alpha_s)$, but for $p_T \lesssim (p_T)_{peak}$, where

$$(p_T^2)_{peak} \simeq \frac{s}{2} \exp[-3\pi/4\alpha_s]$$
$$\simeq \frac{s}{2} \left(\frac{\Lambda^2}{s}\right)^{25/16}, \tag{3.84}$$

radiation damping occurs, and the spectrum goes rapidly to zero. This is all very jolly; however, just as in the case of $\gamma^* \to q\bar{q}(GG\ldots)$, the leading log perturbative methods used to derive eq. (3.76) become entirely invalid at such small p_T, where subleading log perturbative contributions and non-perturbative hadronic effects undoubtedly dominate. The behavior of the hadroproduced γ^* p_T spectrum at small p_T implied by eq. (3.76) is, in fact, probably even less to be believed than the corresponding result in e^+e^- annihilation. In the above discussion, we have tacitly assumed that any transverse momentum carried by the γ^* must be a result of gluon emissions by the annihilating $q\bar{q}$. This would presumably be the case if the p_T were measured with respect to q and $\bar{q}$ which had propagated from infinity to the interaction. However, as discussed in Sec. 2.7, the incoming colored q and $\bar{q}$ must inevitably carry with them a cloud of gluons whose transverse momenta are determined by the size of the hadron state which was, in reality, the true incoming wavepacket. In perturbation theory, it is approximated by an incoming jet of limited transverse momentum $\sim 1/r_h^2 \sim \Lambda^2$. It is with respect to this composite system which represents the incident hadron that the γ^* transverse momentum must be measured. The resulting p_T will differ from that measured with respect to the quark direction by the deviation of the quark momentum from the total momentum of its accompanying jet. This deviation will typically be of order the transverse momentum spread of the incoming jet which is very roughly $\sim \Lambda^2$. The prediction (3.76) of the γ^* p_T spectrum with respect to the incoming quark direction must,

therefore, be smeared by this 'primordial transverse momentum' before it can be compared with experimental results obtained with incident hadrons rather than quarks. As a perturbative approximation, this smearing can be viewed as the result of including not only diagrams in which the incoming q, $\bar{q}$ emit gluons but also in which they absorb gluons from the initial jet and are thereby deflected through angles determined by the spread of the jet. From this aspect, the role of the initial jet may be viewed as follows. Consider calculating not the probability that the γ^* should be produced with some definite p_T, but rather finding the integrated probability for production with a p_T less than q_T. This is analogous to obtaining $\mathcal{F}_B(\theta)$ rather than $\langle F_2^{pt}(\chi)\rangle$ in the e^+e^- annihilation case. In calculating $\mathcal{F}_B(\theta)$, we simply subtracted from one the integral of $\langle F_2^{pt}(\chi)\rangle$ from $\chi = \cos\theta$ to $\chi = 0$. Here, however, it is convenient to discuss direct evaluation of the integral of the p_T spectrum from $p_T = 0$ to $p_T = q_T$. In any order of perturbation theory, the contribution to this integral from gluon emissions by the q, $\bar{q}$ will diverge like $[\alpha_s \log^2(q_T^2/\mu^2)]^k$ where μ is some infrared regularization parameter (e.g., gluon mass). However, the integral also receives a contribution from $\delta(p_T^2)$ terms arising from loop corrections to $q\bar{q} \to \gamma^*$. These corrections give simply the quark electromagnetic (Sudakov) form factor whose leading terms are of order $[\alpha_s \log^2(\hat{s}/\mu^2)]^k$. Adding this contribution, the double logs in the integral of the p_T spectrum are rendered finite and are of order $[\alpha_s \log^2(q_T^2/\hat{s})]^k$. However, the addition of the processes $q\bar{q} \to \gamma^*(GG\ldots)$ and $q\bar{q} \to \gamma^*$ (loop corrections) serves only to cancel the $\log^2(\mu^2)$ terms at each order; $\log(\mu^2/(q_T^2,s))$ terms still remain uncanceled. (In contrast, in $\gamma^* \to q\bar{q}(GG\ldots)$ + loop corrections, no $\log(\mu^2)$ terms appear.) The existence of such (collinear) divergences is a consequence of the presence of colored particles in the initial state. They are canceled by the inclusion of processes in which the quark absorbs a gluon from the

initial jet; the logarithms are then tamed to the form $\log(k_T^2/(q_T^2,s))$ where k_T is the spread associated with the initial jet. Hence, in perturbation theory, the effects of 'primordial transverse momentum' (the spread of the initial jet) are at least formally of subleading order relative to the terms in eq. (3.76) for the p_T spectrum. Nevertheless, any discussion based on perturbation theory is entirely inadequate at very small p_T, as discussed above.

Above, we have considered the process $q\bar{q} \to \gamma^*(GG\ldots)$ which, for our leading log purposes, is essentially a simple crossing of the case $\gamma^* \to q\bar{q}(GG\ldots)$ discussed at length in previous sections. In the same vein, we may use our results (3.42), etc., on $\chi \to GG(GG\ldots)$ (where χ is a spin 0 $Q\bar{Q}$ bound state) to estimate the transverse momenta of χ produced in hadron-hadron collisions through $GG \to \chi(GG\ldots)$. Since a large fraction of the ζ (ψ, Υ, ...) produced in hadron interactions presumably arises from the decay $\chi \to \zeta\gamma$ of the χ produced, the ζ transverse momenta should reflect those of the χ. Comparison of eq. (3.42) with (3.76) suggests that the transverse momentum distributions of hadroproduced ζ should be broader than those of direct γ^* by roughly a factor 9/4. The qualitative support of this result from dimuon production data is again encouraging.

The methods applied here to the Drell-Yan process may also be used in other cases of experimental relevance. Their results for deep inelastic lepton-hadron scattering will be discussed in Ref. [6] [F3.17]; here we consider very briefly the case of hadron-hadron collisions involving large transverse momenta. The most convenient observables for this process are probably the C_ℓ, defined by [2]

$$C_\ell = \left|\sum_i \frac{(p_T)_i}{\sqrt{s}} e^{i\ell\phi_i}\right|^2 = \sum_{i,j} \frac{(p_T)_i (p_T)_j}{s} \cos[\ell(\phi_i - \phi_j)]. \qquad (3.85)$$

To lowest order, a 2 → 2 subprocess (e.g., $qq \to qq$) gives $\langle C_{2\ell}/C_o\rangle = 1$, $\langle C_{2\ell-1}/C_o\rangle = 0$. In this case, $C_o = (2p_T/\sqrt{s})^2 = x_T^2$. For large ℓ, the effects of higher orders may be estimated by a leading log approximation. In the leading log approximation, emissions from the incoming partons will have small p_T and will, therefore, not contribute to $\langle C_\ell\rangle$. The dominant corrections to the $\langle C_\ell\rangle$ will thus come from deflections of the final high-p_T partons by emissions. We make the rough approximation that any parton deflected by an angle $\gtrsim 1/\ell$ does not contribute to $\langle C_\ell\rangle$. Then the $\langle C_\ell/C_o\rangle$ are given by formulae analogous to these derived for the $\langle H_\ell\rangle$ in Sec. 3.5. To $O(\alpha_s)$ we find, for example,

$$\begin{aligned} \langle C_{2\ell}/C_o\rangle &\simeq 1 - \frac{4\alpha_s}{3\pi}\log^2\ell \qquad (qq \to qq(G)) \\ \langle C_{2\ell}/C_o\rangle &\simeq 1 - \frac{3\alpha_s}{\pi}\log^2\ell \qquad (GG \to GG(G)). \end{aligned} \qquad (3.86)$$

Since gluon distributions tend to be softer than quark ones, the second behavior should be prominent at small C_o (x_T) while the first result should dominate at large C_o (x_T). Of course, the results (3.86) may be summed to all orders in α_s and will exponentiate as described for the $\langle H_\ell\rangle$ in Sec. 3.5.

3.9 Real Photon Production in e^+e^- Annihilation

Photon production in e^+e^- annihilation events provides another test of their structure. By measuring suitable observables, one can probe photons which were emitted by quarks at early times before hadronization has smeared their energies. The angular correlation between two final photons would be a particularly clean measure of the angular distribution of the partons at early times, but it is probably inaccessible experimentally. Instead, let us consider complete final states consisting of hadrons and a single identified

photon of momentum k. Defining $z = 2|\vec{k}|/\sqrt{s}$, we require z to be sufficiently large that the photon is constrained to be a relic of early times [F3.18] and not to have been generated in the hadronization process (e.g., by $\pi^0 \to \gamma\gamma$). We consider the angular distribution of energy in events with respect to the photon direction using the observables:

$$\frac{d\Gamma_\ell}{dz} = \sum_i \frac{|\vec{p}_i|}{\sqrt{s}} P_\ell(\hat{p}_i \cdot \hat{k}), \tag{3.87}$$

where the sum runs over all hadrons in the event. Then $d\Gamma_0/dz = (2-z)$ so that the distribution of events in Γ_0 gives simply the photon energy spectrum. This suffers collinear divergences wherever the photon direction comes close to one of the quark directions, which would usually be canceled by final states containing no photons. However, as usual, one may extract this divergent (leading log) term and then compare results obtained at two different values of s, so that the infrared divergences factorize off between them. This procedure has been used to predict the leading log s dependence of the photon energy spectrum ('quark fragmentation function into photons') [34, 35]. Here, we consider the infrared finite observables $d(\Gamma_{\ell_1} - \Gamma_{\ell_0})/dz$, where ℓ_1 and ℓ_0 are relatively even. By performing this subtraction, we explicitly remove the contribution of the collinear region by weighting it with zero so that we obtain a definite finite result at each value of s, rather than having to compare two values of s. The procedure of subtracting two Γ_ℓ removes $O(\alpha)$ QED infrared divergences; QCD infrared divergences cancel just as in the total cross-section. Similarly to the purely hadronic observables H_ℓ and B_ℓ, the mean values and distributions in $d\Gamma_\ell/dz$ may be calculated. We find, for example

$$\left\langle \frac{d(\Gamma_2 - \Gamma_0)}{dz} \right\rangle \simeq \frac{3\alpha}{\pi} \frac{\sum e_i^4}{\sum e_i^2} \frac{(1-z)(2-z)}{z^2} [(z-2)\log(1-z) - z], \tag{3.88}$$

where the e_i are the charges of quarks with masses much less than $\sqrt{s}$, and we have normalized the mean with the total hadronic e^+e^- annihilation rate. Other interesting observables available using real photons in the final state include ones sensitive to angular correlations between the beam direction and the outgoing γ.

	Feynman	$n=q$	$n=q$ (including n^2 term)	$n=p_1$	$n=q-p_1/x_1$	$n=q-p_3/x_3$
D_{11}	$\frac{2(1-x_1)}{(1-x_2)}$	$\frac{2(1+x_1^2)}{(1-x_1)(1-x_2)}$ $- 4/(1-x_1)x_3$	$\frac{2(1+x_1^2)}{(1-x_2)} - \frac{4}{x_3}$ $+ 2(1-x_1)$	$\frac{2(1-x_1)}{(1-x_2)}$	$\frac{2(1+x_1^2)}{(1-x_1)(1-x_2)}$	$\frac{2(1+x_1^2)}{(1-x_1)(1-x_2)} + \frac{4[x_1(1-x_3)-1]}{(1-x_1)x_3^2}$
D_{22}	$\frac{2(1-x_2)}{(1-x_1)}$	$\frac{2(1+x_2^2)}{(1-x_1)(1-x_2)}$ $- 4/(1-x_2)x_3$	$\frac{2(1+x_2^2)}{(1-x_1)} - \frac{4}{x_3}$ $+ 2(1-x_2)$	$\frac{2[x_1^2+(1-x_3)^2]}{(1-x_1)(1-x_2)}$	$\frac{2(1-x_2)}{(1-x_1)}$	$\frac{2(1+x_2^2)}{(1-x_1)(1-x_2)} + \frac{4[x_2(1-x_3)-1]}{(1-x_2)x_3^2}$
D_{12}	$\frac{4(1-x_3)}{(1-x_1)(1-x_2)}$	0	$\frac{8(1-x_3)}{x_3^2}$	$\frac{4(1-x_3)}{(1-x_2)}$	$\frac{-4}{1-x_1}$	$\frac{8(1-x_3)}{x_3^2}$

Table 3.1: Partial cross-sections for the process $e^+e^- \to q\bar{q}G$ in Feynman gauge and in various axial gauges specified by the vector n. $x_i = 2E_i/\sqrt{s}$, where $i = 1, 2, 3$ correspond to q, $\bar{q}$, G.

Section 3 - Footnotes

F3.1 Note that the form depends critically on the method of infrared regularization. If, instead of retaining a finite gluon mass, we had kept the quark off shell by an amount $\sqrt{\gamma s}$, then the kinematic limits change, and roughly β is replaced by $\sqrt{\gamma}$ so that the form of (3.9) is modified, becoming [19]

$$C_{-1} \simeq \frac{2\alpha_s}{3\pi}\,[-\,2\log^2\gamma - 3\log\gamma + 8\zeta(2) - 1].$$

For on-shell fermions of mass $\sqrt{\gamma s}$, a finite β must be retained to regularize soft divergences and [11]

$$C_{-1} \simeq \frac{2\alpha_s}{3\pi}\,[-\,\log^2\gamma - 4\log\beta\log\gamma - 4\log\gamma + 8\zeta(2) - 5/2].$$

Double logarithmic terms like (3.9) may be summed to all orders in α_s to obtain a leading log estimate for the quark form factor. The estimate will be dual (as by the usual inclusive-exclusive correction) to results for quark fragmentation functions close to $x = 1$. The dependence of the form factor on the infrared regularization procedure will be manifest in the various ways in which the limit $x \to 1$ is taken for the fragmentation function.

F3.2 In addition to the direct gauge constraint $n.\epsilon = 0$, the equations of motion for the gluon (or photon) field introduce the further constraint $\partial_n(k.\epsilon) = 0$ which may be satisfied by taking $k.\epsilon = 0$. Feynman gauge corresponds to integrating over all possible values of $k.\epsilon$.

F3.3 Note, however, that for genuine scalar gluons, the collinear singularities are damped. Here D_{11} gives $(1-x_1)/(1-x_2)$, D_{22} $(1-x_2)/(1-x_1)$ and D_{12} 2, yielding a total of $x_3^2/(1-x_1)(1-x_2)$ which exhibits no double-logarithmic ('soft and collinear') singularity as $x_1, x_2 \to 1$.

F3.4 This form was recently conjectured in Ref. [23] on the basis of an explicit $O(\alpha_s^2)$ calculation.

F3.5 One contribution to these subleading log terms comes from the 'two-loop anomalous dimensions', and is process independent. The process-dependent part comes from a product of 'constant (non-logarithmic) terms' with leading log iterations.

F3.6 Such a form factor is not directly amenable to measurement. One may roughly consider it to give corrections to dimensional-counting results for the pion form factor. However, in this case, one should not only include virtual gluon exchanges but also real gluon emission up to transverse momenta which may no longer be supported in the pion wave-function, leading to a single log at each order in α_s. In fact, in all exclusive processes involving hadrons, an infrared cutoff p^2 is presumably provided by the size of the hadrons; real emissions at transverse momenta up to this cut-off should, therefore, be included.

F3.7 For the massive QED of relevance to muon decay, all subleading logs (which must here come from soft, rather than collinear, divergences) also exponentiate and are presumably unimportant close to the kinematic boundary.

F3.8 This is defined to couple directly only to the q and $\bar{q}$, in contrast to the scalar source χ, which couples only to GG. The relevant differential cross-section is then simply

$$\frac{d\sigma}{dx_1 dx_2} = \frac{\alpha_s}{3\pi}\left[\frac{x_1^2 + x_2^2}{(1-x_1)(1-x_2)} + 2\right].$$

F3.9 The definition of $\mathcal{E}_F(\theta)$ for a single jet must be made carefully. We take the corresponding energy correlation function to be

$$(F_2^{pt}(\chi))_J = \sum_{i,j} \frac{E_i E_j}{E_J^2}\,\delta(\chi - \cos\phi_{ij}),$$

where i and j are particles in the same jet J of energy E_J. This definition differs from our usual definition (1.2) of $F_2^{pt}(\chi)$, which contains an extra factor of 2, and is thus normalized to 2 rather than 1 when integrated over χ from -1 to +1. We take the single jet $\mathcal{E}_F(\theta)_i$ to be the integral of $(F_2^{pt}(\chi))_J$ from $\chi = 1$ to $\chi = \cos(\theta)$. This must be summed over the number of jets and weighted by $2E_{jet}^2/s$ to obtain the complete $\mathcal{E}_F(\theta)$ (from which the $\langle H_\ell \rangle$ will be derived) for an n-jet event.

F3.10 This requires use of the quark number conservation (Adler) sum rule: $\int_0^1 (P_{qq}(z) + P_{Gq}(z))dz = 1$, together with the corresponding sum rule for gluons $2\int_{1/2}^1 (P_{GG}(z) + P_{qG}(z))dz = 1$. (One could integrate here from 0 to 1 using suitable kernels regularized at z = 0 as well as z = 1).

F3.11 To prove this result directly from eq. (3.51), let Q be the matrix that diagonalizes the matrix A of n = 3 anomalous dimensions: $Q^{-1}AQ = D$. Integrating (3.51), one finds that $\mathcal{E}_F(\theta \sim 1)$ is $-2VQD^{-1}Q^{-1} = -2VA^{-1}$ so that the result required becomes

$$\begin{pmatrix} V_{q\to\chi} \\ V_{G\to\chi} \end{pmatrix} = \frac{1}{2}\begin{pmatrix} A_2^{qq} - A_3^{qq} + A_2^{Gq} - A_3^{Gq} \\ A_2^{GG} - A_3^{GG} + A_2^{qG} - A_3^{qG} \end{pmatrix}$$

$$= -\frac{1}{2}\begin{pmatrix} A_3^{qq} + A_3^{Gq} \\ A_3^{GG} + A_3^{qG} \end{pmatrix} = -\frac{1}{2}\begin{pmatrix} A_3^{qq} & A_3^{Gq} \\ A_3^{qG} & A_3^{GG} \end{pmatrix}\begin{pmatrix} 1 \\ 1 \end{pmatrix}$$

F3.12 Extreme care must be exercised in the derivation of this result; in most parts of the calculation, the regularizer $\beta = \mu^2/s$ must be retained until the very end. The contribution of the q, $\bar{q}$ term in $\langle F_2^{pt}(\chi)\rangle$ is, however, quite simple since it exhibits no divergence as $\chi \to 1$. For this term, one may explicitly integrate the $\langle F_2^{pt}(\chi)\rangle_{q\bar{q}}$ obtained after setting β to 0 from η to 1. One finds at $\eta = 0$

$$I_{q\bar{q}}(0) = 1 + \frac{2\alpha_s}{3\pi}\,[269+9\zeta(2)-408\log(2)] \simeq 0.074\,\alpha_s .$$

The integral of $\langle F_2^{pt}(\chi)\rangle$ up to $\chi = 1$ for the $\overset{(-)}{q}G$ terms exhibits a logarithmic divergence which must be canceled against the one appearing in C_{+1} (the coefficient of $\delta(1-\chi)$ in $\langle F_2^{pt}(\chi)\rangle$ at $O(\alpha_s)$ given in eq. (3.7)). In intermediate stages, the integral must be regularized by retaining all terms proportional to β. Usually this leads to entirely intractable integrals. However, it is possible to compute $I_{qG}(0)$ directly by integrating $x_1x_3\, d\sigma/dx_1dx_3$ for $e^+e^- \to q\bar{q}G$ over the region $1 - x_1 - \beta/(1-x_1) \le x_3 \le 2(1+\beta-x_1)/(2-x_1)$, $0 \le x_1 \le 1 - \sqrt{\beta}$. (The apparently $O(\beta)$ terms in $d\sigma/dx_1dx_3$ give $O(1)$ contributions by virtue of end-point singularities.) This is then added to C_{+1} to obtain the complete $I_{qG}(0)$. Then, having set β to zero, one may evaluate the integral of $\langle F_2^{pt}(\chi)\rangle$ from $\chi = 0$ to $\chi = \eta$. It is in this last step that dilogarithm functions are introduced. Note that the mass corrections to $I(\eta)$ appear always to be $O(\beta)$.

F3.13 In Ref. [2] we used the prescription for treating fragmentation and independent (leading log) jet evolution advocated in Sec. 2.1. We defined the time or resolution which delineated two or three jet events by making a cut on the H_2 of the partons. The partons which existed at the time corresponding to the cut were then taken to form hadrons according to a phenomenological model which accounts both for the hadronic effects and for some perturbative

QCD effects. The model does not, however, treat correctly the violations of scaling associated with these; in fact, as discussed in Sec. 2.1, some non-scaling component, reflecting the results given in Fig. 3.7, must be added. A simple phenomenological improvement [30] of the Field-Feynman model is to use an energy dependent transverse momentum distribution adjusted to give a $\langle\phi\rangle_E$ which includes estimated perturbative QCD effects.

F3.14 If we consider the cross-section also as a function of the c.m. rapidity y of the γ^*, then the argument of the log becomes $(p_T^2/[s(1+\tau-2\sqrt{\tau}\cosh y)])$. The rapidity clearly does not enter the leading log estimate (3.76) which, therefore, suggests that, as observed, the γ^* p_T spectrum should be roughly independent of rapidity, at least away from the boundaries of phase space, where the leading log approximation fails.

F3.15 This form has also been obtained in Ref. [33] where it is viewed as an eikonal approximation. It differs in leading log order at $O(\alpha_s^2)$ from the results of Ref. [20]. We do not understand the phase space boundaries used in [20].

F3.16 An analogous condition exists for the validity of leading single log results (e.g., $\langle F_2^{pt}(\chi)\rangle$ near $\chi = +1$ as discussed in Sec. 3.7): $\alpha_s^{k-1}\omega^{k-2}/[\alpha_s]^\gamma \lesssim f$ (γ is the relevant anomalous dimension) so that, as usual, $\alpha_s\log(\frac{s}{p_T^2}) \lesssim 1$ in this case.

F3.17 One might imagine that our analysis could be applied directly to $\sigma_L/\sigma_T \simeq 4k_T^2/Q^2$ in deep inelastic scattering. However, integrating a suitable double log form like eq. (3.76) over p_T with this weight function reduces it to a single log form which must be handled by other techniques (renormalization group methods analogous to those in Sec. 3.6).

F3.18 It is also prudent to consider photons at large angles to the incoming beam direction so as to avoid background processes in which the photon is emitted by the initial e^+, e^- rather than from the final state [34].

Section 3 - Figure Captions

3.1 The schematic form of part of an $e^+e^- \to q\bar{q}(GG...)$ event showing some kinematic definitions.

3.2 Forms for the energy correlation functions $\langle F_2^{pt}(\chi = \cos\theta)\rangle$ in $e^+e^- \to q\bar{q}(GG...)$ events found explicitly at $O(\alpha_s)$ and summed to all orders in α_s in the leading log approximation. The leading log results for the region $\theta \approx 180°$ are discussed in Sec. 3.5 while those at $\theta \approx 0°$ are derived in Sec. 3.6. The cross-hatched barrier represents the angles beyond which perturbative methods should definitely fail. Note the proximity of the $O(\alpha_s)$ and summed leading log results for $\alpha_s(s) = 0.2$; they are still closer for smaller α_s. The smallness of the leading log form around $\theta \approx 90°$ suggests that in this region, the $O(\alpha_s)$ result should be accurate. Beyond the order shown here, $\langle F_2^{pt}(\chi)\rangle$ will develop δ functions at all values of χ, whose effects cancel in suitable integrals of $\langle F_2^{pt}(\chi)\rangle$ over χ.

3.3 The $O(\alpha_s)$ and summed leading log results for the $\langle H_\ell\rangle$ at large ℓ in the processes $e^+e^- \to q\bar{q}(GG...)$ and $\zeta \to GGG(GG...)$. (For $\zeta \to GGG(GG...)$ only the leading log part of the $O(\alpha_s)$ term is known.) Beyond the cross-hatched barriers, our perturbative results will be completely invalidated by hadronic effects.

3.4 $\langle H_\ell\rangle$ as a function of α_s for the process $e^+e^- \to q\bar{q}(GG..)$ with the notation of Fig. 3.3.

3.5 The ratios of various approximate results for the mean square energy into a cone of full angle θ ($\mathcal{E}_F(\theta)$) around quark and gluon jets.

3.6 The mean square energy into a cone of full angle θ around quark and gluon jets, using various approximations.

3.7 The mean and r.m.s. energy-weighted angle $\langle\phi\rangle_E$ for quark and gluon jets as a function of the total jet energy. The angular cut for the dashed curves is taken to be at twice the mean angle of hadrons produced according to the Field-Feynman phenomenological jet fragmentation model [31].

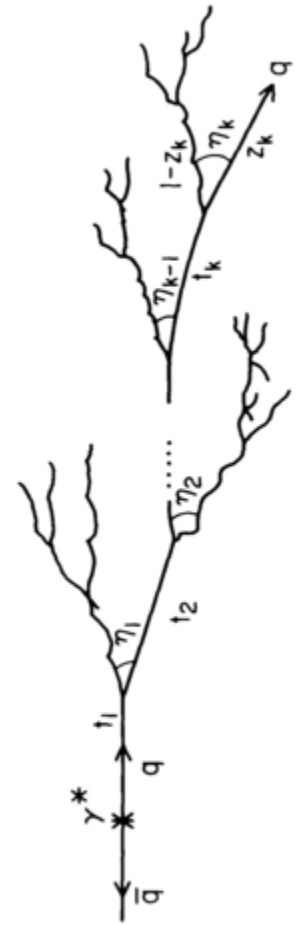

Fig. 3.1

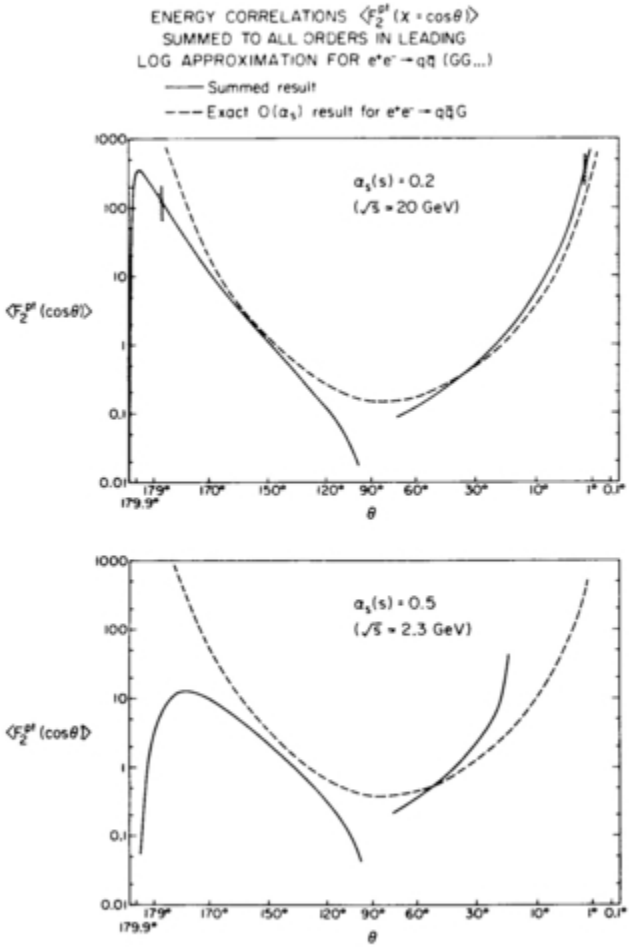
ENERGY CORRELATIONS $\langle F_2^{gf}(x = \cos\theta)\rangle$
SUMMED TO ALL ORDERS IN LEADING
LOG APPROXIMATION FOR $e^+e^- \to q\bar{q}$ (GG...)
Summed result
Exact $O(\alpha_s)$ result for $e^+e^- \to q\bar{q}G$
$\alpha_s(s) = 0.2$
($\sqrt{s} = 20$ GeV)
$\langle F_2^{gf}(\cos\theta)\rangle$
θ
$\alpha_s(s) = 0.5$
($\sqrt{s} = 2.3$ GeV)
$\langle F_2^{gf}(\cos\theta)\rangle$
θ

Fig. 3.2

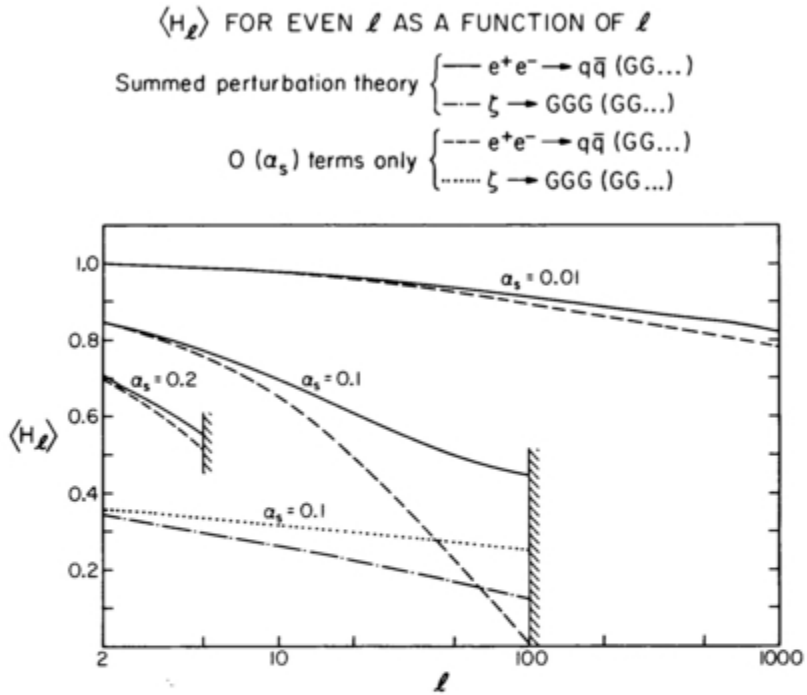
$\langle H_\ell \rangle$ FOR EVEN ℓ AS A FUNCTION OF ℓ
Summed perturbation theory
$e^+e^- \to q\bar{q}$ (GG...)
$\zeta \to$ GGG (GG...)
O (α_s) terms only
$e^+e^- \to q\bar{q}$ (GG...)
$\zeta \to$ GGG (GG...)
$\alpha_s = 0.01$
$\alpha_s = 0.2$
$\alpha_s = 0.1$
$\alpha_s = 0.1$
$\langle H_\ell \rangle$
ℓ

Fig. 3.3

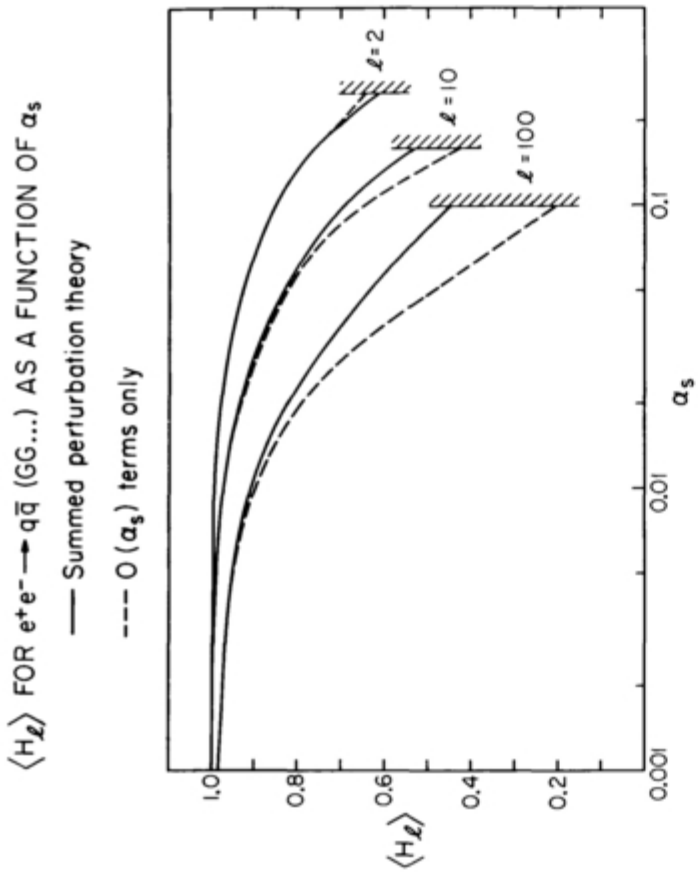
⟨H_ℓ⟩ FOR e⁺e⁻ → qq̄ (GG...) AS A FUNCTION OF α_s
— Summed perturbation theory
--- O (α_s) terms only
ℓ = 2
ℓ = 10
ℓ = 100
1.0
0.8
0.6
0.4
0.2
⟨H_ℓ⟩
0.001
0.01
0.1
α_s

Fig. 3.4

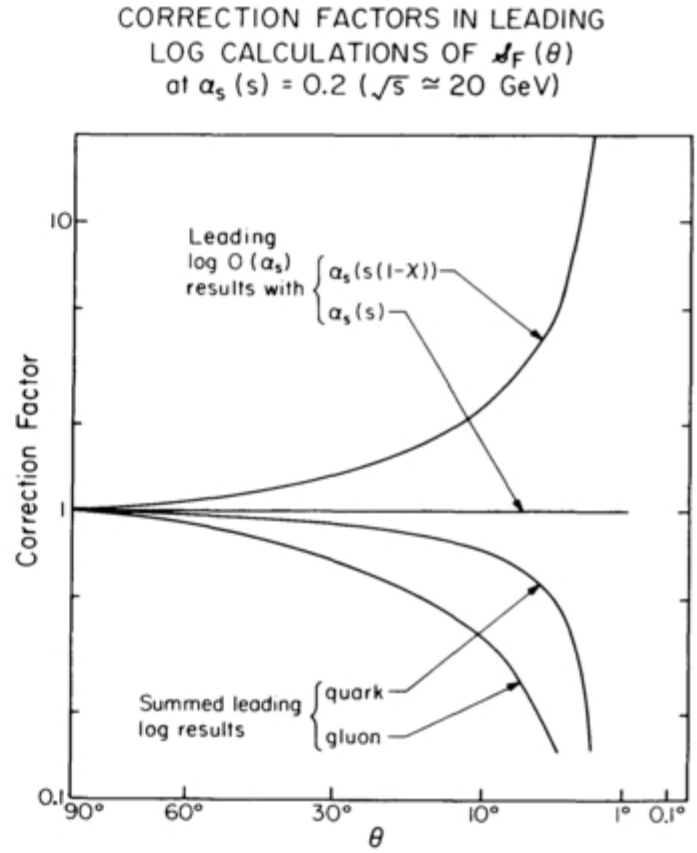
CORRECTION FACTORS IN LEADING
LOG CALCULATIONS OF 𝒟_F (θ)
at α_s (s) = 0.2 (√s ≃ 20 GeV)
Correction Factor
10
1
0.1
Leading
log O (α_s)
results with
α_s(s(1-X))
α_s(s)
Summed leading
log results
quark
gluon
90°
60°
30°
10°
1°
0.1°
θ

Fig. 3.5

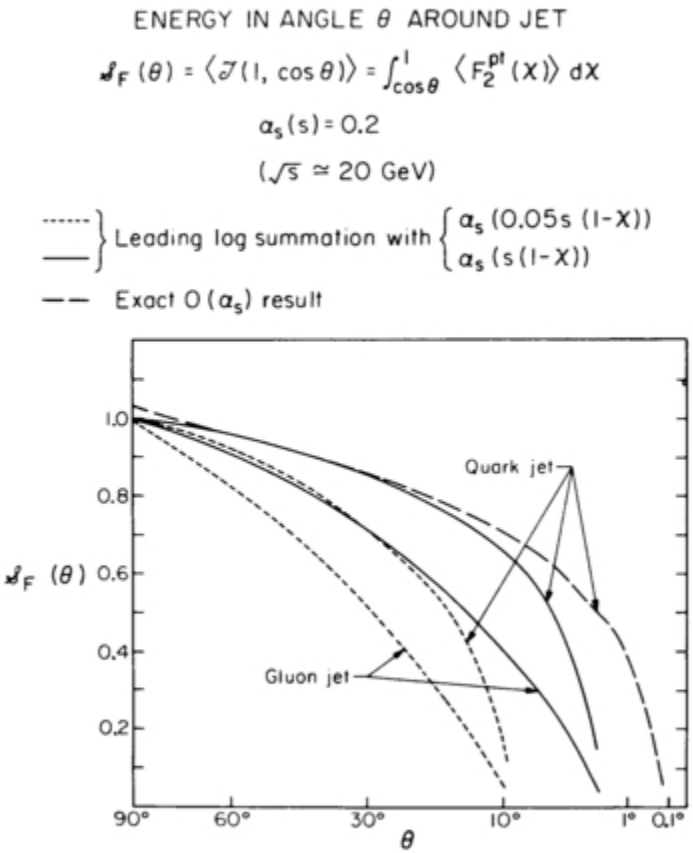
ENERGY IN ANGLE θ AROUND JET
$\mathcal{J}_F(\theta) = \langle \mathcal{J}(1, \cos\theta) \rangle = \int_{\cos\theta}^{1} \langle F_2^{pt}(X) \rangle \, dX$
$\alpha_s(s) = 0.2$
$(\sqrt{s} \simeq 20$ GeV)
Leading log summation with $\alpha_s(0.05s(1-X))$, $\alpha_s(s(1-X))$
Exact $O(\alpha_s)$ result
Quark jet
Gluon jet
$\mathcal{J}_F(\theta)$
1.0
0.8
0.6
0.4
0.2
90°
60°
30°
10°
1°
0.1°
θ

Fig. 3.6

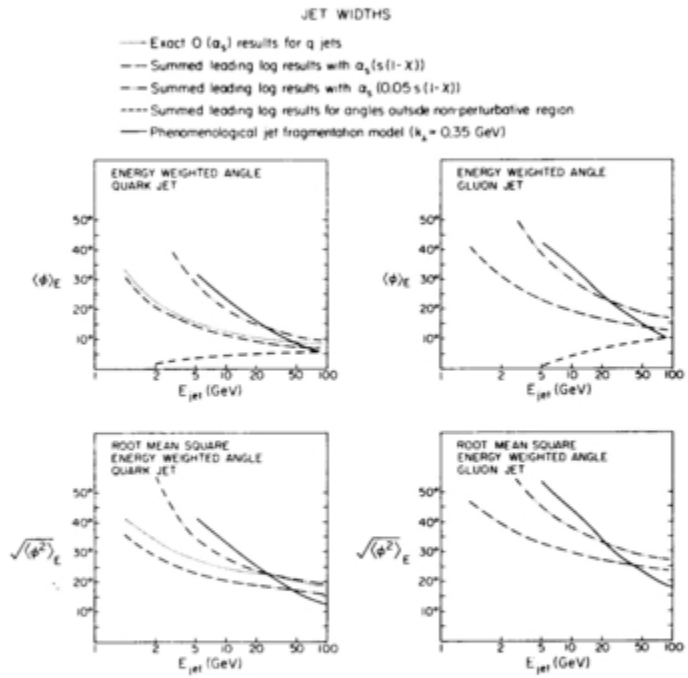
JET WIDTHS
Exact $O(\alpha_s)$ results for q jets
Summed leading log results with $\alpha_s(s(1-X))$
Summed leading log results with $\alpha_s(0.05s(1-X))$
Summed leading log results for angles outside non-perturbative region
Phenomenological jet fragmentation model ($k_\perp$ = 0.35 GeV)
ENERGY WEIGHTED ANGLE QUARK JET
ENERGY WEIGHTED ANGLE GLUON JET
ROOT MEAN SQUARE ENERGY WEIGHTED ANGLE QUARK JET
ROOT MEAN SQUARE ENERGY WEIGHTED ANGLE GLUON JET
$\langle\phi\rangle_E$
$\sqrt{\langle\phi^2\rangle_E}$
E_{jet} (GeV)

Fig. 3.7

4. Rotationally-Averaged Two-Detector Energy Correlations

4.1 Formalism and Calculational Techniques

In this section we discuss the rotationally invariant observable F_2 defined in eq. (1.2) [36]. The two detectors used in this definition occupy areas $\sigma_i (i = 1,2)$ which are, in general, of arbitrary shape. However for simplicity, we shall restrict ourselves in this paper to the case in which the σ_i are congruent circular patches of angular radius $\cos^{-1}(\delta)$. Hence $|\sigma_i| = 2\pi(1-\delta)$ and F_2 is a function only of χ and δ, where $\cos^{-1}(\chi)$ is the angle between the centers of the two detectors σ_i. The arrangement is illustrated in Fig. 4.1. The generalization of our treatment to detectors of arbitrary shape is straightforward. The best method of calculating F_2 from events appears to be the use of the formula

$$F_2(\chi;\delta) = 2 \sum_{i,j} \frac{|\vec{p}_i||\vec{p}_j|}{s} U(\chi;\delta;\cos\phi_{ij}) \tag{4.1}$$

where the sums on i and j run over all the particles in the event (including the case i = j). The smearing function U is given by

$$U(\chi;\delta;\cos\phi_{ij}) = \frac{1}{|\sigma_1||\sigma_2|} \int d\hat{\Omega}_{d1} \Theta(\hat{n}_{d1},\hat{n}_{pi};\hat{n}_{d2},\hat{n}_{pj};\delta). \tag{4.2}$$

Here $\hat{n}_{dk}$ is a unit vector in the direction of detector k and $\hat{n}_{pi}$ the unit vector in the direction of particle i. If $\hat{\Omega}_{d1}$ runs over all elements of the rotation group, so that $\int d\hat{\Omega}_{d1} = 8\pi^2$, then

$$\begin{aligned} \hat{n}_{d1} &= \hat{\Omega}_{d1}\hat{z} \\ \hat{n}_{d2} &= \hat{\Omega}_{d1}\hat{R}(\chi)\hat{z} \end{aligned} \tag{4.3}$$

where $\hat{z}$ is a unit vector in the z direction and $R(\chi)$ a rotation through $\cos^{-1}(\chi)$ about the y axis. Finally in (4.2), the function Θ takes on the values 1 or 0, and is zero unless both the pairs $\hat{n}_{d1}$, $\hat{n}_{pi}$ and $\hat{n}_{d2}$, $\hat{n}_{pj}$ lie within an angle $\cos^{-1}(\delta)$ of each other, so that particle i is incident on detector 1 and particle j on detector 2. The rotational invariance of F_2 is exhibited by the fact that it has the same value for any choice of particle directions $\hat{n}_{pi}$, $\hat{n}_{pj}$ so long as the angle ϕ_{ij} between them remains fixed. For some purposes, it is more convenient to write U in the symmetrical form

$$\begin{aligned} U(\chi;\delta;\cos\phi_{ij}) = \frac{1}{8\pi^2|\sigma_1||\sigma_2|} \int d\hat{\Omega}_{d1} d\hat{\Omega}_{pi} \\ \Theta(\hat{\Omega}_{d1}\hat{z},\hat{\Omega}_{pi}\hat{z};\hat{\Omega}_{d1}\hat{R}(\chi)\hat{z},\hat{\Omega}_{pi}\hat{R}(\cos\phi_{ij})\hat{z};\delta). \end{aligned} \tag{4.4}$$

Note that

$$\int_{-1}^{+1} U(\chi;\delta;\cos\phi_{ij})d\chi = 2 \tag{4.5}$$

which implies the same normalization for F_2:

$$\int_{-1}^{+1} F_2(\chi;\delta)d\chi = 2, \tag{4.6}$$

independent of the value of δ.

In the limit $\delta \to 1$, σ_1 and σ_2 become point detectors separated by an angle $\cos^{-1}(\chi)$. We define [F4.1]

$$F_2^{pt}(\chi) \equiv \lim_{\delta\to 1}[F_2(\chi;\delta)]. \tag{4.7}$$

In this case, U becomes simply

$$U(\chi;1;\cos\phi_{ij}) = \delta(\chi-\cos\phi_{ij}), \tag{4.8}$$

and we may rewrite

$$F_2^{pt}(\chi) = 2\sum_{i,j}\frac{|\vec{p}_i||\vec{p}_j|}{s}\,\delta(\chi-\cos\phi_{ij}) \tag{4.9}$$

and

$$F_2(\chi;\delta) = \int_{-1}^{+1} d\chi' F_2^{pt}(\chi')\,U(\chi;\delta;\chi'). \tag{4.10}$$

F_2 may be expressed in terms of the H_ℓ, defined in eq. (1.1) as

$$\begin{aligned} H_\ell &\equiv \left(\frac{4\pi}{2\ell+1}\right)\sum_{m=-\ell}^{+\ell}\left|\sum_i Y_\ell^m(\Omega_i)\frac{|\vec{p}_i|}{\sqrt{s}}\right|^2 \\ &= \sum_{i,j}\frac{|\vec{p}_i||\vec{p}_j|}{s}P_\ell(\cos\phi_{ij}) \end{aligned} \tag{4.11}$$

where the indices i and j run over the hadrons which are produced in the event, and ϕ_{ij} is the angle between particles i and j. When the first form for the H_ℓ is used, a particular set of axis must be chosen to evaluate the angles (Ω_i) of the momenta, but the values of the H_ℓ deduced will be independent of the choice. The Legendre expansion of F_2 is

$$F_2(\chi;\delta) = \sum_\ell(2\ell+1)H_\ell(\delta)P_\ell(\chi) \tag{4.12}$$

where the H_ℓ as defined in (4.11) are $H_\ell(1)$, and correspondingly,

$$F_2^{pt}(\chi) = \sum_\ell(2\ell+1)H_\ell P_\ell(\chi). \tag{4.13}$$

The relation between $H_\ell(\delta)$ and H_ℓ is

$$H_\ell(\delta) = \sum_{i,j}\frac{|\vec{p}_i||\vec{p}_j|}{s}\int_{-1}^{+1} d\chi P_\ell(\chi)U(\chi;\delta;\cos\phi_{ij}) \tag{4.14}$$

so that (for circular detectors)

$$H_\ell(\delta) = \frac{I_\ell^2(\delta)}{(1-\delta)^2}H_\ell, \tag{4.15}$$

or equivalently

$$U(\chi;\delta;\cos\phi_{ij}) = \sum_\ell\frac{(2\ell+1)I_\ell^2(\delta)P_\ell(\chi)P_\ell(\cos\phi_{ij})}{2(1-\delta)^2} \tag{4.16}$$

which clearly illustrates the symmetry between χ and $\cos\phi_{ij}$ also visible in (4.4). $I_\ell(x)$ was defined in [2] as

$$I_\ell(x) = \int_x^1 P_\ell(y)dy = \sqrt{1-x^2}\,P_\ell^{-1}(x). \tag{4.17}$$

Note that as $\ell \to \infty$, $H_\ell \sim 1$ but $H_\ell(\delta < 1) \sim 1/\ell^3$. Thus the series (4.12) is always absolutely convergent whereas (4.13) diverges (for point particles).

$F_2(\chi;\delta)$ receives a contribution from events in which the same particle passes through both detectors. Although this is of little practical interest, it must be kept if the normalization condition (4.6) is to be maintained. In the point detector limit, $\delta = 1$, this configuration contributes to $F_2^{pt}(\chi)$ a term

$$F_2^{same}(\chi) = 2 \sum_i \frac{|\vec{p}_i|^2}{s} \delta(1-\chi), \tag{4.18}$$

where the coefficient of the delta function is related to the asymptotic limit of the H_ℓ by

$$\frac{1}{2} \lim_{\ell\to\infty} [H_{2\ell}+H_{2\ell+1}] = \sum_i \frac{|\vec{p}_i|^2}{s}. \tag{4.19}$$

The result (4.18) reveals an important difficulty of $F_2^{pt}(\chi)$. In [2], we argued that for observables to be infrared stable when computed in QCD perturbation theory, they should not discriminate between the various final state configurations for which the differential cross-section is divergent, so that when their mean values are calculated, the divergences will cancel just as in the total cross-section. This is clearly not true for the coefficient of $\delta(1-\chi)$ in $F_2^{same}(\chi)$ with point detectors: since it is not linear in the momenta of collinear particles, configurations containing pairs of nearly collinear particles are weighted differently depending on the partitioning of momentum between them. Hence, the coefficient of $\delta(1-\chi)$ in $F_2^{same}(\chi)$ will be divergent as found at $O(\alpha_s)$ in eq. (3.7). As discussed in Sec. 3.1, this divergence at $O(\alpha_s)$ is canceled by a $1/(1-\chi)$ term in $\langle F_2^{pt}(\chi)\rangle$ away from $\chi = +1$ when $\langle F_2^{pt}(\chi)\rangle$ is integrated over χ with a smooth function, such as the $P_\ell(\chi)$ used to obtain $\langle H_\ell\rangle$. The form of $\langle F_2^{pt}(\chi)\rangle$ calculated from perturbation theory is therefore a generalized function or distribution. Only when integrated over χ with some smooth test function (such as $P_\ell(\chi)$) does it yield physical results. This behavior is familiar [2] from the form of, for example, the q energy spectrum or $1/\sigma\, d\sigma/dH_\ell$ in $e^+e^- \to q\bar{q}(GG\ldots)$. The $\langle F_2^{pt}(\chi)\rangle$ obtained from perturbation theory may be smeared by considering instead the energy correlation $\langle F_2(\chi;\delta)\rangle$ for detectors of non-zero area. $\langle F_2(\chi;\delta)\rangle$ then takes on a definite value at each χ, but, for example, $\langle F_2(1;\delta)\rangle$ diverges like

$\log(1-\delta)$ to $O(\alpha_s)$ as the detector size is taken to zero. The presence of a divergence in $\langle F_2^{pt}(\chi)\rangle$ at some value of χ is a consequence of the fact that the $\langle F_2^{pt}(\chi)\rangle$ there can receive contributions from final states in which, for example, one of the final gluons is soft so that the differential cross-section is divergent. At a given order in α_s, this can occur at any value of χ for which $\langle F_2^{pt}(\chi)\rangle$ is non-zero in lower orders. At $O(\alpha_s)$, $e^+e^- \to q\bar{q}(G)$ gives divergences only at $\chi = \pm 1$, where $\langle F_2^{pt}(\chi)\rangle$ for $e^+e^- \to q\bar{q}$ is non-vanishing. However, at $O(\alpha_s^2)$, $\langle F_2^{pt}(\chi)\rangle$ will exhibit divergences at all values of χ and will have no definite value at a particular χ; it will only be defined when smeared over χ.

In practice, the $\langle F_2^{pt}(\chi)\rangle$ for actual events are finite at all χ. The intrinsic resolution associated with the fragmentation of quarks and gluons into hadrons provides the angular smearing of the perturbative result for $\langle F_2^{pt}(\chi)\rangle$. Unless the size of the hadron detectors is very large, it will be the angular smearing associated with the fragmentation which provides the dominant contribution to the effective $|\sigma_i|$ which determine $F_2(\sigma_1,\sigma_2)$. Since the angular resolution introduced by fragmentation cannot at present be deduced directly from QCD, the strong dependence of $F_2(\sigma_1,\sigma_2)$ on it is undesirable. Nevertheless, if one adopts a phenomenological model for the fragmentation of quarks and gluons into hadrons, then one obtains definite predictions for the distributions of events in F_2, although their violent dependence on parameters discussed in Sec. 4.2 probably renders them worthless in practice. We use the model developed by Field and Feynman [31] to simulate the fragmentation of quarks and gluons into jets of hadrons. Our methods were described in Ref. 2. We investigated there the consequences of various cuts on the hadronic final state and found that the effects of fragmentation were lessened if one used only particles whose momentum was greater than a cutoff value p_c. In

the present paper, we follow this prescription with the choice $p_c = 0.5$ GeV. In addition, we consider only events containing four or more final particles; lower multiplicity events contain little information on the underlying dynamics, and their inclusion often induces spurious effects.

In the next section, we present predictions for $\langle F_2 \rangle$ and $1/\sigma\, d\sigma/dF_2$ for two and three jet events.

We discuss there the processes $e^+e^- \to q\bar{q}$, $e^+e^- \to q\bar{q}G$ and $e^+e^- \to \zeta \to GGG$ in the approximation of free final quarks and gluons and also simulated hadronic events resulting from these subprocesses. In Sec. 4.3 we give $\langle F_2 \rangle$ for various classes of heavy quark and lepton production events; we do not give the distributions $1/\sigma\, d\sigma/dF_2$ for these cases.

4.2 $\langle F_2 \rangle$ and $1/\sigma\, d\sigma/dF_2$ for Two- and Three-Jet Events

In this section we discuss the processes $e^+e^- \to q\bar{q}$, $q\bar{q}(G)$ and $e^+e^- \to \zeta \to GGG$. The final state $q\bar{q}(G)$ represents the $O(g^2)$ QCD prediction for e^+e^- annihilation to free quarks and gluons away from resonances, as discussed in detail in [2]. It consists of a sum of $q\bar{q}$ and $q\bar{q}G$ final states. As described in Ref. [2], there are difficulties in estimating the effects of hadron fragmentation in the $q\bar{q}(G)$ case and we were forced to use a rather ad hoc prescription. However, tests contained in Ref. [2] suggested that our results are not sensitive to this prescription. Our method for calculating the hadron final states from $q\bar{q}(G)$ consists in generating true three-jet events when the $q\bar{q}G$ produced in the subprocess satisfy $H_2 < 0.8$, and two jet events otherwise in such a way as to give the correct total $O(g^2)$ cross-section: $\simeq \sigma_0(1+\alpha_s/\pi)$. The cut on H_2 represents the resolution of the hadron final state to changes in the subprocess final state: the hadrons do not reflect the presence of the extra gluon if its transverse momentum is too small. Note that QCD predicts that the two-jet process $e^+e^- \to q\bar{q}$ should never occur in isolation and

that only the combination $e^+e^- \to q\bar{q}(G)$ should ever be observed away from resonances. QCD suggests that heavy resonances (ζ) produced in e^+e^- annihilation should decay dominantly to GGG.

In Appendix A we give analytical forms for $\langle F_2^{pt}(\chi) \rangle$ for the two and three jet processes discussed above in the free quark and gluon approximation. $\langle F_2(\chi,\delta) \rangle$ may be obtained from these formulae using eq. (4.10). The results are shown as curves marked "free quark and gluon approximation" in Figs. 4.2 and 4.3. These figures also give our estimates for the $\langle F_2 \rangle$ of realistic hadronic events in which the quarks and gluons have fragmented into hadrons [F4.2]. At high enough energy, the effects of this fragmentation (which decreases like $(\Lambda^2/s)^p$) should become negligible. However, even in the energy range $20 \leq \sqrt{s} \leq 40$ GeV of PEP and PETRA, fragmentation cannot be neglected. Figure 4.4 shows in more detail the comparison between $q\bar{q}$ and $q\bar{q}G$ final states at $\sqrt{s} = 20$ GeV.

In Fig. 4.2 we present $\langle F_2(\chi;0.95) \rangle$ for detectors with an angular radius of $\simeq 18°$ ($\delta = 0.95$). Although the modifications to the free quark and gluon predictions are large even at $\sqrt{s} = 40$ GeV, we believe that one can estimate the effects of fragmentation sufficiently well [F4.3] that $\langle F_2(\chi,\delta) \rangle$ can be used to study the underlying production mechanism. In Ref. [2] we also found that the $\langle H_\ell \rangle$ suffered significant changes due to fragmentation. However, the distributions $1/\sigma\, d\sigma/dH_\ell$ of events in the H_ℓ did become close [2] to the free quark and gluon approximation at $\sqrt{s} = 40$ GeV at least for $\ell = 2$ or 3. Later in this section, we shall discuss the distributions of events in $F_2(\chi)$, and show that an extremely high center-of-mass energy is required for fragmentation to become unimportant for these distributions.

In the free quark and gluon approximation, the $\langle F_2(\chi;\delta) \rangle$ for $e^+e^- \to q\bar{q}$ events is symmetrical under $\chi \to -\chi$. Fragmentation destroys this symmetry. Near $\chi = 1$, $\langle F_2(\chi;\delta) \rangle$ probes energy correlations within a single jet, while

near $\chi = -1$, it receives contributions only from pairs of particles in opposite jets. If $\delta = 1$, then $\langle F_2(\chi;\delta)\rangle$ would contain a term proportional to $\delta(1 - \chi)$ arising from events in which the same particle passed through both (point) detectors, but for hadronic events, there would be no corresponding $\delta(1 + \chi)$ term. The most significant breakdown of $\chi \to -\chi$ symmetry in $\langle F_2(\chi;\delta)\rangle$ occurs for the process $e^+e^- \to \zeta \to GGG$, and this may allow the $\langle F_2\rangle$ to be used to isolate events of this type. However, the H_2 [2] and H_1 [3] distributions of events probably provide better discrimination. Momentum conservation requires

$$\langle H_1\rangle = \frac{1}{2}\int_{-1}^{1} \chi\langle F_2^{pt}(\chi)\rangle d\chi = 0, \tag{4.20}$$

but a measure of the asymmetry in $\langle F(\chi)\rangle$ may be obtained by using

$$\langle H_3\rangle = \frac{1}{2}\int_{-1}^{1} P_3(\chi)\langle F_2^{pt}(\chi)\rangle d\chi. \tag{4.21}$$

Figure 4.3 gives a comparison between the $\langle F_2\rangle$ obtained with detectors of size $\delta = 0.95$ (18°) and $\delta = 0.9$ (26°) for simulated hadronic events at $\sqrt{s} = 20$ GeV and in the free quark and gluon approximation. It is clear that these two values of δ give very similar $\langle F_2(\chi;\delta)\rangle$. For $\delta = 0.9$, the effects of fragmentation are slightly less important than for $\delta = 0.95$. This is to be expected since the larger $(1 - \delta)$ is, the more the energy correlation function is smeared, and the less evident are the infrared divergences which appear in its calculation for free quarks and gluons as $\delta \to 1$. The fact that the change shown in Fig. 4.3 between $\delta = 0.95$ and $\delta = 0.9$ is so small indicates that the smearing of the free quark and gluon energy correlation by fragmentation to hadrons occurs over much larger angles than those by which the use

of detectors even with $\delta = 0.9$ would smear. Much smaller values of δ (larger detectors) are necessary to obtain significantly better agreement with the free quark and gluon approximation. When δ becomes very small, however, the smearing is so great that little information on the events remains in F_2. In fact, one must then introduce weight functions into the smearing thereby reducing to a calculation of the $\langle H_\ell\rangle$ [2].

In Figs. 4.5 and 4.6 we present calculations for the distributions $1/\sigma\, d\sigma/dF_2$. These are rather disappointing. In our study of the H_ℓ [2], we found that the distributions $1/\sigma\, d\sigma/dH_\ell$ (at least for $\ell = 2$ and 3) were not seriously affected by hadron fragmentation and provided very distinctive tests of the basic dynamics. In the case of F_2, the free quark and gluon calculations show striking structure (see, for example, the lower right-hand graph in Fig. 4.5); however, hadron fragmentation is a huge effect even for the case $\delta = 0.9$ shown in Fig. 4.6. It is worth remembering here that whereas knowledge of $\langle F_2^{pt}(\chi)\rangle$ (as a function of χ) and $\langle H_\ell\rangle$ (as a function of ℓ) are essentially equivalent, the distributions $1/\sigma\, d\sigma/dF_2$ and $1/\sigma\, d\sigma/dH_\ell$ contain inequivalent information. It appears that the shape information contained in $1/\sigma\, d\sigma/dH_{2,3}$ is less sensitive to hadron fragmentation than that in $1/\sigma\, d\sigma/dF_2$. The figures include the case $\chi = 0$, corresponding to two detectors at right angles. As expected, two-jet events give a distribution in $1/\sigma\, d\sigma/dF_2$ sharply peaked at $F_2(\chi = 0,\delta) = 0$ whereas 3 jet final states give a broader distribution. On comparing $e^+e^- \to \zeta \to GGG$ and $e^+e^- \to q\bar{q}(G)$, one sees that the former gives many more events with large values of $F_2(\chi = 0,\delta)$. This behavior is qualitatively as expected and should be preserved regardless of how one treats the hadron fragmentation. This case of two perpendicular detectors gives perhaps the best intuitive way of distinguishing 2 from 3 jets and is probably the only feature of energy correlation distributions worthy of exploration.

Note that the extreme sensitivity of $1/\sigma\ d\sigma/dF_2$ to fragmentation is to be expected because of the infrared instability of F_2. The inadequacy of $1/\sigma\ d\sigma/dF_2$ compared to $1/\sigma\ d\sigma/dH_{2,3}$ is in strong support of the relevance of the criterion of infra-stability for successful shape parameters.

4.3 Heavy Quark and Lepton Production Events

In [2] we discussed various possible mechanisms for heavy quark (Q) decay. Using approximations which are valid only near the threshold for $Q\bar{Q}$ production, we obtain the $\langle F_2(\chi;0.95)\rangle$ for heavy quark pair production events shown in Fig. 4.7. Assuming that the heavy quarks are contained in mesons $M = Q\bar{q}_s$, where q_s is a light (spectator) quark, we consider the various possible decay mechanisms [2]

$$\begin{aligned} M &\to q'q\bar{q}\bar{q}_s && \text{(3-jet)} \\ M &\to q'G\bar{q}_s && \text{(2-jet)} \\ M &\to q'\bar{q} && \text{(2-jet)} \end{aligned} \tag{4.22}$$

which are shown separately in Fig. 4.7. However, it is clear that the different decay modes give essentially identical forms for $\langle F_2(\chi;0.95)\rangle$.

We also give the mean energy correlation function for events in which a pair of heavy leptons are produced and then decay to $u\bar{d}\nu_L$. We assume that the neutrinos will not be detected and therefore divide the F_2 for each event by the square of the observed energy in the event, H_0. Note that our approximations for heavy lepton production events hold only when the energies of the heavy leptons are small compared to their masses. At higher energies, heavy lepton production events should take on a two-jet structure. From Fig. 4.7 it is clear that the $\langle F_2(\chi;0.95)\rangle$ for simulated hadronic events at $\sqrt{s} = 20$ GeV involving heavy quark or lepton production near threshold are closer to those

for isotropic events than the $\langle F_2(\chi;0.95)\rangle$ for $e^+e^- \to q\bar{q}(G)$ or $e^+e^- \to \zeta \to GGG$. The difference between the heavy quark or lepton production events and $\zeta \to GGG$ ones is, in fact, not very great; however, this should not pose a serious problem for any experimental investigation based on $\langle F_2\rangle$ since we expect $\zeta \to GGG$ to occur only on resonances below the thresholds for heavy quark pair production and so heavy quark and lepton production events will compete with $e^+e^- \to q\bar{q}(G)$ ones, from which they are quite well distinguished in $\langle F_2\rangle$.

Section 4 - Footnotes

F4.1 In Ref. [2], $F_2^{pt}(\chi)$ was called simply $F(\chi)$.

F4.2 In practical calculations, $F_2^{pt}(\chi)$ can be found easily from (4.9), and then (4.10) can be used to obtain $\langle F_2(\chi,\delta)\rangle$. Alternatively, one may use the rapidly convergent series (4.12). The latter method has the advantage that it also allows the calculation of the distribution $1/\sigma\ d\sigma/dF_2$. It is clear that for both means and distributions, the H_ℓ are somewhat easier to extract from events than the energy correlation F_2.

F4.3 A precise comparison of theory and experiment would require a refinement of our jet decay model along the lines described in Secs. 2 and 3.

Section 4 - Figure Captions

4.1 Two circular detectors σ_1, σ_2 of half angle $\cos^{-1}(\delta)$. $\cos^{-1}(\chi)$ is angle between the centers of the detectors. $F_2(\chi,\delta)$ is obtained by averaging over all positions for the detectors which preserve the angle χ.

4.2 The mean value of the rotationally invariant energy correlation F_2 as a function of detector separation χ for fixed detector size given by $\delta = 0.95$ (opening angle $\sim 18°$). The curves given are for simulated hadronic final states at $\sqrt{s} = 10$, 20 and 40 GeV and in the approximation of free quarks and gluons. The free quark calculation marked $q\bar{q}(G)$ is, in fact, just the contribution of the $q\bar{q}G$ final state calculated with no H_2 cut and with no $q\bar{q}$ component added (this would contribute only at $\chi \sim +1$).

4.3 A comparison at $\sqrt{s} = 20$ GeV of the mean value of the energy correlation F_2 for two different detector sizes given by $\delta = 0.9$ or $\delta = 0.95$ (corresponding to detectors of half-angle 26° and 18°, respectively).

4.4 The ratio of the mean energy correlation between point detectors $\langle F_2^{pt}(\chi)\rangle$: $\langle F_2(\chi;\delta = 1)\rangle$ for hadrons produced by the processes $e^+e^- \to q\bar{q}G$ and $e^+e^- \to q\bar{q}$ at $\sqrt{s} = 20$ GeV. Note that at this energy, our prescription for treating fragmentation takes 65% of $q\bar{q}(G)$ final states to contain two jets and, therefore, to evolve roughly like $q\bar{q}$ final states.

4.5 The distributions $1/\sigma\ d\sigma/dF_2(\chi,\delta)$ calculated for various separations χ of two detectors with size $\delta = 0.95$ ($\sim 18°$) resulting from the processes $e^+e^- \to q\bar{q}$, GGG and $q\bar{q}(G)$. Calculations in the free quark and gluon approximation are shown as well as those obtained from an estimate of the effects of fragmentation to hadrons at $\sqrt{s} = 10$, 20 and 40 GeV. In the free quark approximation $e^+e^- \to q\bar{q}$ gives a delta function contribution, smeared to angles $\chi = \pm(2\delta^2-1)$ by the finite detector sizes. The curve marked $q\bar{q}(G)$ in the free

quark and gluon approximation is $q\bar{q}G$ with an $H_2 < 0.8$ cut but without the $q\bar{q}$ (delta function) term added.

4.6 $1/\sigma\, d\sigma/dF_2(\chi,\delta)$ for $(e^+e^- \to)\ \gamma \to GGG$ in the free gluon approximation, and using a phenomenological model of hadron formation, for various separations of two detectors with size $\delta = 0.9$ (corresponding to half-angles of 26°), to be compared with the results in Fig. 4.5 obtained with $\delta = 0.95$.

4.7 The mean energy correlation function $\langle F_2(\chi,\delta)\rangle$ for events containing heavy quark or lepton production with various mechanisms for heavy meson decay. For comparison, we show results for the continuum reaction $e^+e^- \to q\bar{q}(G)$ from Fig. 4.5.

ARRANGEMENT OF DETECTORS
FOR MEASUREMENT OF $F_2(X,\delta)$

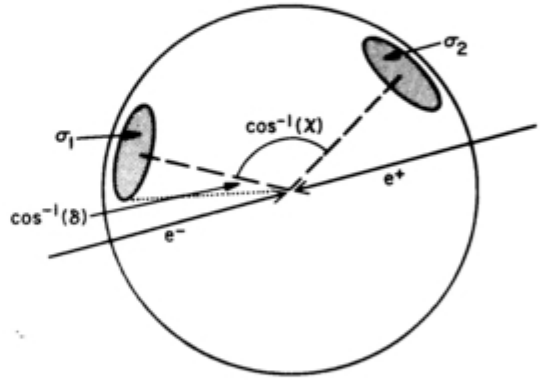

Fig. 4.1

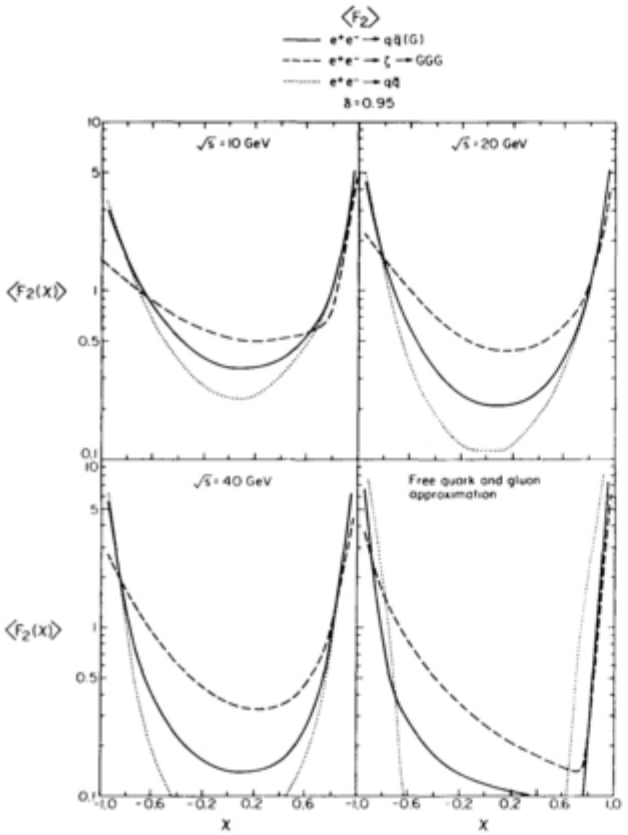
⟨F2⟩
e+e- → qq̄(G)
e+e- → ζ → GGG
e+e- → qq̄
δ = 0.95
√s = 10 GeV
√s = 20 GeV
√s = 40 GeV
Free quark and gluon approximation
⟨F2(x)⟩
x

Fig. 4.2

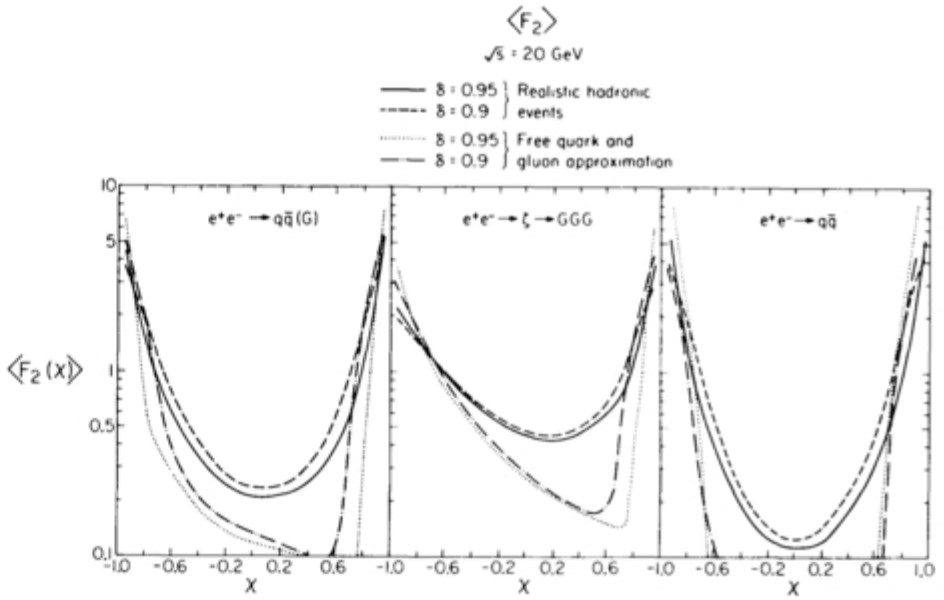
⟨F2⟩
√s = 20 GeV
δ = 0.95
δ = 0.9
Realistic hadronic events
δ = 0.95
δ = 0.9
Free quark and gluon approximation
e+e- → qq̄(G)
e+e- → ζ → GGG
e+e- → qq̄
⟨F2(x)⟩
x

Fig. 4.3

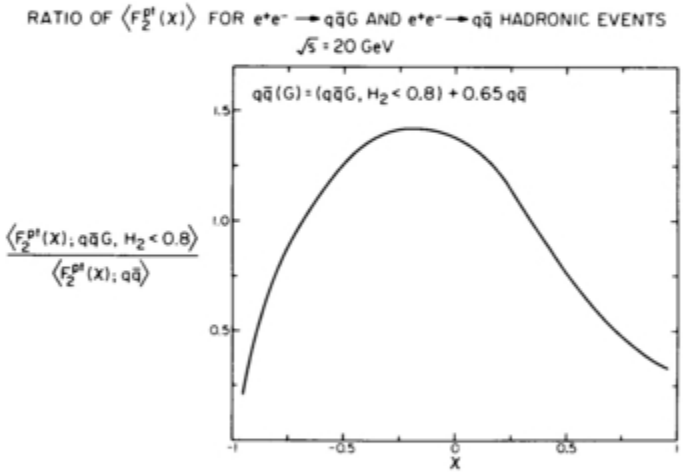
RATIO OF $\langle F_2^{pt}(x)\rangle$ FOR $e^+e^- \to q\bar{q}G$ AND $e^+e^- \to q\bar{q}$ HADRONIC EVENTS
$\sqrt{s} = 20$ GeV
$q\bar{q}(G) = (q\bar{q}G, H_2 < 0.8) + 0.65\, q\bar{q}$
$\frac{\langle F_2^{pt}(x); q\bar{q}G, H_2 < 0.8\rangle}{\langle F_2^{pt}(x); q\bar{q}\rangle}$
1.5
1.0
0.5
-1
-0.5
0
0.5
1
x

Fig. 4.4

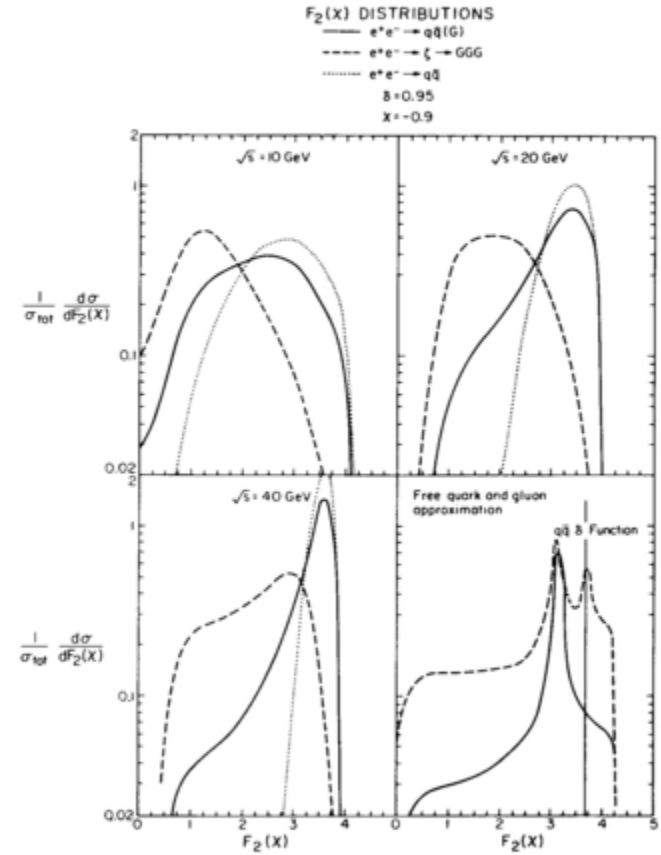
$F_2(x)$ DISTRIBUTIONS
$e^+e^- \to q\bar{q}(G)$
$e^+e^- \to \zeta \to GGG$
$e^+e^- \to q\bar{q}$
$\delta = 0.95$
$x = -0.9$
$\sqrt{s} = 10$ GeV
$\sqrt{s} = 20$ GeV
$\sqrt{s} = 40$ GeV
Free quark and gluon approximation
$q\bar{q}$ δ Function
$\frac{1}{\sigma_{tot}} \frac{d\sigma}{dF_2(x)}$
2
1
0.1
0.02
0
1
2
3
4
5
$F_2(x)$

Fig. 4.5

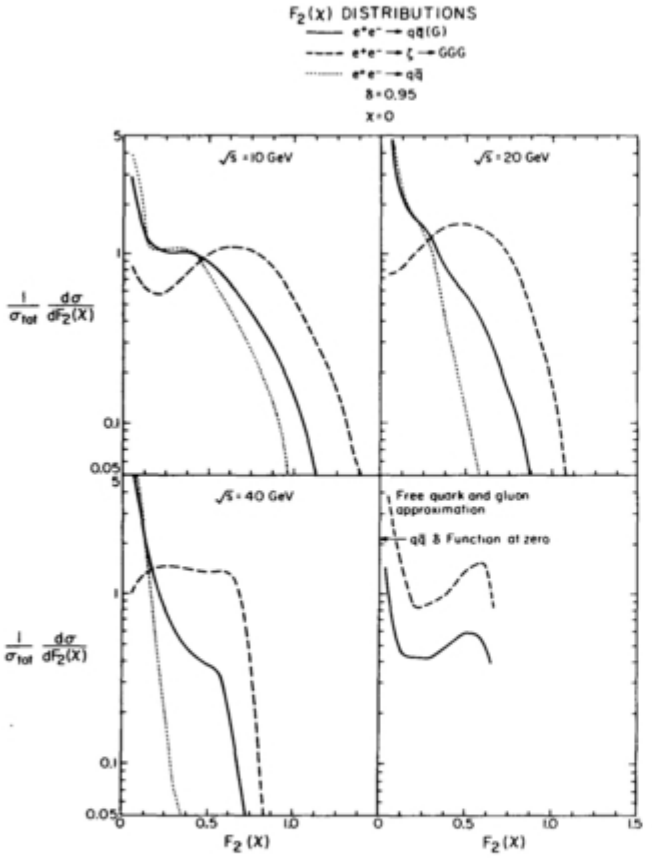
F2(X) DISTRIBUTIONS
e+e- → qq̄(G)
e+e- → ζ → GGG
e+e- → qq̄
δ=0.95
x=0
√s = 10 GeV
√s = 20 GeV
√s = 40 GeV
Free quark and gluon approximation
qq̄ δ Function at zero
1/σtot dσ/dF2(X)
F2 (X)

Fig. 4.5

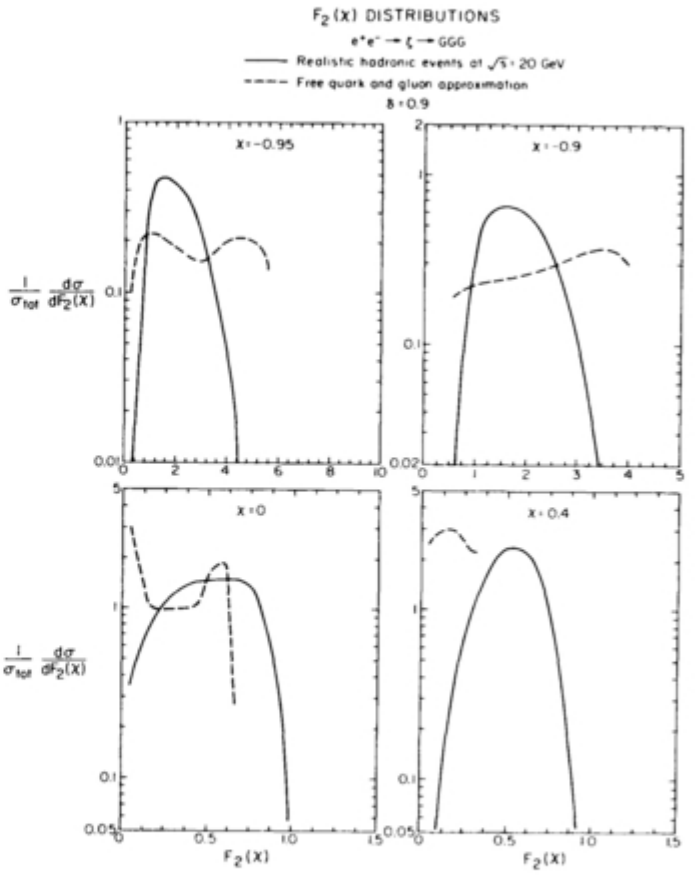
F2(X) DISTRIBUTIONS
e+e- → ζ → GGG
Realistic hadronic events at √s = 20 GeV
Free quark and gluon approximation
δ=0.9
x=-0.95
x=-0.9
x=0
x=0.4
1/σtot dσ/dF2(X)
F2(X)

Fig. 4.6

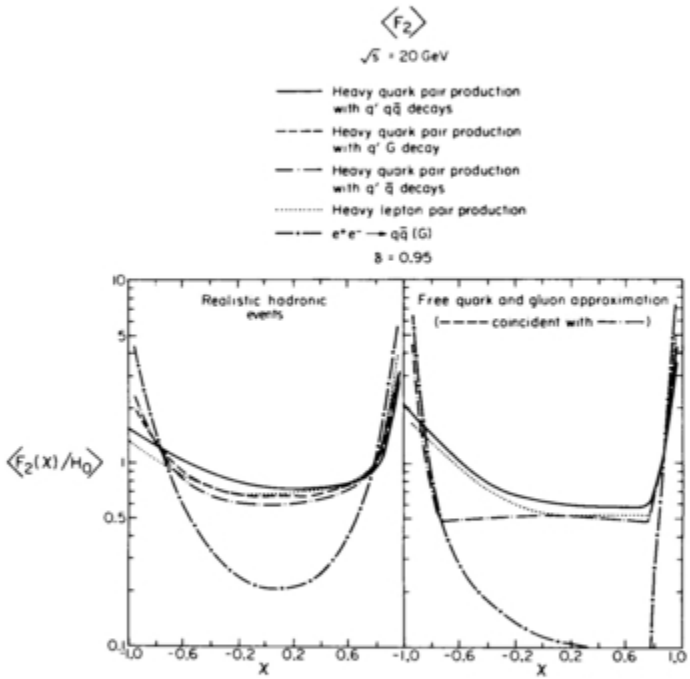

Fig. 4.7

5. Correlations with Respect to the Beam Axis

5.1 Introduction

We have discussed above the rotationally invariant observable $F_2(\chi;\delta)$ obtained by averaging $\tilde{F}_2$, defined in (1.2), over all possible positions of the two detectors which preserve their relative orientation. This averaged $F_2(\chi;\delta)$ characterizes the shapes of events and is probably the most direct probe of their dynamical mechanisms. However, QCD also makes unambiguous predictions for the dependence of the shapes of events on their orientation with respect to the beam axis, which dependence we have thus far brusquely averaged away. In this section we consider this angular dependence using both the energy correlation $\tilde{F}_2$ and its moments with respect to χ, which represent rotationally-non-invariant analogues of the H_ℓ. In Sec. 5.2 we analyze the general form of the angular dependence of $\tilde{F}_2$ and describe a particularly convenient choice of angular coordinates. In Sec. 5.3 we define the moments Ξ of $\tilde{F}_2$ which provide an infrared stable measure of the angular correlations, and in Sec. 5.4 we present results for the three basic processes $e^+e^- \to q\bar{q}$, $e^+e^- \to q\bar{q}(G)$ and $e^+e^- \to \zeta \to GGG$. We consider these both in the free quark and gluon approximation and including the effects of hadron fragmentation. However, we shall not consider either heavy quark or lepton production events [F5.1]; further, our results are specialized to the case of unpolarized electron and positron beams. It is straightforward to generalize our results in these two areas.

5.2 General Form of the Angular Dependence of Energy Correlations

Consider two detectors fixed at particular positions in space separated by an angle χ. The directions of these detectors from the point of interaction (and the normal to the plane defined by them) may be used to define an orthogonal set of axes xyz with respect to which one can specify the direction of

the beam axis. Temporarily we consider the detectors to be fixed and take the beam direction as variable. In the next paragraph, we shall use the alternative choice of a fixed beam direction and detectors at variable angles. With the detectors fixed, one assigns one of the axes to be the normal and the other two to be in the plane formed by the two detectors. The direction of the axes in the plane may be chosen arbitrarily. All choices, if consistently used, are, of course, equivalent; however, some may be more convenient than others. As we shall see, the best choice is to take the z axis to be the normal to the plane of the detectors, and the x and y axes to be in the plane, with the x axis defined to be on the line bisecting the angle between the two detectors. We denote this choice by the subscript N (z axis Normal to plane). We shall also sometimes discuss the P system (z axis in Plane) whose y axis is normal to the plane and z axis is in the same direction as the x axis in the N system. The careful reader will perceive that various signs are undefined in these definitions (e.g., one can reverse directions of z and y axes in the N system). However, no parity-conserving observable is sensitive to the ambiguities.

Now consider the energy correlations between two detectors for an e^+e^- annihilation event. Clearly, the correlation depends on the direction of the beam referred to the axis sets we described above; this beam direction may be specified by spherical polar angles (θ',ϕ') and so we are led to define a beam-orientated energy correlation $\tilde{P}_2^{pt}$ that is a function of χ, δ, θ' and ϕ'. To be precise, we shall actually not define θ', ϕ' exactly in this way but rather fix the e^+e^- direction and define a fixed set of axes $x_R y_R z_R$ with z_R along the e^+e^- direction. Then we take the "reference" orientation of the two detectors so that $x_R y_R z_R$ coincides with the detector-defined axis set described in the paragraph above. Any orientation of the two detectors is

then specified by a rotation R acting on the reference orientation. Let R be in the standard Euler angle form

$$R = \hat{R}_z(\tilde{\phi})\hat{R}_y(\theta)\hat{R}_z(\phi) \tag{5.1}$$

where $\hat{R}_y(\theta)$ is a rotation about the y axis through angle θ and $\hat{R}_z$ a rotation about the z axis. θ and ϕ are the angles to be used in the specification of $\tilde{P}_2^{pt}$ [F5.2]. For unpolarized beams, $\tilde{P}_2^{pt}$ is independent of $\tilde{\phi}$. The unit spin of the photon severely limits the possible dependence of $\tilde{P}_2^{pt}$ on θ and ϕ; we now turn to a discussion of these constraints.

Consider the general process

$$e^+e^- \to 1 + 2 + \text{anything}, \tag{5.2}$$

where we have specialized to the case of point detectors and consider 1 and 2 as particles heading in the directions of the two detectors. Working in the virtual photon rest frame, let λ be the spin component of the virtual photon referred to the e^+e^- direction as a quantization axis, and let μ be the spin component of the virtual photon with respect to the 'reference' final state axes. Then if α denotes the unmeasured momenta and helicities of the final particles, the amplitude for $e^+e^- \to \gamma^* \to 1 + 2 + \text{anything}$ may be written as

$$A_{\lambda\alpha} = \sum_{\mu} G_\lambda d^1_{\lambda\mu}(\theta)\exp(-i\mu\phi)H_{\mu\alpha} \tag{5.3}$$

where G_λ, $H_{\mu\alpha}$ are vertex functions, which give the helicity amplitudes for $e^+e^- \to \gamma^*$ and $\gamma^* \to 1 + 2 + \text{anything}$, respectively. Taking $H_{1\alpha} = a_\alpha$, $H_{0\alpha} = b_\alpha$,

$H_{-1\lambda} = c_\lambda$, and using $G_1 = -G_{-1}$, $G_0 = 0$ (for massless $e^\pm$), the square of the amplitude (5.3) becomes

$$\frac{d^2\sigma}{d(\cos\theta)d\phi} = \sum_\lambda \{|d^1_{11}(\theta)e^{-i\phi}a_\lambda + d^1_{10}(\theta)b_\lambda + d^1_{1-1}(\theta)e^{i\phi}c_\lambda|^2 + |d^1_{-11}(\theta)e^{-i\phi}a_\lambda + d^1_{-10}(\theta)b_\lambda + d^1_{-1-1}(\theta)e^{i\phi}c_\lambda|^2\}, \tag{5.4}$$

which gives the inclusive cross-section $e^+e^- \to 1 + 2 +$ anything. For point detectors, one must simply multiply it by $\frac{E_1E_2}{s}$ to obtain $\tilde{F}_2^{pt}(\chi,\theta,\phi)$. One may expand the resulting expression and derive the general form for the θ and ϕ dependence of $\tilde{F}_2^{pt}$. The parity invariance of the interaction places some constraints on this form. The constraints take a different form depending on whether the z axis lies in the 12 plane (as in the P system) or along the normal to it (N system). In a P-type system, parity invariance implies

$$\left.\begin{aligned} b_\lambda &= \eta_\lambda b_{-\lambda} \\ a_\lambda &= -\eta_\lambda c_{-\lambda} \end{aligned}\right\} \text{ z axis in 12 plane} \tag{5.5}$$

where $\eta_\lambda = \pm 1$ is some phase and $-\lambda$ denotes the state obtained by application to λ of the symmetry operator $S = P\hat{R}_y(\pi)$ (P = parity operator, $\hat{R}_y(\pi)$ a rotation through π about the y direction). S, of course, leaves the directions of 1 and 2 invariant. Combining (5.5) and (5.4), one finds

$$\frac{d^2\sigma}{d\cos\theta_P d\phi_P} = A_P(1+\cos^2\theta_P) + B_P\sin^2\theta_P + C_P\sin^2\theta_P\cos 2\phi_P + D_P\sin 2\theta_P\cos\phi_P \tag{5.6}$$

where A_P through D_P (which, of course, depend on χ) can be related to bilinear sums over a_λ, b_λ and c_λ.

If now the z axis is taken along the normal to the 12 plane, the symmetry operator for the system becomes $S = P\hat{R}_z(\pi)$, so that the constraints from parity invariance become

$$\left.\begin{aligned} a_\lambda &= -\eta_\lambda a_\lambda \\ c_\lambda &= -\eta_\lambda c_\lambda \\ b_\lambda &= \eta_\lambda b_\lambda \end{aligned}\right\} \text{ z axis along normal to 12 plane.} \tag{5.7}$$

Combining (5.7) and (5.4), one finds

$$\frac{d^2\sigma}{d\cos\theta_N d\phi_N} = A_N(1+\cos^2\theta_N) + B_N\sin^2\theta_N + C_N\sin^2\theta_N\cos 2\phi_N + D_N\sin 2\theta_N\sin 2\phi_N. \tag{5.8}$$

Comparing (5.6) and (5.8), we see that there are, in general, 4 independent beam-oriented energy correlation functions. The specific expansion coefficients in the complete energy correlation as a function of the directions of the detectors with respect to the beam (or, equivalently, at least for the point detector case considered here, the inclusive differential cross-section for $e^+e^- \to \gamma^* \to 1 + 2 +$ anything) depend, however, on the choice of coordinate system. The results (5.6) and (5.8) hold for any choice of orthogonal axes in the 12 plane. However, they must be symmetric under the interchange $1 \leftrightarrow 2$. This constraint may be expressed most simply if one chooses one of the axes

in the plane along the bisector of the angle between the directions of 1 and 2. In this case, the terms D_P and D_N vanish and one may write the angular distribution in either the N or P system as

$$\frac{d^2\sigma}{d(\cos\theta)d\phi} = \langle \tilde{F}_2^{pt}(\chi,\theta,\phi)\rangle = T(\chi)\{1 + J(\chi)P_2(\cos\theta) + K(\chi)\sin^2\theta\cos 2\phi\}. \tag{5.9}$$

With the above choice, our previous rotational averaged $\langle F_2(\chi)\rangle$ is just the function $T(\chi)$ while moments of $\tilde{F}_2^{pt}(\chi,\theta,\phi)$ with respect to the orthogonal functions $P_2(\cos\theta)$ and $\sin^2\theta\cos 2\phi$ give J and K:

$$\langle 1\rangle = \frac{1}{4\pi}\int d\Omega\langle \tilde{F}_2^{pt}(\chi,\theta,\phi)\rangle = T(\chi)$$

$$\langle P_2(\cos\theta)\rangle/\langle 1\rangle = J(\chi)/5 \tag{5.10}$$

$$\langle \sin^2\theta\cos 2\phi\rangle/\langle 1\rangle = 4K(\chi)/15.$$

5.3 Moments of Angular Correlations

The H_ℓ observables discussed in [2] were of the form

$$\sum_{i,j} \frac{|\vec{p}_i||\vec{p}_j|}{s} f(\hat{p}_i\cdot\hat{p}_j) \tag{5.11}$$

where $\hat{p}_i$, $\hat{p}_j$ are unit vectors along the momenta of particles i and j and the f were chosen to be the Legendre polynomials. The H_ℓ give a complete specification of the rotationally invariant two-point energy correlation function

in an event. In [3] and in Sec. 6 below, we discuss the expansion of the three-point energy correlation defined as

$$\sum_{i,j,k} \frac{|\vec{p}_i||\vec{p}_j||\vec{p}_k|}{s^{3/2}} f(\hat{p}_i\cdot\hat{p}_j\cdot\hat{p}_k). \tag{5.12}$$

In this section, we consider another extension of (5.11) in which f now depends on the direction of the incoming beams, $\hat{b}$. We take

$$\Xi_f = \sum_{i,j} \frac{|\vec{p}_i||\vec{p}_j|}{s} f(\hat{b}\cdot\hat{p}_i\cdot\hat{p}_j). \tag{5.13}$$

We find that these observables provide information on the angular distributions of planar structures in events with respect to the beam direction.

The general analysis of Sec. 5.2 allows us to write any f in terms of the linearly independent functions

$$f_0^\ell = \sin^2\phi_{ij}P_\ell(\cos\phi_{ij})$$

$$f_1^\ell = \sin^2\phi_{ij}P_2(\cos\theta_{N_{ij}})P_\ell(\cos\phi_{ij}) \tag{5.14}$$

$$f_2^\ell = \sin^2\phi_{ij}\sin^2\theta_{N_{ij}}\cos 2\phi_{N_{ij}}P_\ell(\cos\phi_{ij}),$$

where ϕ_{ij} is the angle between particles i and j. $\theta_{N_{ij}}$ and $\phi_{N_{ij}}$ are the angles which specify the beam direction in the N_{ij} coordinate system. This set of axes (xyz) is defined as described in Sec. 5.2, but with the directions of particles i and j replacing the detector directions of the previous discussion. The subscript N indicates that the z axis is normal to the plane defined by $\hat{p}_i$ and $\hat{p}_j$. The explicit factor $\sin^2\phi_{ij}$ in (5.14) is necessary to make the

f_i^ℓ well defined in the limits $\phi_{ij} = 0$ or π. This can be seen from the expressions for the beam angular functions in terms of scalar products of $\hat{b}$, $\hat{p}_i$ and $\hat{p}_j$:

$$\sin^2\theta_{N_{ij}} \cos^2\phi_{N_{ij}} = \frac{1}{4\cos^2\phi_{ij}/2} [\hat{b}\cdot(\hat{p}_i+\hat{p}_j)]^2$$

$$\sin^2\theta_{N_{ij}} \sin^2\phi_{N_{ij}} = \frac{1}{4\sin^2\phi_{ij}/2} [\hat{b}\cdot(\hat{p}_i-\hat{p}_j)]^2, \tag{5.15}$$

$$f_o^\ell = [1-(\hat{p}_i\cdot\hat{p}_j)^2]P_\ell(\hat{p}_i\cdot\hat{p}_j)$$

$$f_1^\ell = [1 - \tfrac{3}{2}((\hat{b}\cdot\hat{p}_i)^2 + (\hat{b}\cdot\hat{p}_j)^2) + 3(\hat{b}\cdot\hat{p}_i)(\hat{p}_i\cdot\hat{p}_j)(\hat{p}_j\cdot\hat{b})]P_\ell(\hat{p}_i\cdot\hat{p}_j)$$

$$f_2^\ell = [2(\hat{b}\cdot\hat{p}_i)(\hat{b}\cdot\hat{p}_j) - (\hat{p}_i\cdot\hat{p}_j)((\hat{b}\cdot\hat{p}_i)^2 + (\hat{b}\cdot\hat{p}_j)^2)]P_\ell(\hat{p}_i\cdot\hat{p}_j). \tag{5.16}$$

which illustrates the necessity of the $\sin^2\phi_{ij}$ factor in the definition of f_k^ℓ to avoid problems at $\phi_{ij} = 0$ or π. We define Ξ_k^ℓ using (5.13) with f_k^ℓ as taken from eq. (5.14) or (5.16). It is clear that the $\langle\Xi_k^\ell\rangle$ share the infrared stability of the $\langle H_\ell\rangle$ when they are computed in QCD perturbation theory.

Another possible set of observables, which appears to be less sensitive to hadron fragmentation than the Ξ_k^ℓ (see below), is defined in analogy with (5.13):

$$\bar{\Xi}_k^\ell = \sum_{i,j} \frac{|\vec{p}_i||\vec{p}_j|}{s} \bar{f}_k^\ell(\hat{b},\hat{p}_i,\hat{p}_j)$$

$$\bar{f}_k^\ell = f_k^\ell/(\sin^2\phi_{ij}). \tag{5.17}$$

The $\bar{\Xi}_k^\ell$ are only independent of the Ξ_k^ℓ for $\ell = 0$ and 1. The definition (5.17) is singular at $\sin^2\phi_{ij} = 0$, for k = 1 or 2. For $\phi_{ij} = 0$, the x axis remains well defined (along the $\hat{p}_i$, $\hat{p}_j$ direction) but the y and z axes of the N_{ij} system are undefined. In this case, we take the $\bar{f}_{1,2}^\ell$ to have the values obtained by averaging uniformly over all possible directions of the y and z axes in the plane perpendicular to $\hat{p}_i$, $\hat{p}_j$, so that

$$\bar{f}_1^\ell(\phi_{ij} = 0) = -\tfrac{1}{2} P_2(\cos\alpha_i)P_\ell(\cos\theta_{ij})$$

$$\bar{f}_2^\ell(\phi_{ij} = 0) = P_2(\cos\alpha_i)P_\ell(\cos\theta_{ij}) \tag{5.18}$$

where α_i is angle between beam direction and the particles i or j.

In the case $\phi_{ij} = \pi$, an analogous situation pertains and only the y axis is well defined. We take $\bar{f}_{1,2}^\ell$ to have the value obtained by averaging over all possible directions for the x and z directions, so that

$$\bar{f}_1^\ell(\phi_{ij} = \pi) = -\tfrac{1}{2} P_2(\cos\alpha_i)P_\ell(\cos\theta_{ij})$$

$$\bar{f}_2^\ell(\phi_{ij} = \pi) = -P_2(\cos\alpha_i)P_\ell(\cos\theta_{ij}). \tag{5.19}$$

Note that in both limits, $\bar{f}_{1,2}^\ell$ is proportional to $P_2(\cos\alpha_i)$, giving the only possible non-trivial dependence on α_i.

The $\bar{\Xi}_k^\ell$ cannot be written in a form analogous to the H_ℓ from which their infrared stability would be evident. Their values depend, of course, on the treatment of the singular case $\sin\phi_{ij} = 0$. We give evidence below that the prescription for this described above is correct and renders the $\bar{\Xi}_k^\ell$ infrared stable. It is clear that the energy weighting in eq. (5.17) protects the $\bar{\Xi}_k^\ell$ from soft infrared divergences. Collinear quarks and gluons also give rise to divergences

in the differential cross-section. The $\bar{\Xi}^{\ell}_{k}$ can only be infrared stable if they take on the same value for divergent configurations in which two separate particles are exactly collinear ($\phi_{ij} = 0$) and in which a single particle carries their total momentum. This will be the case with our prescription for handling collinear particles only if, in configurations where the particles are nearly collinear, all potential divergences are independent of the azimuthal directions of the particles with respect to the axis defined by the vector sum of their momenta. Any dependence on the azimuthal direction will appear in the amplitude as terms proportional to $\gamma \cdot k_{\perp}$, where $k_{\perp}$ is the transverse momentum of one of the particles with respect to the total momentum axis. Divergences in the amplitude are (up to logarithms) of the form $dk_{\perp}/k_{\perp}$. Hence, any contribution to the amplitude which is not independent of azimuthal angle will be finite as $k_{\perp} \to 0$. Thus the divergent parts of amplitudes for collinear production of particles are azimuthally-symmetrical, so that (with our prescription) the $\bar{\Xi}^{\ell}_{k}$ take on the same value for this configuration as when a single particle is produced in place of several collinear ones. Hence it appears that the moments of the $\bar{\Xi}^{\ell}_{k}$ should be infrared stable when computed in QCD perturbation theory.

Consider now an event in which three partons are produced. Then the angular distribution of the plane defined by their momenta with respect to the beam axis will be characterized by $\Xi^{\ell}_{1,2}/\Xi^{\ell}_{o}$ or $\bar{\Xi}^{\ell}_{1,2}/\bar{\Xi}^{\ell}_{o}$. In actual events, where the final state consists of hadrons, the values of these ratios will approach the free quark and gluon results as $\sqrt{s}$ increases. The $\overset{(-)}{\Xi}{}^{\ell}_{k}$ therefore provide a method for determining the angular distributions of planes of particles with respect to the beam direction without requiring the plane to be found by minimizing an observable [37], which might well induce spurious effects. The $\overset{(-)}{\Xi}{}^{\ell}_{k}$ give the moments of the angular distributions of planes just as the B_{ℓ} described in Ref. 2 describe the angular distributions of jets.

The angular distributions of planes in general depend both on their polar (θ) and azimuthal (ϕ) angles with respect to the beam direction. The polar and azimuthal dependences can, of course, be rearranged by making different choices of frame (e.g., N or P). One might expect that in some frame two jet events should contribute on average only to the polar distribution. However, while this is clearly the case for pure $q\bar{q}$ final states, it is no longer possible after fragmentation to hadrons to choose a frame in which the azimuthal dependence vanishes. Hence both $\overset{(-)}{\Xi}{}^{\ell}_{1}$ and $\overset{(-)}{\Xi}{}^{\ell}_{2}$ should be considered; no particular feature of the angular distribution appears to be especially distinguished.

Finally we note that $\overset{(-)}{\Xi}{}^{\ell}_{k}$ are the Legendre transforms (with respect to χ) of the angular terms (5.10) in the energy correlation function $\tilde{F}^{pt}_{2}$. Their relation to $\tilde{F}^{pt}_{2}$ is, therefore, analogous to the relation of the H_{i} to the rotationally-averaged F^{pt}_{2}.

5.4 Some Analytical Results for $\tilde{F}^{pt}_{2}$

For the process $e^{+}e^{-} \to q\bar{q}$, $\tilde{F}^{pt}_{2}(\chi,\theta,\phi)$ is only nonzero at $\chi = \pm 1$ where the "plane" given by the two detectors is undefined. We use the same azimuthally symmetric prescription for defining the plane here as we described for $\bar{\Xi}^{\ell}_{k}$ at $\sin\phi_{ij} = 0$ in the previous section. If α is the angle between the $e^{+}e^{-}$ and $q\bar{q}$ direction, then the $\frac{3}{8}(1+\cos^{2}\alpha) = \frac{1}{2} + \frac{1}{4} P_{2}(\cos\alpha)$ angular distribution gives for the parameters in $\tilde{F}^{pt}_{2}$ defined according to eq. (5.10)

$$T(\chi) = \delta(\chi-1) + \delta(\chi+1)$$

$$J(1) = J(-1) = -\frac{1}{4} \qquad (5.20)$$

$$K(1) = -K(-1) = \frac{3}{8}.$$

To estimate the modifications to our results when the q and $\bar{q}$ fragment into hadrons, we would usually simulate complete hadronic events. We do this in the next section but present here a simple estimate for the effects of fragmentation on $J(\chi)$ and $K(\chi)$ which agrees closely with the results from the more complicated model. Our simple estimate is obtained by assuming that $\tilde{F}_2(\chi)$ away from $\chi = \pm 1$ is dominated by a complete jet entering one detector and a single hadron from the other jet being incident on the second detector. The first jet then has an angular distribution $(1 + \cos^2\alpha)$ with respect to the beam direction, while we take the single hadron to be distributed uniformly in azimuth about the direction of the jet from which it came. This picture leads to the simple predictions

$$J_{q\bar{q}\ \text{fragmentation}}(\chi) = -\frac{1}{4}$$
$$K_{q\bar{q}\ \text{fragmentation}}(\chi) = \frac{3}{8}\chi \tag{5.21}$$

which are in remarkably good agreement with the full Monte Carlo simulation of $q\bar{q}$ fragmentation shown in Figs. 5.1 and 5.2. Of course, this simple picture predicts only the angular correlations $J,K(\chi)$ and not the overall normalization $T(\chi)$.

For $e^+e^- \to q\bar{q}G$, the function $T(\chi) = \langle F_2^{pt}(\chi)\rangle$ is given in (A.5). One can also calculate $J(\chi)$ and $K(\chi)$ in the free quark and gluon approximation to find (at $O(\alpha_s)$)

$$T_{q\bar{q}G}(\chi)J_{q\bar{q}G}(\chi) = \frac{-T_{q\bar{q}G}(\chi)}{4} + C_J\delta(1-\chi)$$

$$T_{q\bar{q}G}(\chi)K_{q\bar{q}G}(\chi) = \frac{2\alpha_s}{\pi}\frac{1}{(1+\chi)(1-\chi)^5}\{4(5\chi^2+8\chi+5)\log((1+\chi)/2) \tag{5.22}$$
$$+ (\chi-1)(\chi^3-7\chi^2-16\chi-14)\} + C_K\delta(1-\chi)$$

where the coefficients of the delta functions are, as usual, infrared divergent constants. For $e^+e^- \to \zeta \to GGG$, one also finds

$$J_{GGG}(\chi) = -\frac{1}{4}, \tag{5.23}$$

while $K(\chi)$ for this case can be calculated using the results of Ref. [38]. The analytical results for $e^+e^- \to q\bar{q}G$ and $\zeta \to GGG$ are shown in Figs. 5.1 and 5.2 for both $J(\chi)$ and $K(\chi)$. The result $J(\chi) = -\frac{1}{4}$ is a surprisingly common one (see eqs. 5.20, 21, 22 and 23). We know of no simple explanation for this (see Appendix B); it appears to be 'accidental'. An isotropic (phase space) model would, of course, give zero for $J(\chi)$ and so the common nonzero value of $J(\chi)$ for the low order QCD processes in e^+e^- annihilation should provide a useful method of identifying them.

Inspection of eq. (5.22) reveals that (ignoring delta function terms) both $J(\chi)$ and $K(\chi)$ tend to the values given in eq. (5.20) for the pure $e^+e^- \to q\bar{q}$ process (with our prescription for defining the final plane) as $\chi \to \pm 1$. This supports our argument in the last section for the infrared stability of $\bar{\Xi}_k^k$; the equality of the $q\bar{q}$ and $q\bar{q}G$ values for $J(\chi)$ and $K(\chi)$ at $\chi = \pm 1$ will allow the infrared divergences to cancel between the contributions of the two final states. Remembering that the coefficient of $\delta(1-\chi)$ in $T(\chi)$ is just $C_T = 2\sum_i\langle E_i^2\rangle/s$, we may form the infrared finite combinations of the coefficients of $\delta(1-\chi)$ in $J(\chi)$ and $K(\chi)$:

$$-\frac{2}{5}(C_J+C_T/4) = \frac{4}{15}(C_K-3C_T/8)$$

$$= 2\langle(\sum_i E_i^2/s(P_2(\cos\alpha_i) - \tfrac{1}{10}))\rangle \qquad (5.24)$$

$$= -2\alpha_s/15\pi$$

where α_i is the angle between particle i and the beam. The infrared finiteness of these combinations of $\delta(1-\chi)$ terms on their own occurs only at $O(\alpha_s)$. In higher orders, only the complete moments $\langle\bar{\Xi}_k^{\ell}\rangle$ integrated over all possible final state configurations will be infrared finite. It is amusing that the result $J(\chi) = -\frac{1}{4}$ for $e^+e^- \to q\bar{q}G$ is only violated in the coefficient of $\delta(1-\chi)$ to $O(\alpha_s)$.

5.5 Some Results on $\bar{P}_2^{pt}$ and its Moments $\bar{\Xi}_k^{\ell}$ for Hadronic Events

The observables $J(\chi) = \langle P_2(\cos\theta_N)\rangle$ and $K(\chi) = \langle\sin^2\theta_N\cos(2\phi_N)\rangle$ introduced in Sec. 5.3 are shown in Figs. 5.1 and 5.2 as a function of χ for events of several types, both in the free quark and gluon approximation, and for simulated hadronic final states. $J(\chi)$ and $K(\chi)$ completely specify the dependence of $\bar{P}_2^{pt}$ on the orientation of the two detectors with respect to the beam direction. The most striking feature of the curves in Figs. 5.1 and 5.2 is the similarity between results from the different QCD processes. An isotropic model with $J(\chi) = K(\chi) \equiv 0$ would be easy to distinguish from the QCD reactions. These figures also confirm that our simple model for $q\bar{q}$ fragmentation reproduces rather well the hadron final state angular functions given by the full Monte Carlo calculation. The effects of hadron fragmentation are minor except for the GGG final state and even there the hadron final states show beam correlations very different from the isotropic case.

In Tables 1 through 3, we give the mean values of the moments defined in Sec. 5.3. These are infrared stable and probably preferable to $J(\chi)$ and $K(\chi)$

discussed above. The latter have particular problems near $\chi = 1$ which are properly averaged in the moments. The tables give $\langle\bar{\Xi}_k^0\rangle$, $\langle\bar{\Xi}_k^3\rangle$ and $\frac{3}{2}\langle\bar{\Xi}_k^0\rangle = \langle\bar{\Xi}_k^0\rangle - \langle\bar{\Xi}_k^2\rangle$. $\bar{\Xi}_k^0$ is the simplest moment and provides the cleanest tests of the theory with the smallest effects from hadron fragmentation. In fact, the effects of hadron fragmentation appear to be less severe in $\bar{\Xi}_k^0$ than in the analogous single energy correlation in B_2 discussed in [2]. We currently consider $\bar{\Xi}_{1,2}^0$ as the best way of measuring beam angular dependence of the energy distribution of e^+e^- annihilation final states. $\langle\bar{\Xi}_k^3\rangle$ has a weighting function $P_3(\cos\chi)$ that is odd in χ and so is useful for investigating $K(\chi)$, which is predicted to be approximately odd in χ. Thus $\langle\bar{\Xi}_2^0\rangle$ and $\langle\Xi_2^0\rangle$ should always be small while $\langle\bar{\Xi}_2^3\rangle$ provides a measure of the absolute magnitude of K. We have not discussed the simplest odd function $\langle\bar{\Xi}_k^1\rangle$ because of its sensitivity to missing particles in incomplete final states observed experimentally (recall that $\langle\bar{\Xi}_0^1\rangle = \langle H_1\rangle$ vanishes because of momentum conservation). Finally the tables show $\frac{3}{2}\langle\Xi_k^0\rangle$, which is the simplest example of a moment observable with an explicit $\sin^2\chi$ suppression of the $\chi = \pm 1$ regions.

Tables 1 and 2 also show results with an H_2 cut < 0.35 (applied to the final hadrons) which selects "true" 3 jet events. The fact that these results are similar to those without the H_2 cut is an indication that the beam correlations do not depend importantly on the 'shapes' of the events.

Table 1: The Beam Moments $\langle \bar{\Xi}_k^{\ell} \rangle$ for $e^+e^- \to q\bar{q}$ at $\sqrt{s}$ = 20 GeV [F5.3].

		$\ell = 0$: $\langle \bar{\Xi}_k^{o} \rangle$	$\ell = 3$: $\langle \bar{\Xi}_k^{3} \rangle$	$\ell = 0,2$: $\langle \bar{\Xi}_k^{o} - \bar{\Xi}_k^{2} \rangle$
$\langle \bar{\Xi}_o^{\ell} \rangle$, Hadrons		1	0.032	0.27
$\langle \bar{\Xi}_o^{\ell} \rangle$, FQGA		1	0	0
$\langle \bar{\Xi}_o^{\ell} \rangle$, Hadrons	$H_2/H_o <$ 0.35	0.001		
$\langle \bar{\Xi}_o^{\ell} \rangle$, FQGA	$H_2/H_o <$ 0.35	0		
$\langle \bar{\Xi}_1^{\ell} \rangle$, Hadrons		-0.047	-0.001	-0.013
$\langle \bar{\Xi}_1^{\ell} \rangle$, FQGA		-0.05	0	0
$\langle \bar{\Xi}_2^{\ell} \rangle$, Hadrons		0.0004	0.06	-0.001
$\langle \bar{\Xi}_2^{\ell} \rangle$, FQGA		0	0.1	0

Table 2: The Beam Moments $\langle \bar{\Xi}_k^{\ell} \rangle$ for $e^+e^- \to q\bar{q}(G)$ at $\sqrt{s}$ = 20 GeV [F5.3].

		$\ell = 0$: $\langle \bar{\Xi}_k^{o} \rangle$	$\ell = 3$: $\langle \bar{\Xi}_k^{3} \rangle$	$\ell = 0,2$: $\langle \bar{\Xi}_k^{o} - \bar{\Xi}_k^{2} \rangle$
$\langle \bar{\Xi}_o^{\ell} \rangle$, Hadrons		1	0.072	0.36
$\langle \bar{\Xi}_o^{\ell} \rangle$, FQGA		1	0.073	0.15
$\langle \bar{\Xi}_o^{\ell} \rangle$, Hadrons	$H_2/H_o <$ 0.35	0.09	0.018	0.067
$\langle \bar{\Xi}_o^{\ell} \rangle$, FQGA	$H_2/H_o <$ 0.35	0.028	0.015	0.02
$\langle \bar{\Xi}_1^{\ell} \rangle$, Hadrons		- .044	- .0027	- .015
$\langle \bar{\Xi}_1^{\ell} \rangle$, FQGA		- .048	- .0027	- .0076
$\langle \bar{\Xi}_1^{\ell} \rangle$, Hadrons	$H_2/H_o <$ 0.35	- .0031	- .0007	- .0024
$\langle \bar{\Xi}_1^{\ell} \rangle$, FQGA	$H_2/H_o <$ 0.35	- .0014	- .0006	- .0012
$\langle \bar{\Xi}_2^{\ell} \rangle$, Hadrons		.0007	.049	- .002
$\langle \bar{\Xi}_2^{\ell} \rangle$, FQGA		.0008	.080	- .0003
$\langle \bar{\Xi}_2^{\ell} \rangle$, Hadrons	$H_2/H_o <$ 0.35	.00022	.0011	- .0002
$\langle \bar{\Xi}_2^{\ell} \rangle$, FQGA	$H_2/H_o <$ 0.35	.00025	.00040	.00001

Table 3: The Beam Moments $\langle \bar{\Xi}^{\ell}_{k} \rangle$ for $e^+e^- \to \zeta \to GGG$ at $\sqrt{s} = 10$ GeV [F5.3].

	$\ell = 0$: $\langle \bar{\Xi}^{o}_{k} \rangle$	$\ell = 3$: $\langle \bar{\Xi}^{3}_{k} \rangle$	$\ell = 0,2$: $\langle \bar{\Xi}^{o}_{k} - \bar{\Xi}^{2}_{k} \rangle$
$\langle \bar{\Xi}^{\ell}_{o} \rangle$, Hadrons	1	0.19	0.69
$\langle \bar{\Xi}^{\ell}_{o} \rangle$, FQGA	1	0.22	0.38
$\langle \bar{\Xi}^{\ell}_{1} \rangle$, Hadrons	- .014	- .0017	- .0093
$\langle \bar{\Xi}^{\ell}_{1} \rangle$, FQGA	- .04	.0003	- .019
$\langle \bar{\Xi}^{\ell}_{2} \rangle$, Hadrons	0.0008	.0061	- .0021
$\langle \bar{\Xi}^{\ell}_{2} \rangle$, FQGA	0.008	.022	0

Section 5 - Footnotes

F5.1 For heavy meson pair production near threshold, the spinless nature of the mesons prevents any angular dependence of energy correlations, but for spin - $\frac{1}{2}$ heavy lepton pair production, there should be a definite non-trivial angular dependence.

F5.2 $\theta' = -\theta$, $\phi' = -\phi$ relates this to previous description. In (5.9) one can use either choice as allowed transformation functions are independent of a sign change for θ and ϕ.

F5.3 As usual, when not all the energy in the events is included in the calculation of the $\langle \bar{\Xi}^{\ell}_{k} \rangle$, the value in each event is divided by H_o [2]. FQGA denotes the perturbative QCD calculation of the free quark and gluon final state.

Section 5 - Figure Captions

5.1 The beam angular correlation $J(\chi)/5 = \langle P_2(\cos\theta_N)\rangle$ defined in eq. (5.10) for the processes $e^+e^- \to q\bar{q}$, $e^+e^- \to q\bar{q}(G)$ and $\chi \to GGG$, in the free quark and gluon approximation ('idealized calculation') and for simulated hadronic final states. We also show results for $e^+e^- \to q\bar{q}$ events obtained from the simple fragmentation model described in Sec. 5.4. There is a severe nonuniformity in the curves near $\chi = +1$, as discussed at the end of Sec. 5.4 (c.f., eq. (5.22)). The figures do not attempt to illustrate this phenomenon correctly.

5.2 The second independent beam angular correlation $4K(\chi)/15 = \langle \sin^2\theta_N \cos 2\phi_N\rangle$ for the same processes as given in Fig. 5.1. For both $J(\chi)$ and $K(\chi)$, the subscript N on the angles denotes the use of the frame where the z axis is perpendicular to plane defined by the two particles.

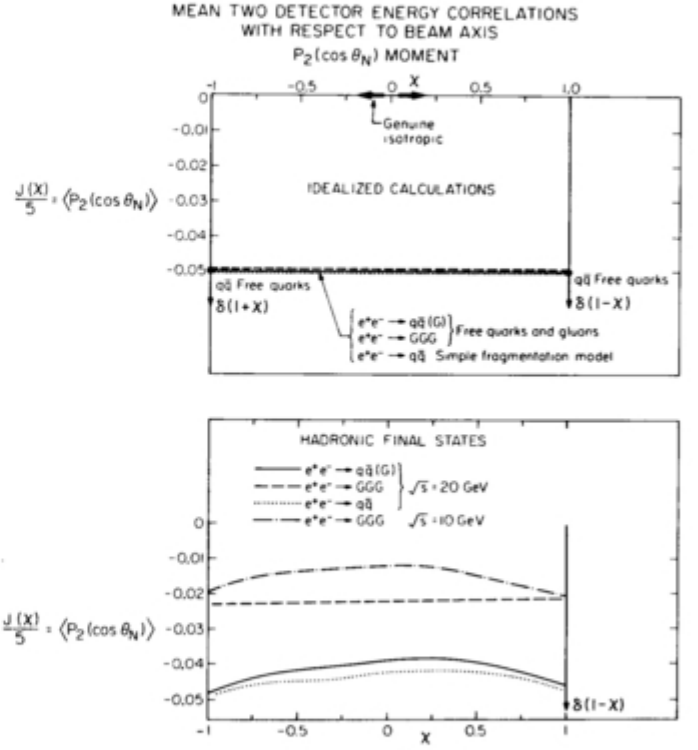

Fig. 5.1

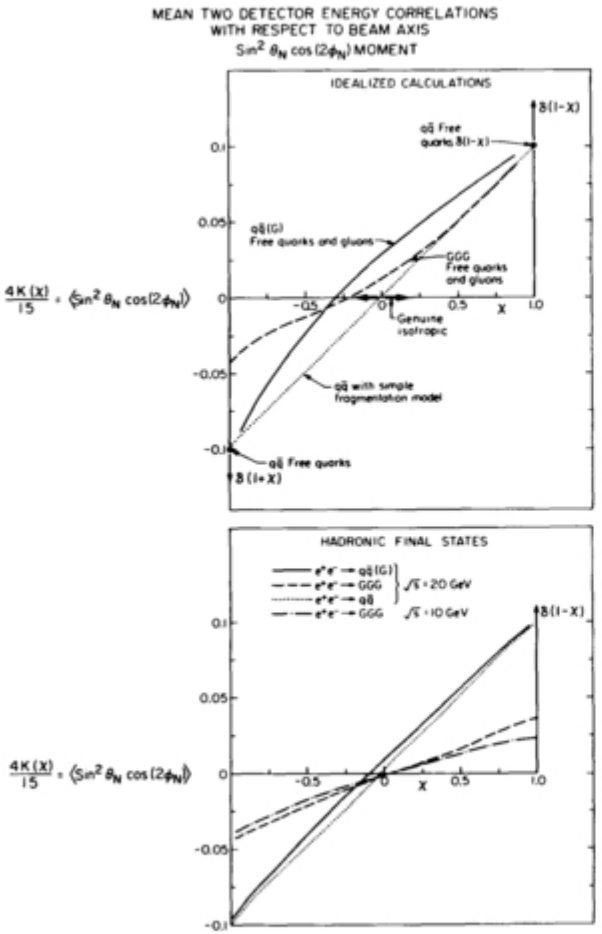

Fig. 5.2

6. Three-Detector Energy Correlations

6.1 $F_{3\perp}$ as a Test for Planar Structure

In this section we consider the three-detector energy correlation, defined by

$$\tilde{F}_3(\sigma_1, \sigma_2, \sigma_3) = \frac{64\pi^3}{|\sigma_1||\sigma_2||\sigma_3|} \frac{|\vec{p}_1||\vec{p}_2||\vec{p}_3|}{(\sqrt{s})^3} \tag{6.1}$$

where detector i has area $|\sigma_i|$ on which a total momentum $|\vec{p}_i|$ is incident. We shall consider only the function $F_3(\sigma_1, \sigma_2, \sigma_3)$ obtained by averaging over all positions of the detectors that maintain their relative orientation. Thus we ignore the correlations with the beam direction that were treated in Sec. 5 for the two detector case. The main purpose in considering three detector correlations is to find tests for planar momentum configurations. Two particle final states contribute to the two detector energy correlation function only when the angle between the two detectors is near 180°. On the other hand, three particle final states, as from $e^+e^- \to q\bar{q}G$ or $e^+e^- \to \zeta \to GGG$, have no such simple signatures in the two detector case. However, the momenta in a three particle final state lie in a plane and hence the three detector energy correlation vanishes for such events unless the detectors themselves are nearly coplanar. In order to extract the most demanding test of coplanarity, we define $F_{3\perp}$ as the value of the rotationally averaged $F_3(\sigma_1, \sigma_2, \sigma_3)$ when all the three detector directions are mutually orthogonal. We take the three detectors to be circular and of equal angular radius $\cos^{-1}(\delta)$. The normalization of F_3 is such that it has the value one for isotropic events. Thus the value of $F_{3\perp}$ is zero for idealized three jet events and one for isotropic events. Hence a measurement of $\langle F_{3\perp}\rangle$ provides a method for distinguishing these two event structures. Of course, the naive prediction that $\langle F_{3\perp}\rangle = 0$ for three-jet

events is only true at infinite energy, where there are neither perturbative nor hadronic corrections. At finite energies which are sufficiently large that fragmentation is unimportant, one may estimate that $\langle F_{3\perp}\rangle = k\alpha_s^2 + O(\alpha_s^3)$ for $e^+e^- \to q\bar{q}(GG\ldots)$, while for $\zeta \to GGG(GG\ldots)$, $\langle F_{3\perp}\rangle \approx k'\alpha_s + O(\alpha_s^2)$. (Analogous results hold for $\langle C_{1\perp}\rangle$.) There are indications that k and k' are of order one. Note that the decay $\zeta \to GGGG$ (which gives rise to non-coplanar final states) where ζ is, as above, a $^3S_1$ $Q\bar{Q}$ state, is not forbidden by symmetry (as would the corresponding positronium decay) because the gluons can be antisymmetric in color. Hence, one expects that, at values of $\sqrt{s}$ for which fragmentation is unimportant, $\langle F_{3\perp}\rangle$ should be larger on resonances than in the continuum by a factor of order $1/\alpha_s$. For lower $\sqrt{s}$, the hadronization of the final state will modify perturbative predictions for $\langle F_{3\perp}\rangle$, and one must make a model to study the size of the changes. We consider the particular question of to what extent a measurement of $\langle F_{3\perp}\rangle$ enables one to test for 3 jet decay of the Υ and possible higher mass heavy quark bound states. In our calculations of the effects of fragmentation, we ignore the perturbative $O(\alpha_s)$ or $O(\alpha_s^2)$ corrections to the result $\langle F_{3\perp}\rangle = 0$ for two and three jet events. We compare only mechanisms that lead to the same single hadron momentum distributions. We found [3] two models that gave the same z distributions as $e^+e^- \to \zeta \to GGG$. The first was obtained by construction; we generated hadrons from genuine $\zeta \to GGG$ events and then randomly rotated each hadron in the final state. We term this model 'isotropic.' For the second model, we noted that $e^+e^- \to M\bar{M}$, where each meson M decays into 3 jets (cf. Sec. 4.3), happens to give essentially the same single hadron momentum distribution as $e^+e^- \to \zeta \to GGG$. This '6 jet' model is, of course, not isotropic but it is certainly more so than would be expected from a GGG final state. In Fig. 6.1 we plot $\langle F_{3\perp}\rangle$ as a function of $\sqrt{s}$ for these three types of events. The GGG final state is easily

distinguished, even at the Υ mass, from the more isotropic mechanisms. Of course, the discrimination improves as $\sqrt{s}$ increases.

Although $\langle F_{3\perp}\rangle$ appears to be a very useful experimental observable, we should point out that it is not trivial to calculate. We found no simple analogue of the eq. (4.1) for the two detector case. Thus we calculated $\langle F_{3\perp}\rangle$ by doing the angular average (integral) in its definition by a simple Monte Carlo technique. Note that this integral has to be done separately for each event.

We have chosen to emphasize one particular angular configuration for the three detectors: the case where they are mutually perpendicular. One can, of course, consider other angular separations but we do not believe they will lead to qualitatively different results.

6.2 Moments of Three-Detector Energy Correlations

The two jet form for the H_ℓ:

$$\langle H_\ell\rangle = 0 \quad \ell \text{ odd}$$
$$\langle H_\ell\rangle = 1 \quad \ell \text{ even} \tag{6.2}$$

is a moment analogue of the result for the two detector energy correlation:

$$F_2^{pt}(\chi) = \delta(1-\chi) + \delta(1+\chi) \tag{6.3}$$

It is natural to ask if there is a moment analogue for the prediction that the three detector correlation function F_3^{pt} is zero for three particle final states unless the detectors are coplanar. In Ref. 3, we showed that there were such moment analogues but did not discuss their relation to F_3^{pt}. We defined two classes of moments that vanished for planar events:

$$\Pi_S = \sum_{i,j,k} \frac{|\vec{p}_i||\vec{p}_j||\vec{p}_k|}{(\sqrt{s})^3} (\hat{p}_i \times \hat{p}_j \cdot \hat{p}_k)^2 S(\hat{p}_i, \hat{p}_j, \hat{p}_k)$$
$$\Psi_A = \sum_{i,j,k} \frac{|\vec{p}_i||\vec{p}_j||\vec{p}_k|}{(\sqrt{s})^3} (\hat{p}_i \times \hat{p}_j \cdot \hat{p}_k) A(\hat{p}_i, \hat{p}_j, \hat{p}_k), \tag{6.4}$$

where the functions S and A are respectively symmetric and antisymmetric polynomials in the scalar products of the unit vectors $\hat{p}_i$ in the directions of the particles i. The simplest example of the Π class of observables has S = 1 and was denoted Π_1, while the simplest non-trivial member of the Ψ class (denoted by Ψ_1) has $A = [(\hat{p}_i \cdot \hat{p}_k)^2(\hat{p}_k \cdot \hat{p}_j) + (\hat{p}_j \cdot \hat{p}_i)^2(\hat{p}_i \cdot \hat{p}_k) + (\hat{p}_k \cdot \hat{p}_j)^2(\hat{p}_j \cdot \hat{p}_i) - (\hat{p}_i \cdot \hat{p}_j)^2(\hat{p}_j \cdot \hat{p}_k) - (\hat{p}_k \cdot \hat{p}_i)^2(\hat{p}_i \cdot \hat{p}_j) - (\hat{p}_j \cdot \hat{p}_k)^2(\hat{p}_k \cdot \hat{p}_i)]$. It is clear from our previous arguments that the moments of Π_S and Ψ_A are infrared stable when computed in QCD perturbation theory. As discussed in Ref. 3, we found Π_1 to be the most useful observable in that it offered the greatest discrimination between 3 jet and isotropic processes at the Υ mass. In Fig. 6.2 we show $\langle\Pi_1\rangle$ as a function of $\sqrt{s}$ for the three processes discussed in the previous subsection. There are again reasonably large differences between the results for $e^+e^- \to \zeta \to GGG$ events and for our models with isotropic ζ decay. However, comparison of Figs. 6.1 and 6.2 shows that $\langle F_{3\perp}\rangle$ is somewhat better than $\langle\Pi_1\rangle$ at distinguishing the processes. Π_1 does have two advantages, however: first, it is much easier to calculate than $\langle F_{3\perp}\rangle$, and further it is not only possible to find easily the mean $\langle\Pi_1\rangle$ but also the distribution $1/\sigma\, d\sigma/d\Pi_1$. The latter provides additional discrimination as discussed in Ref. 3.

We now describe the relationship of the observables Π_S and Ψ_A to F_3^{pt}; the analogue to the result that the H_ℓ are the Legendre moments of F_2^{pt}. We specialize to the idealized case of point detectors and write F_3^{pt} in the rather formal manner

$$F_3^{pt}(\hat{\Omega}_{d1}, \hat{\Omega}_{d2}, \hat{\Omega}_{d3}) = 8\pi \int d\hat{\Omega}\, \rho(\hat{\Omega}\hat{\Omega}_{d1})\rho(\hat{\Omega}\hat{\Omega}_{d2})\rho(\hat{\Omega}\hat{\Omega}_{d3}). \tag{6.5}$$

Here $\hat{\Omega}$ and $\hat{\Omega}_{dk}$ (k = 1,2,3) are elements of the rotation group. $\hat{\Omega}$ runs over all rotations (labeled by 3 Euler angles so that $\int d\hat{\Omega} = 8\pi^2$) while $\hat{\Omega}_{dk}$ is defined so that the direction of detector k is given by $\hat{\Omega}_{dk}\hat{z}$ where $\hat{z}$ is unit vector in the z direction. We have written (6.5) for the case of a continuous energy density ρ normalized to unity when integrated over <u>independent</u> values of its argument (i.e., dropping the redundant azimuthal integral in $d\hat{\Omega}$), so that

$$\int d\hat{\Omega}\, \rho(\hat{\Omega}) = 2\pi \tag{6.6}$$

and $\rho = 1/4\pi$ for an isotropic event. Of course, for a particle event (6.5) is valid with ρ as a sum of delta functions at the angles of the various particles. We now define the multipole moments A_ℓ^m as in Refs. 2 and 3:

$$A_\ell^m = \frac{1}{2\pi} \int d\hat{\Omega}\, \rho(\hat{\Omega}) Y_\ell^m(\hat{\Omega}) \tag{6.7}$$

or conversely

$$\rho(\hat{\Omega}) = \sum_{\ell,m} A_\ell^m \sqrt{\frac{2\ell+1}{4\pi}}\, D_{m0}^\ell(\hat{\Omega}) \tag{6.8}$$

where D_{mn}^ℓ, are the conventional rotation matrices which can be written as

$$D_{m0}^\ell(\hat{\Omega}) = \exp(-im\phi) d_{m0}^\ell(\theta) \tag{6.9}$$

where $$\hat{\Omega} = \hat{R}_z(\phi)\hat{R}_y(\theta)\hat{R}_z(\psi) \tag{6.10}$$

is expressed as a product of rotations about the y and z axes.

Substituting (6.8) into (6.5), we use the addition theorem for the D matrices to find

$$F_3^{pt}(\hat{\Omega}_{d1},\hat{\Omega}_{d2},\hat{\Omega}_{d3}) = \sum_{\substack{\ell_1\ell_2\ell_3\\ m_1m_2m_3\\ m_1'm_2'm_3'}} \int d\hat{\Omega}\, D^{\ell_1}_{m_1m_1'}(\hat{\Omega})D^{\ell_2}_{m_2m_2'}(\hat{\Omega})D^{\ell_3}_{m_3m_3'}(\hat{\Omega}) \tag{6.11}$$

$$A^{m_1}_{\ell_1}A^{m_2}_{\ell_2}A^{m_3}_{\ell_3}D^{\ell_1}_{m_1o}(\hat{\Omega}_{d1})D^{\ell_2}_{m_2o}(\hat{\Omega}_{d2})D^{\ell_3}_{m_3o}(\hat{\Omega}_{d3})\sqrt{\frac{(2\ell_1+1)(2\ell_2+1)(2\ell_3+1)}{\pi}}.$$

Defining the rotationally invariant three detector moments $T_{\ell_1\ell_2\ell_3}$ by

$$T_{\ell_1\ell_2\ell_3} = (4\pi)^{3/2} \sum_{m_1m_2m_3} \begin{pmatrix}\ell_1\ell_2\ell_3\\ m_1m_2m_3\end{pmatrix} A^{m_1}_{\ell_1}A^{m_2}_{\ell_2}A^{m_3}_{\ell_3} \tag{6.12}$$

the integral $d\hat{\Omega}$ may be expressed in terms of 3-j symbols [39] so that

$$F_3^{pt}(\hat{\Omega}_{d1},\hat{\Omega}_{d2},\hat{\Omega}_{d3}) = \sum_{\ell_1\ell_2\ell_3} T^{\ell_1\ell_2\ell_3}\Lambda^{\ell_1\ell_2\ell_3}(\hat{\Omega}_{d1},\hat{\Omega}_{d2},\hat{\Omega}_{d3}) \tag{6.13}$$

where

$$\Lambda^{\ell_1\ell_2\ell_3}(\hat{\Omega}_{d1},\hat{\Omega}_{d2},\hat{\Omega}_{d3}) = \sqrt{(2\ell_1+1)(2\ell_2+1)(2\ell_3+1)}$$
$$\sum_{m_1m_2m_3} \begin{pmatrix}\ell_1\ell_2\ell_3\\ m_1m_2m_3\end{pmatrix} D^{\ell_1}_{m_1o}(\hat{\Omega}_{d1})D^{\ell_2}_{m_2o}(\hat{\Omega}_{d2})D^{\ell_3}_{m_3o}(\hat{\Omega}_{d3}). \tag{6.14}$$

Λ is a function of general mathematical interest. It is a rotationally invariant function of three directions. This invariance can be expressed as

$$\Lambda^{\ell_1\ell_2\ell_3}(R\hat{\Omega}_{d1},R\hat{\Omega}_{d2},R\hat{\Omega}_{d3}) = \Lambda^{\ell_1\ell_2\ell_3}(\hat{\Omega}_{d1},\hat{\Omega}_{d2},\hat{\Omega}_{d3}) \tag{6.15}$$

for any rotation $\hat{R}$. Λ is the three-direction analogue of the two-direction rotationally-invariant function $P_\ell(\hat{\Omega}_{d1}^{-1}\hat{\Omega}_{d2})$. Of course, the H_ℓ are the two direction analogues of $T^{\ell_1\ell_2\ell_3}$ and F_2^{pt} can be expressed in terms of H_ℓ and $P_\ell(\hat{\Omega}_{d1}^{-1}\hat{\Omega}_{d2})$ in analogy to (6.13). If any ℓ value is zero, $\Lambda^{\ell_1\ell_2\ell_3}$ and $T^{\ell_1\ell_2\ell_3}$ reduce to $P_\ell(\hat{\Omega}_{d1}^{-1}\hat{\Omega}_{d2})$ and H_ℓ, respectively.

Note that if $\ell_1 + \ell_2 + \ell_3$ is even, then T and Λ are real and invariant under any permutation of indices {k} in the ℓ_k and $\hat{\Omega}_{dk}$. On the other hand, if $\ell_1 + \ell_2 + \ell_3$ is odd, then both T and Λ are purely imaginary and permutations of {k} multiply them by the signature of the permutation.

This fact leads to our first test for planes. If in a planar event we choose the x and z axes to be in the plane, then the A^m_ℓ are manifestly purely real and hence all $T^{\ell_1\ell_2\ell_3}$ are real. Therefore, $T^{\ell_1\ell_2\ell_3}$ vanishes for planar events if $\ell_1 + \ell_2 + \ell_3$ is odd. The simplest nontrivial constraint corresponds to $T^{234} = 0$ and one can easily show that

$$\Psi_1 = \frac{8}{35}\,\mathrm{Im}(T^{234}). \tag{6.16}$$

The equivalence between Ψ-like tests (in sense of (6.4)) and $\mathrm{Im}(T^{\ell_1\ell_2\ell_3};\ \ell_1+\ell_2+\ell_3$ odd) is complete. Note that both Ψ_A and $\mathrm{Im}(T^{\ell_1\ell_2\ell_3})$ are pseudoscalars (i.e., change sign on reversal of all the particle momenta) while Ξ_S and $\mathrm{Re}(T^{\ell_1\ell_2\ell_3})$ are scalars.

We now show how to obtain observables of the Ξ type from our new formalism. We first choose a particular configuration for the three detectors with detector 1 along the z axis and detector 2 in the xz plane:

$$\hat{\Omega}_{d1} = 1$$

$$\hat{\Omega}_{d2} = \hat{R}_y(\theta_2) \tag{6.17}$$

$$\hat{\Omega}_{d3} = \hat{R}_z(\phi_3)\hat{R}_y(\theta_3).$$

This makes the degrees of freedom of Λ manifest but loses the elegant symmetry of the original form (6.14). We can now express F_3^{pt} as a Fourier series in the azimuthal variable ϕ_3:

$$\begin{aligned} F_3^{pt}(\theta_2,\theta_3,\phi_3) &= \sum_m \Gamma^m(\theta_2,\theta_3)\exp(im\phi_3) \\ &= 2\sum_{m\geq o}(\mathrm{Re}\Gamma^m)\cos m\phi_3 - 2\sum_{m>o}(\mathrm{Im}\Gamma^m)\sin m\phi_3 \end{aligned} \tag{6.18}$$

where

$$\begin{aligned} \Gamma^m(\theta_2,\theta_3) = &\sum_{\ell_1\ell_2\ell_3}\sqrt{(2\ell_1+1)(2\ell_2+1)(2\ell_3+1)}\; T^{\ell_1\ell_2\ell_3} \\ &\begin{pmatrix}\ell_1 & \ell_2 & \ell_3\\ o & m & -m\end{pmatrix} d^{\ell_2}_{mo}(\theta_2)d^{\ell_3}_{-mo}(\theta_3). \end{aligned} \tag{6.19}$$

For a planar event, F_3^{pt} is proportional to a delta function at $\phi_3 = 0$, and inverting the Fourier series (6.18) this implies

$$\mathrm{Im}\Gamma^m = 0 \qquad (m \text{ integer}) \tag{6.20}$$

$$\mathrm{Re}\Gamma^m = \mathrm{Re}\Gamma^{m'} \qquad (m,m' \text{ integer}). \tag{6.21}$$

The result (6.20) is just the vanishing of $\mathrm{Im}(T^{\ell_1\ell_2\ell_3})$ for planar events that we have already discussed. Some of the information in (6.21) can be turned into new moment constraints that are equivalent to $\Pi_S = 0$ in (6.4). Consider the relation

$$\mathrm{Re}\Gamma^{m_1} = \mathrm{Re}\Gamma^{m_2} \qquad m_1 > m_2 \tag{6.22}$$

where m_1 and m_2 differ by an even integer. Multiply both sides of (6.22) by $d^{\ell_2}_{m_1o}(\theta_2)d^{\ell_3}_{-m_1o}(\theta_3)$ and integrate $d(\cos\theta_2)d(\cos\theta_3)$. Using the orthogonality of the d matrices, we pick up a finite linear combination of $T^{\ell_1\ell_2\ell_3}$ (ℓ_2, ℓ_3 fixed, ℓ_1 varies) on the left hand side. Now we can express $d^{\ell_2}_{m_1o}(\theta_2)$ as a linear combination of $d^{\ell_2'}_{m_2o}(\theta_2)$ with $\ell_2' \leq \ell_2$ and similarly for ℓ_3. (Here we use our choice that m_1 and m_2 differ by an even integer.) It follows that the right hand side is also a finite linear combination of $T^{\ell_1\ell_2\ell_3}$ observables and hence (6.22) gives rise to a set of finite relations between $\mathrm{Re}T^{\ell_1\ell_2\ell_3}$ for planar events. These relations may be translated into constraints of the form $\Pi_S = 0$. For example, the simplest observable Π_1 is obtained from the relation $\mathrm{Re}\Gamma^2 = \mathrm{Re}\Gamma^o$ on multiplying through by $d^2_{20}(\theta_2)d^2_{-20}(\theta_3)$ and integrating. Reference 3 gives some of the simpler Π observables found in this way as linear combinations of the $T^{\ell_1\ell_2\ell_3}$.

Section 6 - Figure Captions

6.1 The mean energy correlation $\langle F_{3\perp}\rangle$ between three orthogonal detectors with angular radii $\cos^{-1}(0.95) \simeq 18°$, as a function of $\sqrt{s}$, for three classes of processes discussed in the text. At infinite energy, coplanar events such as $\zeta \to GGG$ give $\langle F_{3\perp}\rangle = 0$, while a completely isotropic distribution of energy in the final state gives $\langle F_{3\perp}\rangle = 1$. '6 jet' final states give $\langle F_{3\perp}\rangle \simeq 0.2$ as $\sqrt{s} \to \infty$.

6.2 The mean coplanarity parameter $\langle \Pi_1\rangle$ defined in Sec. 6.2 as a function of s. At infinite $\sqrt{s}$, $\zeta \to GGG$ gives $\langle \Pi_1\rangle = 0$, isotropic events $\langle \Pi_1\rangle = 2/9$ and '6 jet' ones $\langle \Pi_1\rangle \simeq 0.07$.

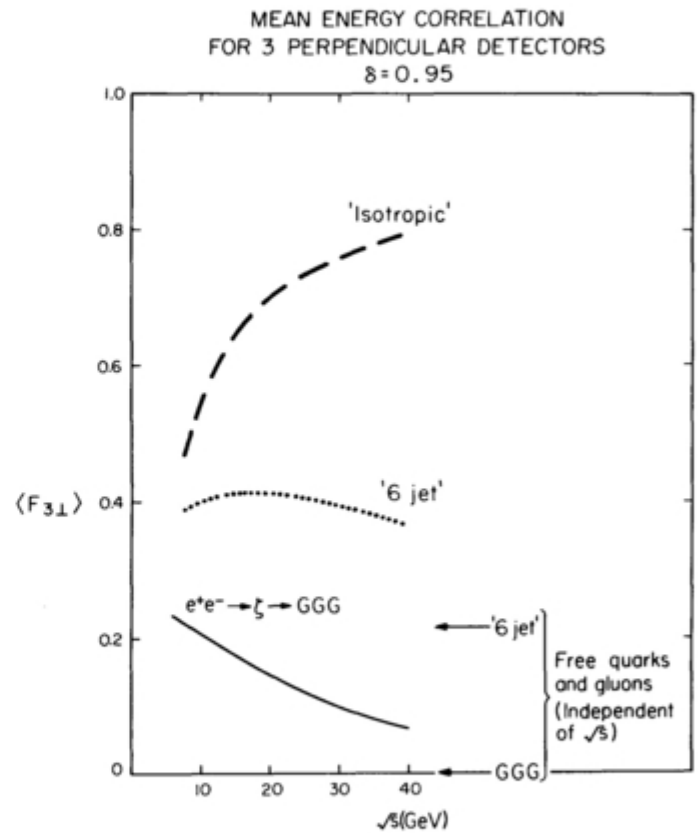

Fig. 6.1

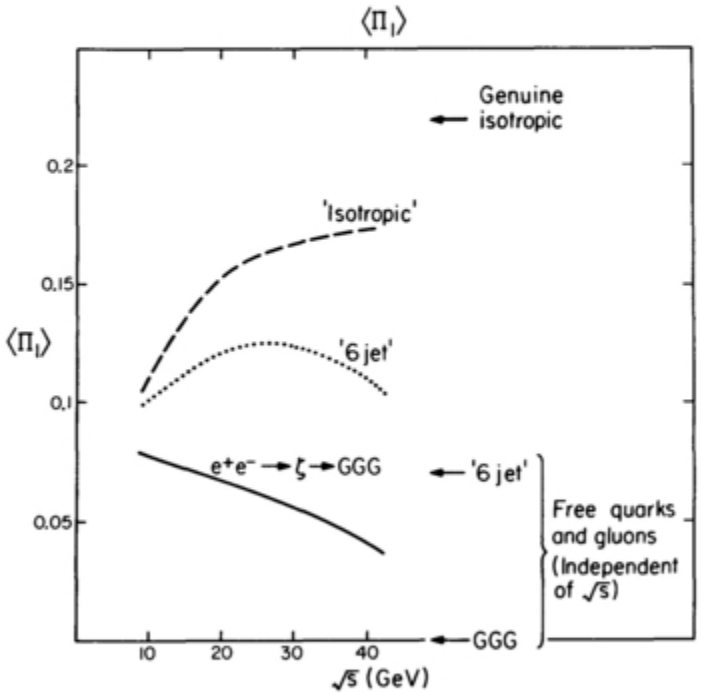

Fig. 6.2

Acknowledgments

We are grateful to R. P. Feynman, H. D. Politzer and especially R. D. Field for discussions and comments and to the MATHLAB group of the MIT Laboratory for Computer Science for the use of MACSYMA.

Appendix A: Analytical Results for Mean Two-detector Energy Correlations in the Free Quark and Gluon Approximation

In this appendix, we give the $\langle F_2^{pt}(\chi)\rangle$ for various processes in the free quark and gluon approximation. The $\langle F_2(\chi,\delta)\rangle$ for detectors of non-zero area can be obtained by smearing $\langle F_2^{pt}(\chi)\rangle$ using the formula (4.10).

All $e^+e^- \to q\bar{q}$ events give

$$F_2^{pt}(\chi) = [\delta(1-\chi) + \delta(1+\chi)]. \tag{A.1}$$

Three-particle final states give rise to a distribution of forms for $F_2^{pt}(\chi)$. Taking the fractional energies of the particles to be $x_i = \frac{2E_i}{\sqrt{s}}$, $\langle F_2^{pt}(\chi)\rangle$ becomes

$$\langle F_2^{pt}(\chi)\rangle = \sum_{\substack{i,j\\ i\neq j}} \frac{1}{2}\int_0^1 dx_i dx_j x_i x_j \frac{1}{\sigma}\frac{d\sigma}{dx_i dx_j}\left|\frac{\partial x_j}{\partial\cos\phi_{ij}}\right| \delta(x_j-\tilde{x}_j) + \frac{1}{2}\langle\Sigma x_i^2\rangle\delta(1-\chi), \tag{A.2}$$

where $\tilde{x}_j$ is determined by requiring that the angle ϕ_{ij} between particles i and j satisfies $\cos\phi_{ij} = \chi$, i.e.,

$$\tilde{x}_j = \frac{2(1-x_i)}{2 + x_i(\chi-1)}. \tag{A.3}$$

The Jacobian is, therefore, simply

$$\left|\frac{\partial x_j}{\partial\cos\phi_{ij}}\right| = \frac{2x_i(1-x_i)}{[2+x_i(\chi-1)]^2}. \tag{A.4}$$

Then, dropping the infrared divergent part of $\langle F_2^{pt}(\chi)\rangle$ at $\chi = 1$ coming from

the case i = j and given in eq. (3.7), one finds that for $e^+e^- \to q\bar{q}G$,

$$\langle F_2^{pt}(\chi)\rangle = \frac{16\alpha_s}{3\pi}\frac{(\chi+2)}{(1+\chi)(1-\chi)^5}\{4(\chi^2+4\chi+1)\log(\tfrac{1+\chi}{2}) + 3(1-\chi)(1+3\chi)\}. \tag{A.5}$$

Hence, for example

$$\langle F_2^{pt}(0)\rangle = \frac{32(3-4\log 2)\alpha_s}{3\pi} \simeq 0.77\,\alpha_s. \tag{A.6}$$

The forms for $\langle F_2^{pt}(\chi)\rangle$ close to $\chi = \pm 1$ are given in eqs. (3.4) and (3.5). The form (A.6) is essentially indistinguishable from that of $\langle F_2(\chi,\delta)\rangle$ in the free quark and gluon approximation when $\delta = 0.95$, shown in Fig. 4.2. Of course, the true form of $\langle F_2^{pt}(\chi)\rangle$ contains a term proportional to $\delta(1-\chi)$ with a divergent coefficient, whereas in $\langle F_2(\chi,\delta)\rangle$ this divergence is smeared out. Note that the result (A.5) is obtained by integrating over all possible $q\bar{q}G$ final states, with no cut on H_2. In our prescription for treating hadronic final states, we only consider $q\bar{q}G$ final states which have $H_2 < H_2^{cut}$. The form of $\langle F_2^{pt}(\chi)\rangle$ for $e^+e^- \to q\bar{q}G$ when $H_2^{cut} = 0.8$ is qualitatively similar to the result (A.5) ($H_2^{cut} = 1$), but there is a slight suppression near $\chi = \pm 1$.

On several occasions, we approximate $\langle F_2^{pt}(\chi)\rangle$ for $e^+e^- \to q\bar{q}G$ by the value obtained by performing the sum (A.2) only over the q and $\bar{q}$ and neglecting contributions from the gluon. In this case,

$$\langle F_2^{pt}(\chi)\rangle = \frac{8\alpha_s}{3\pi}\frac{1}{3(\chi-1)^5(1+\chi)}\{24(3\chi+5)\log(\tfrac{1+\chi}{2}) + (\chi-1)(\chi^2-14\chi-83)\} \tag{A.7}$$

so that

$$\langle F_2^{pt}(0)\rangle = \frac{8(120\log 2-83)\alpha_s}{9\pi} \simeq 0.05\ \alpha_s. \tag{A.8}$$

This is much smaller than the result (A.6) for the complete $q\bar{q}G$ final state since the q and $\bar{q}$ are rarely at 90°. Near $\chi = -1$, (A.7) becomes

$$\frac{-2\alpha_s}{3\pi}\left\{\frac{2\log(\frac{1+\chi}{2})}{(1+\chi)} + \frac{17}{3(1+\chi)} + \ldots\right\}. \tag{A.9}$$

Note that while the leading term here is the same as in (3.4) for the complete case, the subleading terms differ. For $\chi \simeq +1$, $\langle F_2^{pt}(\chi)\rangle$ calculated using only the q and $\bar{q}$ has no divergence and its regular part tends simply to $\alpha_s/30\pi$.

The process $\zeta \to GGG$ at lowest order (g^6) in g^2 gives

$$\begin{aligned}\langle F_2^{pt}(\chi)\rangle = &\left(\frac{6}{\pi^2-9}\right)\frac{1}{(1-\chi)^3}\left\{(2-5\chi)\sqrt{1-\chi^2}\left(\frac{\cos^{-1}\chi}{2}\right)\right.\\ &\left.-(3\chi^2+4\chi+5)\log\left(\frac{1+\chi}{2}\right) + (1-\chi)(2\chi-5)\right\} \qquad (A.10)\\ &+\left(\frac{13\pi^2-127}{2(\pi^2-9)}\right)\delta(1-\chi),\end{aligned}$$

where the last term comes from events in which the same particle passes through both detectors. At $\chi = 0$ one finds

$$\langle F_2^{pt}(0)\rangle = \left(\frac{6}{\pi^2-9}\right)\left[5(\log 2-1) + \frac{\pi}{2}\right] \simeq 0.252. \tag{A.11}$$

Near $\chi = -1$, (A.10) becomes

$$-\frac{3}{2(\pi^2-9)}\left[\log\left(\frac{1+\chi}{2}\right) + 7 + \ldots\right], \tag{A.12}$$

while at $\chi = +1$, the regular part of (A.10) tends to $1/(10(\pi^2-9)) \simeq 0.114$. All these results are very similar to those for a three particle final state generated uniformly in phase space as discussed in Sec. 2.6. Once again, the mean $\langle F_2(\chi,\delta)\rangle$ with $\delta = 0.95$ given in Fig. 4.2 for the free quark and gluon approximation is essentially identical to the form in eq. (A.7), except near $\chi = 1$.

In [2] we discussed various possible mechanisms for the production and weak decay of heavy quark pairs near threshold. Two of these ($Q \to q'G$ and $Q\bar{q}_s \to q'\bar{q}_s$) gave rise to events containing four jets of equal energy in two collinear pairs. If the angle between these pairs of jets in a particular event is ζ, then the energy correlation function for this event will be

$$F_2^{pt}(\chi) = \frac{1}{2}\left[\delta(1-\chi) + \delta(1+\chi) + \delta(\chi-\cos\zeta) + \delta(\chi+\cos\zeta)\right] \tag{A.13}$$

giving immediately

$$\begin{aligned}H_\ell &= \frac{1}{2}\left(P_\ell(\cos\zeta) + 1\right) \qquad (\ell \text{ even})\\ &= 0 \qquad (\ell \text{ odd}).\end{aligned} \tag{A.14}$$

Averaging over all values of $\cos\zeta$, one obtains

$$\begin{aligned}\langle F_2^{pt}(\chi)\rangle &= \frac{1}{2}\left[\delta(1-\chi) + \delta(1+\chi) + 1\right],\\ \langle F_2^{pt}(0)\rangle &= \frac{1}{2}.\end{aligned} \tag{A.15}$$

Three-body heavy quark decays were also considered in [2]. With this decay scheme, $Q\bar{Q}$ production and decay gives

$$\langle F_2^{pt}(\chi)\rangle = \frac{1}{2} + \frac{8}{(1-\chi)^7}\{6(1+\chi)(\chi^3+33\chi^2+171\chi+195)\log(\frac{1+\chi}{2}) + (1-\chi)(25\chi^3+401\chi^2+1163\chi+811)\} + \frac{11}{30}\,\delta(1-\chi), \tag{A.16}$$

so that

$$\langle F_2^{pt}(0)\rangle = \frac{1}{2} + 8(811-1170\log 2) \simeq 0.642. \tag{A.17}$$

At $\chi = -1$, (A.16) becomes 7/2, while the regular part goes to 19/35 as $\chi \to +1$. Note the absence of a $\log(1+\chi)$ divergence as $\chi \to -1$.

Appendix B: $2 + \sin^2\theta_N$ Forever?

A remarkable feature of the results presented in Sec. 4.2 was that four distinct processes gave a $2 + \sin^2\theta_N$ distribution for the angle θ_N between the incoming beam direction and the normal to the plane defined by the (three-particle) final state: $e^+e^- \to q\bar{q}G$, $e^+e^- \to \zeta(^3S_1) \to GGG$, $e^+e^- \to q\bar{q}\phi$, where ϕ is a scalar 'gluon' and $e^+e^- \to q\bar{q}$, where the plane in this case is taken to have a uniform distribution about the $q\bar{q}$ direction. One may wonder whether this common $2 + \sin^2\theta_N$ dependence is accidental or has some fundamental significance. As we will now describe, our tentative conclusion is that it is largely accidental.

The formalism of Sec. 3.2 shows that a $2 + \sin^2\theta_N$ distribution has a simple interpretation in terms of the amplitudes E_λ for virtual photons of helicity λ to decay to a given final state configuration. We work in the virtual photon rest frame and quantize the photon spin along the normal to the plane defined by the final state particles. Then the condition for a $2 + \sin^2\theta_N$ angular distribution is

$$|E_0|^2 = |E_1|^2 + |E_{-1}|^2. \tag{B.1}$$

This may also be expressed as a constraint on the photon polarization amplitude A_μ. If z is the normal to the final state plane, and the x and y are axes in the plane, then (B.1) may be rewritten as

$$|A_z|^2 = |A_x|^2 + |A_y|^2. \tag{B.2}$$

Note that gauge invariance for a photon at rest implies

$$|A_o|^2 = 0. \tag{B.3}$$

We first discuss the origin of the $2 + \sin^2\theta_N$ behavior in the process $e^+e^- \to q\bar{q}G$. As mentioned in Sec. 4.3, this angular distribution is easy to understand in the infrared limit where the virtual quark is nearly on shell. Here, the gluon will be distributed uniformly in azimuth about the $q\bar{q}$ direction, while the q and $\bar{q}$ will have a $1 + \cos^2\theta$ angular distribution with respect to the beam direction. In this limit, therefore, $e^+e^- \to q\bar{q}G$ behaves like $e^+e^- \to q\bar{q}$ with random plane orientation, and the $2 + \sin^2\theta_N$ form follows directly. The same result holds for scalar gluons. Unfortunately, these arguments cannot be extended away from the infrared region where the q and $\bar{q}$ no longer have a $1 + \cos^2\theta$ angular distribution. In Feynman gauge, one finds that for each of the two diagrams contributing to $e^+e^- \to q\bar{q}G$,

$$|A_z|^2 = |A_x|^2 + |A_y|^2 - |A_o|^2. \tag{B.4}$$

However, only in the sum of the diagrams does the $|A_o|^2$ term cancel so that the requirement (B.2) is satisfied. The fact that all diagrams must be included (at least in Feynman gauge) in order to obtain a $2 + \sin^2\theta_N$ angular distribution for $e^+e^- \to q\bar{q}(G)$ suggests that its appearance there is somewhat 'accidental'.

For $e^+e^- \to \zeta + GGG$, the situation is even more mysterious. In this case, two heavy quarks annihilate at rest leaving no hint of a $1 + \cos^2\theta$ beam distribution which might be transmuted into a $2 + \sin^2\theta_N$ plane angular distribution. In fact, one can easily show that the $2 + \sin^2\theta_N$ obtained for ζ decay to spin 1 gluons does not hold for spin 0 gluons. For scalar gluons, $E_o = 0$, while for pseudoscalar ones, $E_1 = E_{-1} = 0$.

We conclude that we are unable to find a fundamental explanation for the widespread $2 + \sin^2\theta_N$ behavior. Perhaps the reader can.

Appendix C: 'Scalar QCD'

In assessing to what extent various measurements constitute tests of QCD, it is convenient to compare QCD predictions for them with results obtained from other theories. In this appendix, we give the forms for some of the results discussed in this paper which would follow from a theory in which the gluons (ϕ) are colored scalars. This theory has many fundamental differences from QCD. In particular, the effective $qq\phi$ coupling λ does not tend logarithmically to zero as s increases but rather goes to a constant value as a power of s. Nevertheless, this behavior is not yet ruled out by deep inelastic scattering measurements. The $\gamma^* \to q\bar{q}\phi$ differential cross-section is

$$\frac{d\sigma}{dx_1 dx_2} = \frac{\lambda}{3\pi} \frac{x_3^2}{(1-x_1)(1-x_2)}. \tag{C.1}$$

Note that this exhibits collinear but not soft infrared divergences. Adding in the one-loop corrections to $\gamma^* \to q\bar{q}$, one finds that for scalar QCD, the e^+e^- total cross-section is [FC.1]

$$\sigma = \sigma_0 (1 + \frac{\lambda}{2\pi} + \ldots). \tag{C.2}$$

From eq. (C.1) one finds that for $e^+e^- \to q\bar{q}(\phi)$:

$$\langle H_2 \rangle = 1 - \frac{\lambda}{3\pi} (21-2\pi^2) \simeq 1 - 0.13\ \lambda \tag{C.3}$$

$$\langle H_3 \rangle = \frac{20\lambda}{9} (7\pi^2-69) \simeq 0.19\ \lambda, \tag{C.4}$$

while for $e^+e^- \to q\bar{q}(G)$ [2]:

$$\langle H_2 \rangle = 1 - \frac{2\alpha_s}{3\pi} (4\pi^2-33) \simeq 1 - 1.4\ \alpha_s \tag{C.5}$$

$$\langle H_3 \rangle = \frac{2\alpha_s}{9\pi} (1980-200\pi^2) \simeq 0.43\ \alpha_s. \tag{C.6}$$

For $e^+e^- \to q\bar{q}\phi$:

$$\langle F_2^{pt}(\chi) \rangle = \frac{2\lambda}{3\pi} \frac{1}{(\chi-1)^5(1+\chi)} [8(1+\chi)(2\chi^2+18\chi+19)\log(\frac{1+\chi}{2}) + (1-\chi)(47\chi^2+160\chi+105)] + C\delta(1-\chi), \tag{C.7}$$

$$\langle F_2^{pt}(0) \rangle = \frac{2\lambda}{3\pi} (152\log 2-105) \simeq 0.076\ \lambda. \tag{C.8}$$

The corresponding results for $e^+e^- \to q\bar{q}G$ are given in Appendix A. Equations (C.3) through (C.8) indicate that, for a given value of the coupling constant, scalar QCD predicts that continuum e^+e^- annihilation events should be closer to the two-jet limit than is expected from QCD.

Near $\chi = -1$, the $\langle F_2^{pt}(\chi) \rangle$ given in (C.7) becomes

$$\frac{\lambda}{3\pi} [\frac{1}{(1+\chi)} + \frac{6\log(\frac{1+\chi}{2})-25}{4} + \ldots], \tag{C.9}$$

while around $\chi = +1$, the regular part goes like

$$\frac{\lambda}{3\pi} [\frac{1}{12(1-\chi)} + \frac{7}{30} + \ldots]. \tag{C.10}$$

Note the absence of a double logarithmic divergence in the integral of $\langle F_2^{pt}(\chi) \rangle$ close to $\chi = -1$. This implies that the $\langle H_\ell \rangle$ for $e^+e^- \to q\bar{q}(\phi)$ depend on $\log(\ell)$ for large ℓ, rather than $\log^2(\ell)$, as in QCD. The $\langle H_\ell \rangle$ at large ℓ for the

process $e^+e^- \to q\bar{q}(\phi\phi....)$ behave like $\ell^{-a\lambda}$ when summed to all orders in λ, in contrast to the result $\sim \ell^{-ba_s \log \ell}$ found in QCD.

Appendix C - Footnote

FC.1 For colored scalar quarks, but vector gluons, this result becomes

$$\sigma = \sigma_0 (1 + \frac{4\lambda}{\pi} + ...).$$

References

1. The Concise Oxford Dictionary of Current English, Clarendon press, Oxford, 1964.
2. G. C. Fox and S. Wolfram, Phys. Rev. Lett. 41, 1581 (1978); Nucl. Phys. B149, 413 (1979).
3. G. C. Fox and S. Wolfram, Phys. Lett B 82, 134 (1979).
4. M. L. Goldberger and K. M. Watson, 'Collision Theory,' Wiley, 1964, p. 552.
5. K. Konishi, A. Ukawa and G. Veneziano, 'Jet Calculus: A Simple Algorithm for Resolving QCD Jets,' Rutherford preprint RL-79-026 (Feb. 1979).
6. G. C. Fox, T.-Y. Tse and S. Wolfram, 'Event Shapes in Deep Inelastic Scattering,' Caltech preprint, in preparation.
7. E. C. Poggio, H. R. Quinn and S. Weinberg, Phys. Rev. D13, 1958 (1976); R. G. Moorhouse, M. R. Pennington and G. G. Ross, Nucl. Phys. B124, 285 (1977).
8. L. D. Landau and E. M. Lifshitz, 'Quantum Mechanics,' Pergamon 1977, Section 136.
9. A. de Rujula, J. Ellis, E. G. Floratos and M. K. Gaillard, Nucl. Phys. B138, 387 (1978).
10. S. Frautschi and A. Krzywicki, Zeit. fur Phys. C, 1, 25 (1979).
11. G. Källén and A. Sabry, Mat. Fys. Medd. Dan. Vid. Selsk, 29 (1955) No. 17; J. Schwinger, 'Particles, Sources and Fields,' Vol. 2, Addison-Wesley, 1973, p. 407; O(8): S. S. Kanwal, private communication.
12. S. Weinberg, Phys. Rev. D8, 3497 (1973).
13. D. A. Ross, A. E. Terrano and S. Wolfram, 'e^+e^- Annihilation to Order α_s^2,' Caltech preprint in preparation; M. Dine and J. Sapirstein, 'Higher Order QCD Corrections in e^+e^- Annihilation,' SLAC preprint (July 1979); K. Khetypkin, A. Kataev and S. Tkakhoy, unpublished telex (1979).

14. A. E. Terrano and S. Wolfram in S. Wolfram, 'MACSYMA Tools for Feynman Diagram Calculations,' Caltech preprint CALT-68-720 (May 1979), and Proceedings of the 1979 MACSYMA Users' Conference, (Washington, D.C., June 1979).
15. A. Ali et al., DESY preprint, 79/03 (Jan. 1979).
16. B. Rossi, 'High-Energy Particles,' Prentice-Hall, 1952; R. L. Ford and W. R. Nelson, 'The EGS Code System,' SLAC preprint SLAC-210 (June 1979).
17. B. Rossi, Ref. [16], p. 238.
18. R. K. Ellis et al., Nucl. Phys. B152, 285 (1979); D. Amati et al., Nucl. Phys. B146, 29 (1978); G. Sterman and S. Libby, Phys. Rev. D18, 3252 (1978).
19. R. D. Field, private communication.
20. Yu. L. Dokshitser, D. I. D'Yakonov and S. I. Troyan, 'Inelastic Processes in QCD,' SLAC Translation 183 (1978).
21. W. J. Stirling, talk given at the 1979 Caltech Workshop on High-Energy Physics, Feb. 1979.
22. G. Altarelli and G. Parisi, Nucl. Phys. B126, 298 (1977); Yu. L. Dokshitser, ZhETF 72, 1216 (1977).
23. C. L. Basham et al., 'Energy Correlations in Perturbative QCD: A Conjecture for All Orders,' Washington preprint RLO-1388-786 (1979).
24. E. M. Lifshitz and L. P. Pitaevskii, 'Relativistic Quantum Theory,' Pergamon 1973, Section 129 et seq.
25. J. M. Cornwall and G. Tiktopoulos, Phys. Rev. D13, 3370 (1976); R. Coquereaux and E. de Rafael, Phys. Lett. 69B, 181 (1977).
26. D. A. Ross, Nuovo Cim. 10A, 475 (1972).
27. G. Sterman and S. Weinberg, Phys. Rev. Lett. 39, 1436 (1977); M. B. Einhorn and B. Weeks, Nucl. Phys. B146, 445 (1978).
28. K. Shizuya and S.-H. H. Tye, 'QCD Phenomenology of Gluon Jets,' Fermilab preprint 79/16-THY (Jan, 1979).